ELSEVIER

Marine Geology 213 (2004) 9–72

MARINE GEOLOGY
INTERNATIONAL JOURNAL OF MARINE GEOLOGY, GEOCHEMISTRY AND GEOPHYSICS

www.elsevier.com/locate/margeo

Slope failure dynamics and impacts from seafloor and shallow sub-seafloor geophysical data: case studies from the COSTA project

M. Canals[a,*], G. Lastras[a], R. Urgeles[a], J.L. Casamor[a], J. Mienert[b], A. Cattaneo[c], M. De Batist[d], H. Haflidason[e], Y. Imbo[d], J.S. Laberg[b], J. Locat[f], D. Long[g], O. Longva[h], D.G. Masson[i], N. Sultan[j], F. Trincardi[c], P. Bryn[k]

[a]*GRC Geociències Marines, Dept. d'Estratigrafia, P. i Geociències Marines, Universitat de Barcelona, E-08028 Barcelona, Spain*
[b]*Institute of Geology, University of Tromso, N-9037 Tromso, Norway*
[c]*Istituto di Geologia Marina, CNR, I-40129 Bologna, Italy*
[d]*Renard Centre of Marine Geology, Ghent University, B-9000 Ghent, Belgium*
[e]*Dept. of Geology, University of Bergen, N-5007 Bergen, Norway*
[f]*Dept. of Geology and Geological Engineering, Université Laval, Québec, Canada G1K 7P4*
[g]*British Geological Survey, Edinburgh, EH9 3LA, United Kingdom*
[h]*Geological Survey of Norway, N-7491 Trondheim, Norway*
[i]*Challenger Division for Seafloor Processes, Southampton Oceanography Centre, Southampton, SO14 3ZH, United Kingdom*
[j]*IFREMER, F-29280 Plouzané Cédex, France*
[k]*Norsk Hydro, N-0246 Oslo, Norway*

Accepted 30 September 2004

Abstract

Holocene and slightly pre-Holocene submarine landslide are found both in high-latitude glacial-dominated margins and in lower latitude, river-dominated margins. This paper constitutes a major assessment on some of the best-studied submarine instabilities in the world. We review and update from original data and literature reports the current state of knowledge of Storegga, Traenadjupet and Finneidfjord slides from the mid-Norwegian margin, Afen Slide from the Faeroe-Shetland Channel, BIG'95 Slide and Central Adriatic Deformation Belt (CADEB) from continental slope and inner continental shelf settings off the Ebro and Po rivers in the Mediterranean Sea, Canary Slide west of the westernmost, youngest Canary Islands and Gebra Slide off the northern tip of the Antarctic Peninsula in the southern hemisphere, i.e. those studied in the Continental Slope Stability (COSTA) project. The investigated slides range in size from the gigantic 90,000 km^2 and almost 3000 km^3 Storegga Slide to the tiny 1 km^2 and 0.001 km^3 Finneidfjord Slide. Not only do individual submarine landslides rarely involve processes precisely fitting with pre-established categories, mostly based on subaerial research, but also they display complex mechanical behaviors within the elastic and plastic fields. Individual events can involve simultaneous or successive vertical to translational movements including block detachment, block gliding, debris flow, mud flow and turbidity currents. The need for an in-depth

* Corresponding author. Tel.: +34 93 402 1360; fax: +34 93 402 1340.
E-mail address: miquelcanals@ub.edu (M. Canals).

doi:10.1016/j.margeo.2004.10.001

revision of the classification criteria, and eventually for a new classification system, based on the new imaging capabilities provided by modern techniques, is more than obvious. We suggest a new system, which, for the moment, is restricted to debris flows and debris avalanches.

Volume calculation methods are critically reviewed and the relations between some key geomorphic parameters are established for the selected slides. The assumed volume missing from scar areas does not necessarily match the actual volume of sediment remobilised by an individual event since in situ sediment can be remoulded and eventually incorporated during the slide downslope journey. CADEB, a shore-parallel prodelta detached from its source, is the exception to the good correlation found between across slope width and alongslope length with slide area. Height drop measured from the headwall upper rim to its foot correlates with the debris deposit maximum thickness unless the slide moves into restricted areas, which prevent farther forward expansion of the deposit, such as Gebra and BIG'95. In such cases, "over-thickened" deposits are found. A particularly loose and fluid behavior can be deduced for slides showing an "over-thinned" character, such as the Canary Slide that traveled 600 km.

Scar areas and slip planes have been investigated with particular emphasis. Although slide headwalls might present locally steep gradients (up to 23° for Storegga Slide), the slope gradients of both the failed segment margins and the main slip planes are very low (max. 2° and usually around 1° and less). An exception is the Finneidfjord Slide (20°–<5°) that occurred in 1996 because of a combination of climatic and anthropogenic factors leading to excess pore pressure and failure. Mechanically distinct, low permeable clayey "weak layers" often correspond to slip planes beyond the slide headwall. Since not only formation of these "weak layers" but also sedimentation rates are climatically controlled, we can state that slide pre-conditioning is climatically driven too.

Run-out distances reflect the degree of disintegration of the failed mass of sediment, the total volume of initially failed material and transport mechanisms, including hydroplanning. Commonly, specific run-outs could be attributed to distinct elements, such as cohesive blocks and looser matrix, as nicely illustrated by the BIG'95 Slide. Total run-outs usually correspond to matrix run-outs since the coarser elements tend to rest at shorter distances. Outrunner blocks are, finally, a very common feature proving the ability of those elements to glide over long distances with independence of the rest of the failed mass.

In addition to pre-conditioning factors related to geological setting and sedimentation conditions, a final trigger is required for submarine landslides to take place, which is most often assumed to be an earthquake. In high latitude margins, earthquake magnitude intensification because of post-glacial isostatic rebound has likely played a major role in triggering landslides. Although it cannot be totally ruled out, there is little proof, at least amongst the COSTA slides, that gas hydrate destabilisation or other processes linked to the presence of shallow gas have acted as final triggers.

Keywords: COSTA project; BIG'95 Slide; mid-Norwegian margin

1. Introduction

A tremendous effort has been made in the last few years to characterize and better understand seafloor failures in European margins (Mienert and Weaver, 2002 and references therein) and elsewhere (Locat and Mienert, 2003 and references therein). The more that is known about continental margins, the clearer it becomes that submarine slides are a widespread phenomenon (Canals, 1985; Hühnerbach et al., 2004). The interests of the oil industry have triggered their study, jointly with other deepwater geohazards, mostly during the last decade as related to the exploration and exploitation of hydrocarbon resources in the deep sea (Campbell, 1999). A variety of slides, often related to fluid escape, is known to occur in the most important offshore oil provinces such as the Norwegian margin, the Gulf of Guinea, the Gulf of Mexico and the Caspian Sea (Barley, 1999). The second largest gas field discovery off Norway, the Ormen Lange field, is located within the scar created by the Storegga Slide, possibly the largest submarine slide in the world ocean (Bryn et al., 2003a).

Seafloor failures represent a major threat not only to the oil and offshore industries but also to the marine environment and coastal facilities. It is well known that large historical seafloor failures have engendered destructive tsunamis. Recent results indicate that the large tsunamis that devastated Lisbon and struck the Gulf of Cadiz and North Atlantic coasts both in Europe and Africa in 1755 following a magnitude ~8.5 earthquake probably had a landslide contribution

(Gracia et al., 2003). Seismicity in the Southwestern Iberian margin results from tectonic activity along the Europe–Africa plate boundary connecting the Azores Triple Junction to the west to the Gibraltar Strait to the east (Zitellini et al., 2001). The Lisbon event, as it is known, represents the largest natural catastrophe in Western Europe since the Roman period, which resulted in about 60,000 casualties in Portugal alone (Baptista et al., 1998). The destruction of Lisbon, at the time one of the main capitals in Europe, terrified European society. At present, there is an important international on-going effort off Portugal to further investigate the source area of the Lisbon earthquake and related submarine landsliding (Zitellini et al., 2001; Gracia et al., 2003).

The breaking of submarine telegraph cables during the Grand Banks event following an earthquake in 1929 is also an outstanding case that had a profound impact on deep sea sedimentological research. The water depth of the area affected ranges from 650 to about 2800 m, and the distance between the scar rim and the most distal deposit is >850 km. It appears that the Grand Banks mass movement may have reached a maximum velocity of about 70 km/h according to Heezen and Ewing (1952). The thickness of the turbidity current was of the order of hundreds of meters as determined from erosional trimlines (Piper and Aksu, 1987). Detailed descriptions of the Grand Banks event and resulting deposits can be found in Rupke (1978) and Piper et al. (1999). This event occurred at a time when the now widely accepted concepts of turbidity currents and the continuum of submarine mass gravity flows (from slumps to debris flows to turbidity currents) had not yet been conceived. Heezen and Ewing (1952) and Heezen and Hollister (1971) shook the scientific community after convincingly identifying the Grand Banks slumps and turbidity current as the cause of cable breaks south of Newfoundland in 1929. Their works followed famous earlier papers by Kuenen (1937) and Kuenen and Migliorini (1950) where these authors demonstrated the existence of turbidity currents and showed some of their properties after conducting a series of classic flume experiments. Other key pioneer papers that greatly helped in establishing the current background on mass gravity flows were those of Morgenstern (1967), Hampton (1972) and Middleton and Hampton (1976) to cite just a few. As correctly pointed out by Rupke (1978), these theories revolutionized the study of clastic sediments and enormously stimulated research on deep-sea sedimentary processes.

Now, we know that sediment failure around the epicenter of the 1929 Grand Banks earthquake shows a downslope transition from retrogressive thin-skinned rotational slumps, through debris flows, to erosional features cut by turbidity currents, to turbidite deposits (Piper et al., 1999). The 1929 turbidity current was thus triggered by prolonged numerous relatively small failures nourishing it over a period of about 11 h (Hughes Clarke, 1988). While limited deep-towed side scan sonar imagery, high resolution seismic reflection profiles, sediment cores, in situ shallow geotechnical measurements and submersible observations are available (Hughes Clarke et al., 1989; Piper et al., 1985, 1999), multibeam mapping of the continental slope area disturbed by the 1929 Grand Banks earthquake has not been completed, a surprising situation. The need for new data including swath bathymetry has steered an international consortium of research teams, which has advanced plans to deploy there the best geophysical tools available for deep seafloor and sub-seafloor imaging. The benefits from such an endeavor are anticipated to be of major importance.

A third recent submarine landslide that had a major impact both on coastal facilities and on the scientific community in Europe occurred off the French town of Nice in the Northwestern Mediterranean the 16th of October 1979. The source area was the prograding prodelta of the Var River that accumulated on a very narrow shelf. The nearby Monaco observatory registered no earthquake that could have triggered the slide (Malinverno et al., 1988). Because of the very steep nature of the seafloor off Nice, undercutting cannot be excluded as a concurrent potential triggering mechanism. In addition, sediment failures off Nice are favored by the common occurrence of underconsolidated, meter-thick sediment layers (Cochonat et al., 1993; Klaucke and Cochonat, 1999) although ridge-forming normally consolidated to overconsolidated sediments could also be involved (Mulder et al., 1993, 1994). Three types of sediment failure have been distinguished by Klaucke and Cochonat (1999): superficial slumping, deep-seated failure often associated with successive rotational slides and gullying of the canyon walls.

The shelf and upper slope 1979 slide evolved into a turbidity current, which, as in the Grand Banks case, broke submarine communication cables. The calculated peak velocity of the mass movement was 40 km/h according to Gennesseaux et al. (1980). The suction effect of the downslope-moving sediment mass generated first a retreat of the sea and, second, a several meters high tsunami wave (Groupe ESCYA-NICE, 1982; Malinverno et al., 1988). As a consequence of the event, part of a land filled area reclaimed to the sea to enlarge the airport of Nice was destroyed, bulldozers were dragged deep into the sea and various people were killed (Savoye, 1991; Mulder et al., 1997). In addition to the work already carried out, the stability of the Nice offshore area is being actively investigated with a priority for observations with highly capable imaging tools, in situ measurements, laboratory tests and modeling (Savoye et al., 2004; Sultan et al., 2004). New in situ instruments such as IFREMER's flexible penetrometer (Penfeld) have been first deployed off Nice.

In a date as recent as July 1998, a tsunami most probably generated by a submarine slump hit the Sissano coast in northwestern Papua-New Guinea (Tappin et al., 1999). Wave heights of 10 m were observed along a 25-km stretch of coastline with maximum heights of 15 m and overland flow velocities of 54–72 km/h. The death toll was over 2200, surpassed in the XXth century only by a tsunami on the coast of Sanriku, Japan, in 1933 (Kawata et al., 1999). The tsunamigenic submarine slump occurred 25 km offshore and was itself probably triggered by an estimated 7.0 magnitude earthquake. The Sissano tsunami is the first that has been comprehensively investigated very soon after its occurrence by seabed and sub-seabed imaging, sediment coring, ROV and manned submersible observations, measurements of potential fields and computer simulations. The approximately 760-m-thick, 5–20-km^3 slump took place in an arcuate, amphitheatre-shaped structure made of fine grained, cohesive and stiff sediments that failed by rotational faulting. Fissures, brecciated angular sediment blocks, vertical slopes, talus deposits and evidence of active fluid expulsion have been found in the amphitheatre area. A failure plane with at most a 100-m high exposed scar has been identified on the slump headwall. Also, the occurrence of several events of different ages in the same source area has been postulated. Local seabed morphology resulted in focusing the magnitude and wave-height distributions of the tsunami along the coast (Tappin et al., 2001).

The most recent submarine landslide generating a tsunami that we are aware of, took place on the flanks of the volcanic island of Stromboli, Thyrrhenian Sea, while writing the present paper (December 30, 2002). According to an oral account by S. Tinti from the University of Bologna, Italy, two successive slides, one subaerial and submarine and the other only subaerial, affected an area prone to instability known as Sciara del Fouco. The total volume of rock and debris remobilised was about 28.5 millions of m^3 (Bosman et al., 2004). The first slide was responsible for the observed tsunami, which flooded part of the lowlands to the north of the island. The observed height of the wave was up to 10 m at specific locations. There were no casualties. The Stromboli tsunami wave was recorded by tide gauges in nearby islands and also in Milazzo, north of Sicily, where tankers were displaced during oil transfer operations, and oil depots on the coast were close from being hit by the wave.

The above accounts only represent a small part of all the known occurrences of submarine slides in historical times. To illustrate our points, we have deliberately chosen a few slides that generated tsunamis since these are the ones that have a stronger social, economical and scientific impact. Many other submarine landslides are known to have occurred not only during the historical epoch but also throughout the Holocene (Canals, 1985; Hühnerbach et al., 2004). Note that submarine landslides, eventually associated with tsunamis, might be rather frequent along European and North Atlantic margins, even on segments that can be considered tectonically quiet (i.e., Lisbon, Grand Banks and Nice slides and tsunamis).

One of the major advantages of studying geologically recent or historical seafloor mass movements is that they can be much better constrained than older events in terms of resulting morphologies, deposits, dynamics, impacts and ages. To achieve such knowledge, state-of-the-art high resolution geophysical tools (i.e., swath bathymetry systems, deep-towed side scan sonars, high to ultra-high resolution 2D and 3D seismic reflection profiling) are required to provide seafloor and sub-seafloor images of unprecedented quality that can then be used to investigate the above points. The

enormous improvement in surveying equipment during the last few years is bringing to the surface events and impacts, jointly with their fine-grained details, that could not be resolved previously. Coring is a necessary complement to get datable samples for events that have occurred in pre-historical times or whose timing is not well known even if historical.

One of the main tasks within the "Continental Slope Stability" (COSTA) project has been to investigate slope failure dynamics and impacts from seafloor and sub-seafloor shallow geophysical data with the aim to assess:

- External morphology and internal structure of slope failures and resulting deposits
- Slip plane geometries for small, medium and megaslide events
- Run-out distances and flow pathways
- Triggering mechanisms
- Ages of slide events, either single-phased or multi-phased, and recurrence intervals

To achieve the above aims, which overall could illustrate the variability of submarine sediment failures, the research effort focused on eight pre-Holocene to present case studies representing the variety of submarine instabilities that can be found along ocean margins. Seafloor instability events in this paper are now among the best studied in the world. Describing the main results achieved through their study, extracting overall conclusions and distillating implications are the primary goals of the current paper, which also includes a review and summary of previously published data.

2. Setting of the studied slides

Six of the slides studied are located in Europe's margin and have been systematically and intensively investigated within the COSTA project. These are from north to south Traenadjupet, Storegga and Finneidfjord Slides, off Norway, Afen Slide from the Faeroe-Shetland Channel, and BIG'95 Slide and the Central Adriatic sediment deformation belt from the Mediterranean Sea (Fig. 1). The Canary Slide affecting an ocean island flank has been added as an end member not represented by the European case studies. A slide that occurred off the Northern Antarctic Peninsula, Gebra Slide, has been included for comparison purposes with slides on the Norwegian margin. These case studies cover from shallow to deep settings, from glacial-dominated to river-dominated margins, from giant to tiny instabilities and from long run-outs to almost in situ deformation (Table 1). Several of the studied instabilities on glacial-dominated margins, such as Traenadjupet, Storegga and Gebra, develop off or at a short distance from the mouths of ancient glacial troughs, which were occupied by fast moving ice streams during glacial times. Ice stream-related basal erosion and till transport led to high sediment inputs at the tidewater terminus of the glacial systems off glacial trough mouths (Canals et al., 2002).

The considered slides extend from 69°10′N (Traenadjupet) to 61°15′N (Afen) along Europe's Atlantic margin and from 1°00′E (BIG'95) to 16°10′E (Adriatic deformation belt) along the northern Mediterranean margins. The Canary Slide is comprised between the crosses of 27°48′N and 31°18′N with 18°30′W and 24°06′W respectively. Finally, the Gebra Slide lies at the crosses of 62°14′S and 62°38′S with 57°40′W and 58°06′W west of the Antarctic Peninsula (Fig. 1; for specific location figures, see different articles in this volume). Their specific geological settings are provided below.

The Traenadjupet Slide is located east and northeast of the marginal Voring Plateau and extends from the shelf break at 400 m to more than 3000 m water depth in the Lofoten Basin abyssal plain. The first published mention to the Traenadjupet Slide, based on 3.5 kHz profiles, was by Damuth (1978) who reported an area of sediment removal on the Norwegian continental slope off Traenadjupet. The name of the slide comes from the close-lying large Traenadjupet glacigenic trough on the shelf. Traena is an island close to coast, while "djupet" means "deep", in this case a trough separating shallower bank areas.

The Traenadjupet Slide developed in a passive continental margin setting with a continental shelf more than 200 km wide. The shelf has experienced various phases of glacial erosion and sediment bulldozing by the advancement of ice to the shelf break during glacial epochs (Ottesen et al., 2001). Shelf and slope bedrock in the area consists of Tertiary and Mesozoic sedimentary rocks (Sigmond, 1992). Quaternary glacigenic debris flow deposits and glacimarine sediments capped

Fig. 1. Location of the studied instabilities. Gebra Slide is located off the northern tip of the Antarctic Peninsula.

by a <2-m-thick Holocene hemipelagic drape cover the continental slope. On the shelf, the Quaternary succession is formed by till units interbedded with stratified glacimarine sediments (Laberg and Vorren, 2000). The slide scar is off Traenadjupet glacial shelf trough where the Quaternary succession is comparatively thin (King et al., 1987). The Traenadjupet Trough is the most pronounced on the mid-Norwegian continental shelf, reaching a water depth of more than 450 m.

Table 1
General depositional settings for the submarine landslides studied in detail within COSTA. CADEB: Central Adriatic Deformation Belt

TARGETS		GLACIAL-DOMINATED	RIVER-DOMINATED	OTHER
SHALLOW (shelf)		Finneidfjord	CADEB	Canary
DEEP (slope)	small	Afen Gebra Traenadjupet Storegga	BIG'95	
	large			
WATER TEMP.		COLD	WARM	

The Storegga Slide ("great edge" slide, in Norwegian, according to Evans et al., 1996, or simply "shelf edge" after geographic location) is located immediately south of the Voring Plateau in the mid-Norwegian margin. Discovered in 1979, the first report to describe the giant Storegga Slide was by Bugge (1983). The 290-km long headwall of the Storegga Slide is situated in water depths of 150–400 m along the shelf break, 100 km off the Norwegian nearest coast. The distalmost deposits passed through 3800 m of water depth northwest of the Aegir Ridge in the southern Norway Basin (Bugge et al., 1987).

It would be more appropriate to refer to the "Storegga slides" or "slide complex" since what is identified as the Storegga Slide is actually the result of

a succession of events extending through several tens of thousand of years according to Bugge et al. (1987, 1988) or almost concurrent and younger according to new AMS ^{14}C datings reported in Haflidason et al. (2003a,b) (see Section 10 below). The southern headwall of the Storegga Slide cuts a prominent outbulge formed off the mouth of the Norwegian Channel glacial trough, in a setting that is similar to the Gebra Slide (see below) except for the size of the area and the volume of sediment involved. Other smaller glacial troughs containing ice-streams may also have converged towards Storegga's head.

The Storegga Slide area partly coincides with a Cenozoic depocentre characterized by a thick prograding sediment wedge developed during the late Pliocene–Pleistocene period (Jansen et al., 1987; Rokoengen et al., 1995; Eidvin et al., 2000; Haflidason et al., 2003a; Evans et al., 2002). Most of the mobilised materials are normally consolidated, stratified and relatively soft fine grained Plio–Quaternary sediments of glacimarine and hemipelagic origin which grade to ice-proximal or diamicton-type sediments towards the upper slope and shelf (Haflidason et al., 2003a). However, more consolidated sediments as well as older sediments are also involved locally (Bouriak et al., 2000). The undisturbed acoustic character of the autochtonous sediments is commonly disrupted by a wide variety of features, which are interpreted to result from fluid expulsion (Evans et al., 1996). Contour current-deposited soft clays have been identified in the two large margin embayments where the Storegga and Traenadjupet slides originated (Bryn et al., 2003a) and could have played a fundamental role as weak layers (see Sections 7 and 9 below).

The so-called Second Storegga Slide, dated at about 7200 yr BP (Bondevik and Svendsen, 1994, 1995), engendered a 10–11-m high tsunami wave that impacted most of the Norwegian coastline and reached the eastern coasts of Scotland and Iceland at least (Dawson et al., 1988, 1993; Svendsen and Mangerud, 1990; Harbitz, 1992; Bondevik et al., 1997).

Last but not least, a major gas discovery, the Ormen Lange field, has been made in a depth of 800–1200 m close to the steep back wall left by the Storegga Slide. A major program has been funded by oil companies to "evaluate large scale margin stability, identify slide release mechanisms, evaluate the risk of new large and small slides, assess the consequences of possible reservoir subsidence as a result of production, evaluate possible measures to reduce the risk in the event of a development, as well as map the seabed to identify good pipeline routes out of the slide area" (www.offshore-technology.com/projects/ormen/). Production is expected to start in 2007 following completion of a gas liquefaction plant onshore. Tanker vessels will carry most of the liquefied gas to the United Kingdom market.

The Gebra Slide off the Trinity Peninsula, Antarctica, also occurred off a glacial trough in a passive margin. It was discovered in 1993 during the Gebra-93 cruise aboard the Spanish research vessel *Hesperides*. First called Gebra Valley, it took the name from the cruise acronym, which means "Geological Evolution of the BRAnsfield Basin" (Canals et al., 1993, 1994). The source area is located in the middle and lower slope, whereas the resulting deposit mostly accumulated in the flat-bottomed King George Basin of the Central Bransfield Basin between the Trinity Peninsula and the South Shetland Islands. The Trinity Peninsula has a total width of about 80 km and includes an inner and an outer continental shelf, a slope and a continental rise that extends down to the basin floor (Gracia et al., 1996b). The inner continental shelf is up to 250 m deep and is incised by four large glacial troughs that behaved as main sediment pathways to the outer shelf during glacial times (Canals et al., 2002). The troughs merge into the outer continental shelf, where the shelf edge varies in depth from about 600 to 750 m in front of the Gebra Slide headwall. The shelf edge is made of basinward-convex till lobes formed at the prolongation of the glacial troughs. It is assumed that the ice was grounded on the shelf edge during glacial maxima. The total water depth range for the Gebra Slide is from 900 m for the uppermost scarp to 1950 m into the deep basin. The slide scar is cut into the toe of the glacial-period continental slope prograding strata (Imbo et al., 2003).

The Gebra Slide itself has not been cored but there are numerous cores from the surrounding non-failed areas (Table 2). The lower section in the King George Basin is covered by a thick late-glacial and post-glacial unit named U8 by Prieto et al. (1999) as illustrated by Imbo et al. (2003). The continental slope around Gebra Slide is formed by alternations of diamictons and hemipelagic/turbiditic layers accumulated during glacial and interglacial periods, respectively (Prieto et al.,

Table 2
Summary of geophysical and shallow sampling techniques used to investigate the slope failure dynamics and impacts of COSTA instabilities

Landslide	Multibeam bathymetry	Side scan sonar	Optical imagery	VHR seismics	HR and DP seismics	Cores	
						Type	Number
Storegga	From various systems, including industry-owned recorded by near-bottom vehicles	Deep tows GLORIA, TOBI and OKEAN	Mostly industry-owned	Deep-tow boomer and several other	Air gun, sleeve guns, sparker, and industrial 2D and 3D multichannel	Gravity Piston Selcore	 100 [+30]
Canary	Simrad EM12 and EM12S	Deep tows GLORIA and TOBI	–	TOPAS and 3.5 kHz	Airgun	Piston	10 [+50]
Trænadjupet	Simrad EM1002	Deep tows GLORIA and TOBI	–	Deep-tow boomer, ROV-mounted chirp and 3.5 kHz	Sparker and industrial 2D multichannel	Gravity	10 [+9]
CADEB	Simrad EM3000 offshore Ortona and Vieste	Surface portable side scan	–	Chirp, 3.5 kHz and 3D seismics (offshore Ortona)	Sparker	Gravity Piston SW104	17 32 [+189] 17
BIG'95	Simrad EM12S, EM12D and EM1000	Deep tows TOBI and MAK-1	Videos along selected transects	Chirp, TOPAS and 3.5 kHz	Airgun, sleeve guns, sparker and industrial 2D multichannel	Gravity Piston	2 5 [+2]
Gebra	Simrad EM12D and EM1000	–	–	TOPAS	Airgun and sleeve guns	Gravity Piston Vibrocorer	[+19] [+5] [+10]
Afen	Bathymetry extracted from 3D seismic blocks	Deep-tow TOBI	–	Deep-tow boomer, and pinger	Airgun, sparker and industrial 3D multichannel	Gravity Kasten Megacorer Vibrocorer	 8 [+11] 8 [+11]
Finneidfjord	Simrad EM100	Surface portable side scan	Slide scar videos	Boomer and TOPAS	–	Niemistoe Vibrocorer	20 [+20] 20 [+20]

Optical imagery includes video, TV shots and photography. Core numbers refer to cores from the slided area and deposit, and to cores from nearby non-failed areas (in brackets, following the "+" sign). Core numbers refer either to the number of cores per coring device and landslide or to the total number of cores per landslide, depending on the available information. Box cores and multicores are not included because of too limited penetration (some tens of centimeters). VHR, HR and DP refer to very high and high resolution, and to deep penetrating seismics. See explanations in the main text.

1998, 1999). Overconsolidated muddy and silty sand glacial tills have been sampled by vibrocoring in the outer continental shelf and the shelf edge (Dingle et al., 1998; Canals et al., 2002). Muddy sands and sandy muds cover most of the continental slope (Barcena et al., 1998 and references therein). Recent massive muds resulting from hemipelagic sedimentation, graded sediments deposited by turbidity currents and siliceous oozes related to productivity blooms have been reported from lower slope and basinal settings by Yoon et al. (1994) and Fabres et al. (2000). Various authors have also identified layers including variable amounts of sand-sized volcanic ashes. Late-glacial and post-glacial sedimentation rates are noticeable high in the Bransfield Basin, from 60 to 490 cm ka^{-1} (Harden et al., 1992).

The Finneidfjord Slide represents slides in the innermost part of formerly glaciated margins that later have been modified by riverine processes. It is the smallest and youngest of all the studied slides. It was observed to happen in June 1996 (see Sections 9 and 10 below). The slide was named after the geographic location, Finneidfjord, which is part of Soerfjorden, Hemmes Commune, Nordland County in Norway. The first report to describe the slide in detail was by Janbu (1996). The slide itself is centered at 66°11′N and 13°48′E with the outer boundary of the resulting depositional lobe lying at less than 60 m of water

depth. The slide developed within the slope of a submarine shore face consisting of glacimarine and marine clayey sediments and retreated inshore and onland. As reported by Longva et al. (2003), ground investigations prior to the slide, in connection with public works inshore, showed that the beach sediments comprised soft sensitive clays with layers of quick clay (Sultan et al., 2004) and silt, overlain by up to 5 m of sand. Rockhead sloped towards the fjord with the clay layer therefore thickening downslope towards the shore. At the shoreline, bedrock was encountered at a level of about −15 m. The role of free gas in the activation of submarine slides in Finneidfjord has been examined by Best et al. (2003).

The Afen Slide occurs on the west Shetland slope of the >1000-m deep, NE–SW oriented, glaciated Faeroe-Shetland Channel, 87 km northwest of the Shetlands Islands, and is centered around 61°18′N and 02°27′W. The Channel is a bathymetrically complex narrow passageway in the exchange of deepwater from the Arctic to the Atlantic. The influence of modern hydrodynamics on seafloor bedforms and sediment distribution on the west Shetland slope has been described by Kenyon (1986), Long and Gillespie (1997) and Masson (2001). Much of the shelf and upper slope is characterized by relict glacigenic features such as morainal ridges and iceberg ploughmarks (Long, 2001). The imprint of the glacial/interglacial cyclicity is of paramount importance for margin development, although the sedimentary style of the margin is believed to have been initiated in the early Pliocene (Leslie et al., 2003). During the Plio–Pleistocene, locally extensive slope sedimentation shifted the shelf edge seaward more than 50 km (Long et al., 2003a). The thickness of the Quaternary deposits on the west Shetland slope typically is less than 200 m, which contrasts with the >0.5 km known in nearby margins such as the mid-Norwegian margin (Long et al., 2003b).

The Afen Slide is the best-studied instability event in the Faeroe-Shetland Channel, where many other failure events dating back to 200 ka ago have been identified (Long et al., 2003a,b). It was first observed in 1996 from TOBI sidescan and pinger data collected during an environmental survey commission by AFEN, the "Atlantic Frontiers Environmental Network" from where it took its name. The Afen Slide moved northwest from a source area bounded by the 825-m isobath and flowed downslope to 1120 m of water depth. The continental slope in the area is almost devoid of significant topography and displays a gentle uniform gradient of around 2° diminishing to less than 1° beyond 1050 m of water depth (Wilson et al., 2003a,b).

The Afen Slide area is mostly made of clayey and silty glacimarine sediments modified by the interaction of along-slope and down-slope transport processes, with a dominance of the first since at least the second glacial stage of the Pleistocene epoch dated at 0.9 Ma ago (see above) (Stoker et al., 1993, 1994; Wilson et al., 2003a,b). Clean sandy layers and pockets are known or have been inferred to exist below and within the slide lobe, as well as sandy contourites are located directly above the slide and within the stable sediment packages surrounding the failed area (Masson, 2001; Sultan et al., 2004). The Afen Slide headwall is cut into an elongated contourite mound field, as illustrated on Fig. 5 of Bulat and Long (2001).

A 3D exploration seismic data cube provided by Shell UK Exploration has been examined to determine the regional setting of the Afen Slide by looking in detail at the seabed pick and examining key subsurface reflectors. This has revealed the presence of faulting and minor downslope channels within the Quaternary sediments in the slide area. There is co-location of these faults and features in the seabed outline of the Afen Slide (Long and Bulat, 2001a). The potential linkage of the Afen Slide with a main structural feature, the Victory Transfer Zone, is under investigation (Long and Bulat, 2001b).

The BIG'95 Slide occurred on the prograding, river-dominated continental slope of the Ebro margin, east of the Iberian Peninsula, in the Northwestern Mediterranean Sea, an area with fewer earthquake activity if compared to other Mediterranean areas (Grünthal et al., 1999). The Ebro margin forms the western side of the Valencia Trough, a late Oligocene/early Miocene–Pleistocene extensional basin between the Balearic Promontory and the Iberian Peninsula, which was almost totally opened at 10 Ma BP (Fernandez et al., 1995; Gueguen et al., 1998). Several volcanic structures related to the Neogene and Quaternary extension are known in the Valencia Trough, including the Ebro margin where the Columbretes Islets are the emerged expression of a 90×40-km, mostly buried volcanic

field (Maillard and Mauffret, 1993). The recentmost volcanic flows in these islets have been dated at 300 ka BP (Aparicio et al., 1991).

The Ebro margin is mainly fed by the 900-km long Ebro River, draining almost one-sixth (~85,000 km^2) of the Iberian Peninsula. The Ebro is the fourth largest sediment source to the Mediterranean Sea, discharging annually five to six million tons of sediment, a volume that probably was about three times larger during Quaternary lowstands when most of the progradation took place (Nelson, 1990). The Plio–Pleistocene thick progradational sequence forming the Ebro continental margin is known as the Ebro Group and includes the lower Ebro Clays, a clayey unit of Pliocene age and the upper Ebro Sands, a Pleistocene clastic shelf complex (Soler et al., 1983). This sequence overlies the erosional Messinian unconformity created when the Mediterranean dried up (Clavell and Berastegui, 1991; Maillard et al., 1992; Escutia and Maldonado, 1992). The growth pattern and sedimentation rates of the Ebro margin were controlled by glacioeustatic sea-level oscillations, a relatively strong subsidence and climatically driven changes in sediment supply (Farran and Maldonado, 1990).

In terms of physiography, the Ebro margin consists of an up to 70-km wide continental shelf, one of widest in the entire Mediterranean, a 10-km narrow slope with a mean gradient of 4° and a smooth continental rise that progressively deepens till encountering the Valencia Channel, a SW–NE-oriented mid-ocean type valley (e.g., Canals et al., 2000c). The continental slope of the Ebro is cut by a number of comparatively small, roughly WNW–ESE-oriented canyon-channel systems forming channel-levee complexes on the lowermost slope and rise. The base-of-slope, which gradually deepens to the NE, lies at water depths of 1300–1800 m. The channel-levee complexes, inter-channel areas, and debris flow and apron deposits at the base of the Ebro slope were referred as the Ebro Turbidite System by Nelson and Maldonado (1988).

The BIG'95 Slide takes its name from the acronym of the cruise ("Biogeoquímica i Geologia", BIG) and year when it was first identified and fully swath-mapped following earlier reports about landsliding in the area (Alonso et al., 1990; Field and Gardner, 1990). Its center is located at 39°47′N and 01°25′E. It developed in <600–2000 m of water depth (Lastras et al., 2002, 2003). The uppermost course of the Valencia Channel is now hardly recognizable since it is buried under the deposits resulting from the BIG'95 Slide (Canals et al., 2000c). Core samples taken both within the BIG'95 remobilised mass of sediment and in adjacent non-failed areas allowed to identify: (i) an upper unit made of rather homogeneous brownish clays and clayey silts with abundant foraminifera of hemipelagic origin; (ii) an intermediate unit with convoluted laminations of interbedded sands, silts and silty clays and low fossil content; and (iii) a lower unit composed of grey massive, sometimes laminated silty clays with little fossil content (Urgeles et al., 2003). It is considered that these three units correspond to the post-, syn- and pre-slide materials, respectively (Willmott et al., 2001). Relatively coarse black sands attributed to a very recent turbiditic event have been identified on top of the upper unit in the uppermost, filled course of the Valencia Channel. While the upper unit is also identified in the non-failed areas, materials below it consist either of massive clays and silty clays in the upper slope, or interbedded clayey silts and sands of turbiditic origin in the leveed lower slope (Urgeles et al., 2003). Massive medium sands have been also recovered in the uppermost continental slope by vibrocoring.

The Canary Slide occurs in a setting, a volcanic ocean island flank, which is unique amongst those of the other slides considered in this paper. It extends for about 600 km from the northwestern lower slope of El Hierro Island in the Canary Archipelago, at 3900 m of water depth, to the eastern edge of the Madeira Abyssal Plain (MAP), at about 5400 m water depth. It can be considered that the Canary Slide is centered at 30°N and 21°W. It was identified as a separate event in 1989 since previously it was believed to be part of the Saharan Slide, discovered in the late 1970s of the XXth century (Embley, 1976).

The Canary Archipelago is made of seven, roughly E–W-oriented large islands and a few islets in the Atlantic Ocean offshore northwest Africa. The basaltic-dominated intraplate Canary oceanic-island volcanoes have been related to an upwelling mantle plume or hotspot, now most probably located close to the island of El Hierro. Notwithstanding its proximity to the African margin, all the islands have been built up on oceanic crust fractured by a WNW–ESE-oriented Atlantic system, and an ENE–WSW- to NNE–SSW-oriented system related to the Atlas Range inland in

northwest Africa (Mezcua et al., 1991; Carracedo and Day, 2002). Since the ocean floor around the islands is 3000–4000 m below sea level, the true heights of the volcanoes that form the islands are all in excess of 4–5 km. Teide, on the island of Tenerife, is the third highest volcano on Earth after Mauna Loa and Mauna Kea in Hawaii. As a general trend, there is an age progression from east to west. Since El Hierro is the westernmost island in the archipelago, it is also the youngest with the oldest rocks dated at 1.2 Ma BP. On El Hierro, three large volcanic edifices have been identified which appear dislocated by subsequent giant landslides. Those are the volcanic edifices of El Tiñor (1.22–0.88 Ma), El Golfo (545–176 ka) and Frontera (37 ka–present) (Carracedo et al., 1995; Guillou et al., 1996). However, Holocene eruptions are known in all of the islands except La Gomera.

At least 18 large lateral collapses and landslides originating from the flanks of the various islands in the Canaries are known, with a majority being partly subaerial and partly submarine (Canals et al., 2000b; Urgeles et al., 2001; Krastel et al., 2001; Masson et al., 2002, and references therein). The occurrence of those landslides seems to be related to volcanic rift zones forming star-shaped three-arm alignments. But the Canary Slide is submarine only (see Section 9 below) (Masson et al., 1998). Onshore, landslide headwalls are most often expressed as arcuate embayments with steep cliffs (Cantagrel et al., 1999; Navarro and Coello, 1989; Ridley, 1971). The discovery of landslide deposits offshore the Canaries proved to be fundamental for an integrated seascape/landscape integrated evolutionary model (Urgeles et al., 1998).

The pattern of sediment influx observed west of the islands of El Hierro and La Palma, the second youngest island (2 Ma BP) shows that the E–W migration of the major volcano-forming episodes controls the sedimentary processes and the location of volcaniclastic depocenters (Urgeles et al., 1998). Above a lower unit believed to consist mostly of pelagic sediments, the intermediate and upper units filling the MAP are dominated by turbidites (Duin et al., 1984; Searle, 1987). MAP turbidites are of three types, volcanic-rich, organic-rich and calcareous, reflecting source areas in the Canary Islands, the NW African continental margin and seamounts to the west of the abyssal plain, respectively (Weaver et al., 1992; Lebreiro et al., 1998; Alibes et al., 1999).

Several studies indicate that the flanks of El Hierro and nearby La Palma are covered predominantly by fragmented sedimentary material, including pelagic sediments, turbidites and volcaniclastic products (Simm et al., 1991; Masson et al., 1992, 1997, 1998). Slope gradients vary from 1° at the source to virtually 0° at the edge of the abyssal plain. This suggests a highly mobile flow. The deposit itself consists of a mixture of clasts and matrix of the above lithologies. Large slabs up to 300 cm across have been identified too (Masson et al., 1997). Similarly to the BIG'95 Slide, the slide deposit is capped by a thin layer of hemipelagic sediment post-dating it and partly filled channels have been also identified within the area of the flow (Masson et al., 1992). These channels can be up to 10 km wide and are typically 10–30 m deep. The Canary Slide deposit correlates with a prominent turbidite in the MAP known as the "b" turbidite (Weaver et al., 1994).

The origin of the Central Adriatic Deformation Belt (CADEB) is object of intense scientific debate. The reader should be aware that, although studied as a submarine landslide within the COSTA project, some authors think that it is not a failure but a depositional feature similar to sediment waves, resulting from hyperpycnal flows out of the Appenine rivers and possibly the Po river (e.g., Lee et al., 2002). This paper will consider CADEB to be an end-term landslide from here onwards, because it differs from the other study cases because downslope sediment displacement is very limited or null, and because the along-slope dimension of the affected sediments is several times larger than the across-slope dimension. CADEB occurs as a narrow deformation fringe parallel to the isobaths between 43°N and 42°N, from offshore Ortona and the northern Gargano Promontory, at water depths of 30–110 m. CADEB is thus, jointly with Finneidfjord Slide, the shallowest of the studied instabilities. CADEB and BIG'95 (see above) provide a view on seafloor instabilities in river-dominated margins covering both deep water and shallow water, and passive and active margin settings. CADEB was first imaged locally in 1989 and at a regional scale in 1992 (Hovland and Curzi, 1989; Correggiari et al., 1992).

The Adriatic Sea is a narrow (92–220 km), NW–SE-elongated (800 km), shallow semi-enclosed basin that communicates with the deep Ionian Sea in the Eastern Mediterranean through the Otranto Strait. The

Adriatic Sea constitutes the latest Apennine foreland basin, which is segmented according to lithospheric thickness, state of deformation and rates of subduction (Ciabatti et al., 1987; Royden et al., 1987). The movement of the westward-dipping Adriatic microplate triggers a shallow distributed seismicity characteristic of the area (Argnani et al., 1993; Doglioni et al., 1994). Substantial Quaternary uplifting has been observed both inland and offshore the Gargano Promontory, where several historical strong earthquakes are also known (Tinti et al., 1995). The northwestern third of the Adriatic Sea is occupied by the largest epicontinental shelf in the Mediterranean Sea, constructed with the sediment input from the Po River and Appenine rivers during and subsequently to the post-glacial sea level rise. The modern shelf overlaps a former glacial alluvial plain (Trincardi et al., 1994).

The CADEB deformed unit belongs to the Central Adriatic shelf mud wedge lying on top of the late Holocene maximum flooding surface and is, therefore, part of the late Holocene highstand systems tract (Correggiari et al., 2001). The modern mean suspended load entering from the western side of the Adriatic Sea, where the Apennine rivers and the large Po River open, has been estimated at 39×10^9 kg yr^{-1} (Frignani and Langone, 1991; Trincardi et al., 1994). Perhaps surprisingly, the main sediment source is the ensemble of Apennine rivers with a total drainage area of 23×10^3 km^2, a mean suspended load of 24×10^9 kg yr^{-1} and a sediment yield exceeding 10^6 kg km^{-2} yr^{-1}. The Po River, which enters the Adriatic Sea at about 45°N forming one of the largest deltas in the entire Mediterranean Sea, has a drainage area of 54×10^3 km^2, a mean suspended load of 15×10^9 kg yr^{-1} and a sediment yield of 0.28×10^6 kg km^{-2} yr^{-1} (Frignani et al., 1992; Milliman and Syvitski, 1992; Bartolini et al., 1996).

The general cyclonic circulation carries fine-grained particles supplied by the Po and Apennine rivers south-eastward along the eastern Italian coast. The sediment accumulates as shore-parallel muddy prodeltaic wedges detached from their river source. The muds are layered, display high water and clay contents, low density and low shear strength (Correggiari et al., 2001; Cattaneo et al., 2003a). CADEB is, therefore, a good representative of the tens of meters thick extensive mud-dominated coastal wedges common in most Mediterranean margins. River inputs resulted in progradation after the present sea-level highstand was reached ca. 5.5 cal ka BP (Correggiari et al., 1996; Cattaneo and Trincardi, 1999).

According to several reports, seafloor crenulations are common in these mud-dominated prodelta slopes offshore river mouths all around the Mediterranean and elsewhere. They generally occur under seafloor gradients of tenths of a degree, display a variety of internal geometries and seem to be associated to high sedimentation rates (Correggiari et al., 2001 and references therein). These have been estimated to be higher than 1.5 cm yr^{-1} for the western Adriatic shelf. In the CADEB area, the mud prism shows a sigmoid section with an almost horizontal topset region (0.02°) and a foreset region inclined about 0.5°, locally up to 1°. The depocenter of the up to 35-m-thick CADEB muddy wedge is at 35–40-m water depth while in the modern Po Delta, further north, it is located at the shoreline (Cattaneo et al., 2003a). Widespread diffused impregnation by biogenic gas in the shallowest topsets has been inferred from acoustic masking in very high resolution (VHR) seismic reflection profiles offshore Ortona and north of Gargano Promontory (Correggiari et al., 2001).

3. Methods

High resolution state-of-the-art geophysical methods were applied to the case studies considered within the COSTA project. These include both seafloor and shallow sub-seafloor imaging tools deployed both near the sea surface and near the ocean bottom. Sediment cores provided materials to groundtruth geophysical interpretations and to perform age analyses of the events. Table 2 summarizes the methods used to investigate the slope failure dynamics and impacts of each of the eight landslides of the COSTA project.

It is beyond the scope of this paper to describe in detail the various methods used, and all of them are widely known by the scientific community. However, we have added at the end of each paragraph below a brief selection of references that are easy to read, handbooks or scientific articles that will allow the interested reader to expand their knowledge of the principles and practicalities of the various groups of techniques mentioned in Table 2. Those interested by

in-depth information would need to search for more specialized literature.

Swath bathymetry data exist for most of the studied landslides although only three (Finneidfjord, BIG'95 and Gebra) are fully swath mapped. For other landslides, multibeam work has started recently and there is still quite a lot to do (Traenadjupet, CADEB). Some are simply too large so that full swath mapping would require an enormous effort (Storegga and Canary). In relation to the future exploitation of the Ormen Lange gas field (see Section 2 above) oil companies have carried out ultra-high resolution swath bathymetry mapping in particularly sensitive areas of Storegga Slide area using autonomous underwater vehicles navigating at a short distance from the seafloor. In some settings, such as CADEB, multibeam mapping requires a lot of time since the shallow water depth greatly limits efficiency because of narrower swaths. In Traenadjupet only, a small area of the slide headwall has been swath mapped (Laberg et al., 2002). In the CADEB area, two small boxes offshore Ortona and Vieste, at the northern and southeastern limits of the study area, have been swath mapped with an EM3000 system (Cattaneo et al., 2003a). In the Afen Slide, good quality bathymetry data have been extracted from 3D seismic reflection blocks provided by the industry. Digital terrain models (DTMs), slope gradient maps, 3D views and other representations are classic subproducts from swath bathymetry data. It must be noticed that, in addition to bathymetry, swath data include backscatter information, which has proved extremely useful for seafloor characterization purposes (e.g., Blondel and Murton, 1997).

Brief reports on swath bathymetry systems can be found in De Moustier (1988), Grant and Schreiber (1990), De Moustier and Matsumoto (1993), Riddy and Masson (1996), Le Bas and Masson (1997), Jones (1999) and Masson (2003). Manuals from manufacturing companies are also a valuable source of information. The consistency and comparability of swath bathymetry data acquired from surface vessels within the COSTA project is to be noted since all of them have been collected using Simrad systems.

The high availability of deep-towed side scan sonar imagery from the COSTA slides is worth mentioning. The 30-kHz TOBI sonographs exist for five out of the eight slides studied. Higher resolution sonographs obtained with the 30 or 100 kHz Russian MAK-1 system also exist for BIG'95. Lower resolution data have been obtained with long-range side scan sonars such as the 6.5-kHz British GLORIA and the 9.5-kHz Russian OKEAN in Traenadjupet, Storegga and Canary Slides (Table 2). Useful very high resolution 7.5- and 5-kHz seismic reflection data are co-registered with the TOBI and MAK-1 data, respectively. See McQuillin and Ardus (1977), Trabant (1984), Le Bas et al. (1995), Riddy and Masson (1996), Blondel and Murton (1997), Jones (1999) and Masson (2003) for reports on both deep-towed and shallow water side scan sonar systems. Such references are also useful to get an historical perspective of the evolution of side scan sonar systems applied to the exploration of the seafloor.

While useful for many other seafloor research objectives, optical imagery yielded, in general, poor results in the COSTA sites since often the slide scar and the deposits, especially in deep water settings are draped by a thin veneer of fine sediments that masks features directly attributable to the instability events. A too small field of vision for the scale of many of the seafloor features to be observed in failed areas is another problem to overcome when using optical imagery for submarine slide studies.

VHR seismic reflection systems are, for the purpose of this paper, those high frequency systems giving penetrations of tens of metres, maximum a few hundred, and vertical and horizontal resolutions better than a few metres. The VHR systems used to obtain sections of the COSTA slides include trawled deep tows, ROV-mounted chirps and near-surface sources, both trawled and hull-mounted (Table 2). TOPAS is a full ocean depth hull-mounted system based on the parametric interference principle according to which a relatively low frequency signal, from 0.5 to 5 kHz, is generated from two higher frequency primary signals. The result is an excellent compromise between penetration and resolution, which nominally is better or equal to 10 cm. Penetrations in excess of 250 m have been obtained both in deep sea pelagic and turbiditic sequences using TOPAS. Penetration in debris flow deposits is less but most often is enough to image the base of several tens of meter thick debris deposits. The TOPAS system is normally used in parallel and synchronized with Simrad swath mapping systems. It allows fast acquisition (up to 10 knots) of VHR seismic profiles.

In addition to TOPAS and the classical 3.5-kHz mud penetrators, the third most often used system for shallow sub-seafloor investigation within COSTA was the BGS deep-tow boomer (DTB), able to collect profiles with a vertical resolution of 1 m and a penetration of up to 200 m in water depths of up to 1500 m. As its name suggests, the boomer fish is towed a long way below the sea surface, usually about two thirds of the way down the water column. DTB was developed from the Huntec deep-tow boomer, first designed for continental shelf water depths (Evans et al., 1996). VHR 3D seismic data covering an area of 800×3600 m, at water depths in between 50 and 75 m have been acquired offshore Ortona in the CADEB area using a new system developed by IFREMER. A description of the method and of the results achieved off Ortona as well can be found in Marsset et al. (2003a,b).

For the purpose of this paper, high resolution (HR) and deep penetrating (DP) seismics incorporates systems able to penetrate from hundreds of metres to few kilometres below the seafloor. Resolution is usually not better than a few tens of metres. Industry has provided valuable HR and DP multichannel data sets, either 2D or 3D. The investigated instability where the industry involvement has been the highest, by far, is the Storegga Slide. The consortium of researchers in COSTA has used various types of guns and sparkers. Seismic reflection principles and techniques, both for shallow and deep water, for VHR, HR and DP, are well described in Leenhardt (1972), McQuillin and Ardus (1977), McQuillin et al. (1979), Geyer (1983), Trabant (1984), Badley (1985), Jones (1999) and Masson (2003).

A wide range of shallow coring techniques has been deployed in the eight study sites of COSTA allowing us to sample both the slide areas and the nearby non-failed areas (numbers in brackets after a "+" sign in the right column of Table 2). Gravity and piston corers, followed by vibrocoring systems, have been the most used coring devices. They all provide cylinders of sediment from less than 1 m long to a few tens of meters long. The number of cores from each of the investigated areas is highly variable, from more than 100 in Storegga to 10 or 20 in some areas. Description of the most commonly used coring systems can be found in Weaver and Schultheiss (1990) and Griffiths and Thorpe (1996).

Deep drills, either ODP or industrial, have not been taken into account for the specific purposes of this article. The geotechnical properties and the mechanical behavior of the sediments involved in the COSTA project submarine landslides are covered by various papers in this volume including those by Sultan et al. (2004), De Blasio et al. (2004) and Vanoudheusden et al. (2004).

4. Mass movement types

Before assigning a specific mass movement type to any of the COSTA instabilities, it is convenient to introduce a word of caution about terminology. There is certainly a terminology problem in the literature since some of the terms (i.e., slide and slump) are often used in a loose way to refer to almost any type of submarine mass movement rather than reserving them for specific mass movement types following precise definitions (Canals, 1985). Indeed, the readers will have noted that the term slide is being used in this paper as a general term for all the instabilities studied. Most of the terminology applied to submarine mass movements is inherited from that applied to subaerial mass movements (Varnes, 1958), which is perhaps one of the sources of confusion given that submarine instabilities are distinct in many aspects from the subaerial ones. Since the earlier papers on submarine mass movements by Dott (1963), Morgenstern (1967) and Middleton and Hampton (1973, 1976), there have been many attempts to address this situation which have resulted in various subsequent classifications (Carter, 1975; Moore, 1978; Lowe, 1979; Nardin et al., 1979; Prior and Coleman, 1979; Cook and Mullins, 1983; Moore et al., 1989; Mulder and Cochonat, 1996). The Glossary of Geology of the American Geological Institute (Bates and Jackson, 1987) is suggested as a reference book for terminological questions although it also requires updating, especially in view of the new data on submarine instabilities contributed by the newest technologies.

The more our imaging capabilities of submarine mass movements and their deposits have improved, the more we have realized how complex and varied they are. That different behaviors could coexist or succeed each other over short distances has been already demonstrated. Also, various parts of an

individual event could belong to several of the categories proposed by the authors cited above. The case studies within the COSTA project perfectly illustrate those situations. With the partial exception of Mulder's and Cochonat (1996), none of the classifications previously proposed is fully based on state-of-the-art swath bathymetry, deep-tow side scan sonars and VHR, HR, DP and 3D seismic reflection tools as those extensively deployed within COSTA. A revision of existing classifications integrating information provided by the new techniques would represent a major benefit. A preliminary attempt has been made by Locat and Lee (2002).

Not only do the seafloor instabilities within the COSTA project occur in a large variety of settings (see Section 3 above), but they also cover a wide range of offshore mass movement types according to the static and dynamic classifications of Mulder and Cochonat (1996) and earlier authors. Taking into account mainly motion, architecture and shape of the failure surface, these authors distinguish between slides/slumps, plastic flows and turbidity currents, of which they differentiate 13 main varieties. Turbidity currents and their deposits are not considered in the present paper.

Table 3 summarizes the main characteristics of the COSTA submarine landslides, from those where sediment has been just deformed but not moved apart nor disintegrated, as CADEB, to those where sediment presumably had, at least partly, a mud flow behavior, such as Afen and Finneidfjord slides, where quick clays have been encountered. Five mass movement types have been identified: (i) creeping, (ii) rock falls and rock/debris avalanches, (iii) translational slides or glides, (iv) debris flows and (v) mud flows. Both alongslope displacement and disturbance of the sediment increase from (i) to (v). Purely rotational slides or slumps do not appear in the COSTA study sites, although rotational components are relatively common in translational mass movements, specially in the upper sections where movement initiates. Before flattening towards the toe of the detachment area, failure planes are often rotational in character. Some authors use the term "mixed slide" to refer to slides with a relatively small hemi-circular scar and a large planar body.

Creeping is defined as "the slow, gradual, more or less continuous, non recoverable (permanent) deformation sustained by ice, soil and rock materials under gravitational body stresses". Many types of creeping

Table 3
Classification of the submarine mass movements studied within the COSTA project

General features			Mass movement type				
			Creeping	Block detachment rock fall debris avalanche	Gliding blocks	Debris flow	Mud flow
Mechanical behavior			Elastic			Plastic	
Failure character			Progressive	Vertical to translational	Translational		
Main failure planes			Incipient	Pre-failure	Pre-and syn-failure		-
Landslide	Retr.	Multi.					
CADEB	–	–	Fig.2A				
Storegga	Y	Y		Fig.2B			
Traenadjupet	Y	Y			Fig.3		
BIG'95	Y	Y					
Finneidfjord	Y	Y			Fig.4A		Quick clays
Canary	?	N					
Afen	Y	Y					
Gebra	Y	Y					

Slides are listed in a different order than in the rest of the tables for ease of organization with respect to mass movement types. Retr.: retrogressive character. Multi.: multi-staged landslide. See explanations in the main text.

have been described in the literature, although "the general term should not be limited by a presumption of mechanism, depth, velocity profile, thickness of creep zone or lateral extent" (Bates and Jackson, 1987). According to Mulder and Cochonat (1996), "creep is the elastic deformation of sediment, usually clay, under constant load and very low deformation rate". If the plastic deformation limit is exceeded, creep could evolve into a slide or a plastic flow. Creep is considered as an indicator of areas prone to failure. Creep deformation within COSTA is best represented by the CADEB area, where detached prodeltaic muds develop pervasive undulations over a sharply marked detachment layer slightly inclined seawards (ca. 0.1–0.2°) (Fig. 2A). This layer corresponds to 1800 years of slower deposition and is located between the Holocene maximum flooding surface dated at 5.5 calibrated ka BP and the so-called Avellino tephra dated at 3.7 calibrated ka BP (Correggiari et al., 2001) (see Section 10 below). The mean slope gradient in the CADEB area is only 0.55°. An attempt was made within the COSTA project to instrument pore pressure variations and rates of deformation under earthquake excitation in the CADEB area (Sultan et al., 2004).

Gravity-driven mass movements include rock falls, rock/debris avalanches and translational slides. All

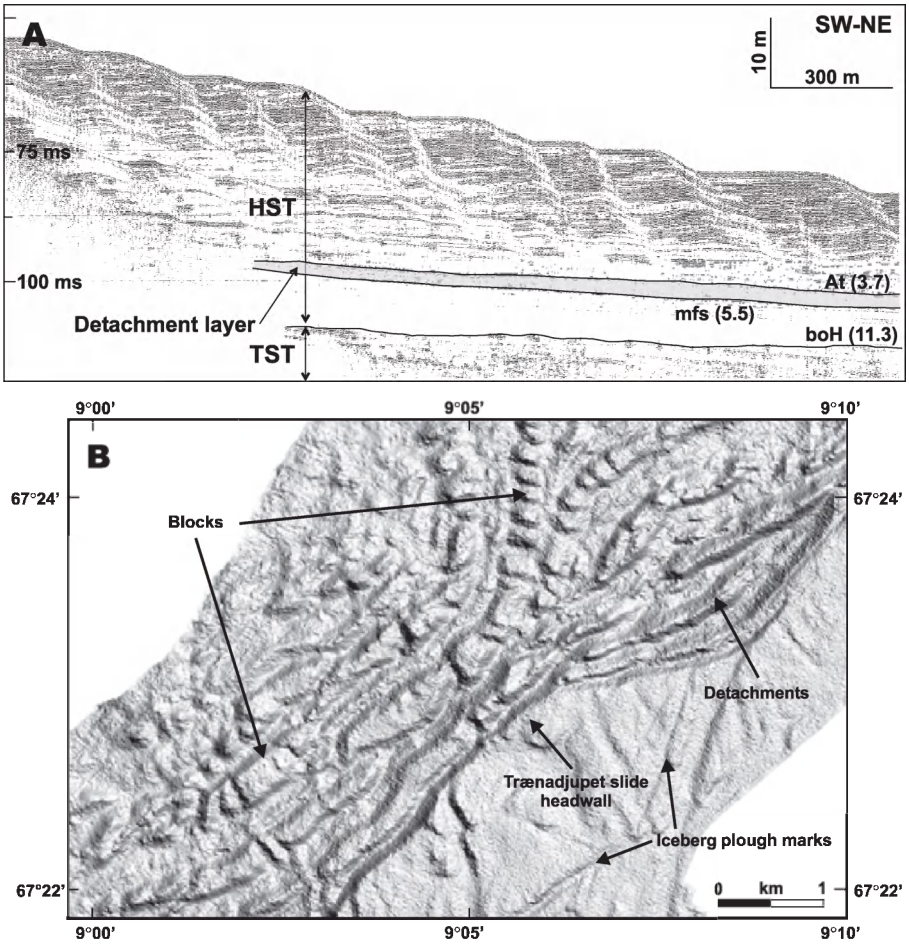

Fig. 2. (A) 3.5 kHz profile across creep-like structures in the CADEB area. mfs: Holocene maximum flooding surface, At: Avellino tephra, boH: base of Holocene, HST: highstand systems tract, TST: transgressive systems tract. Ages are in cal ky BP (modified from Correggiari et al., 2001). (B) Block detachment within the upper Traenadjupet Slide scar area as seen on a shaded relief image extracted from multibeam bathymetry (modified from Laberg et al., 2002).

these movements often initiate as *block detachments* that predetermine future headwall scars. Block detachments from headwall areas might be precursors of rockfalling (see below). Block detachments also relate to retrogradational phases following major landsliding events. Within the COSTA sites, indications of block detachment with open fractures and ridge systems in cohesive sediment exist at least for the Storegga and Traenadjupet Slide escarpments (Haflidason et al., 2003a,c; Laberg and Vorren, 2000; Laberg et al., 2002) (Fig. 2B). These could easily evolve into rockfalling and avalanching.

A *rock fall* is a "relatively free falling or precipitous movement of a newly detached segment of bedrock of any size from a cliff or a steep slope. It is the fastest moving landslide. Movement may be straight down, or a series of leaps and bounds down the slope. It is not guided by an underlying slip surface" (Bates and Jackson, 1987). Volumes involved in rock falls are usually smaller than those involved in debris avalanches (see below). Rockfalls could be rather common components in headwall scar areas of submarine landslides.

Debris avalanche or rock avalanche is defined as "the very rapid downslope flowage of rock fragments, during which the fragments may become further broken or pulverized. They typically result from very large rockfalls and rockslides. Characteristic features include chaotic distribution of large blocks, flow morphology and internal structure, relative thinness in comparison to large areal extent, high porosity, angularity of fragments and lobate form" (Bates and Jackson, 1987). Debris avalanches have been studied extensively on the flanks of oceanic islands (Lipman et al., 1988; Moore et al., 1989, 1994; Watts and Masson, 1995; Urgeles et al., 1997, 1999; Ollier et al., 1998). They typically consist of a large and steep headwall amphitheater, a blocky intermediate reach often starting at the foot of headwall scarps including detached blocks of up to tens of kilometers in diameter, and a distal section with smaller blocks and a finer matrix. Debris avalanche deposits can reach thicknesses in excess of 1 km and volumes of more than 500 km^3 (Moore et al., 1989, 1994; Urgeles et al., 1999; Canals et al., 2000b; Masson et al., 2002). It is thought that they occur as very fast single episodes as revealed by features indicative of hundreds of meters upslope climbing during mobilisation (Moore et al., 1989). Debris avalanches are thus large-scale catastrophic events. The criteria to distinguishing debris avalanches from debris flows (see below) using most of the geophysical tools deployed within the COSTA project are summarized in Table 4. Several of the morphologies observed adjacent to large slide escarpments and the characteristics of some of the deposits can be best explained if involving processes such as block detachment, block falling and avalanches.

A *slide sensu stricto* is defined as "a mass movement or descent resulting from failure of earth, snow, or rock under shear stress along one or several surfaces that are either visible or may reasonably be inferred. The moving mass may or may not be greatly deformed and movement might be rotational or planar" (Bates and Jackson, 1987). According to Mulder and Cochonat (1996), slides (and slumps) are downslope displacements of coherent masses of sediments scarcely disturbed during the movement, which is limited, and bounded by distinct failure planes usually parallel to the stratification, except for the headwall region. *Glide* is the term often used to refer to translational slides in the sense of Mulder and Cochonat (1996). The term "shallow slab slide" refers to shallow translational slides. However, the term "translational" is also applied to slides with a Skempton ratio less than 0.15. Such a ratio expresses the relation between depth (h) and length (l) of slide (Skempton and Hutchinson, 1969). Most submarine slides appear to be translational according to the Skempton ratio (Prior and Coleman, 1984), which is thus not very useful to differentiate between various submarine landslide types. As an example, all the slides investigated into the COSTA project would belong to the translational type of Skempton and Hutchinson (1969) despite their noteworthy differences.

Strictly speaking, true translational movements according to the Mulder and Cochonat (1996) concept, i.e. with substantial preservation of the original internal structure of the mobilised mass of sediment, are lacking within the COSTA landslide set. However, several of the COSTA landslides, either glacial or river-dominated, involve blocks (see below), which preserve the original structure within a looser heterometric matrix resulting from disintegration of initial sediment chunks and, eventually, contributions from other sources. *Gliding blocks* or rafted blocks can be found either as individual entities or embedded within

Table 4
Differences between debris flows and debris avalanches from practical (multibeam bathymetry, VHR and HR seismics) and sediment dynamics viewpoints (transport and support mechanisms, and sedimentary structures)

Mass movement type	Area	Multibeam bathymetry	VHR seismics	HR seismics	Transport and support mechanisms	Sedimentary structures
Debris flow (and mud flow)	Source	Less than 200 m high escarpments, complex scar areas	Hyperbolic and mostly opaque facies	Small listric faults or escarpments cutting the stratigraphic sequence	Gravitational fall involving block and clast rolling and gliding	Grain-supported, disorganized conglomerates with variable matrix proportions
	Depositional	Could remain morphologically unnoticed. Backscatter is very useful for identification purposes	Mostly transparent facies. Internal reflections representative of various pulses and behaviors may appear	Transparent to hyperbolic facies, or a single reflector, depending on the deposit thickness		
Debris avalanche	Source	Headwall escarpments forming large amphitheatres, 500–1500 m high	Hyperbolic facies	Hyperbolic facies	Shear distributed within the sediment mass. Strength mostly due to cohesion, which itself depends on clay content. Additional support by the matrix due to buoyancy. May involve basal hydroplanning	Matrix-supported, strongly variable fabric with clasts of varying sizes and variable matrix proportions. Rip ups, rafted blocks, inverse grading and fluidal structures
	Depositional	100–500 m high mounds and several kilometers in diameter. Backscatter is very useful for identification purposes	Hyperbolic facies	Hyperbolic, transparent or chaotic facies, mostly depending on the deposit thickness		

VHR: very high resolution, HR: high resolution.

deposits resulting from various mass movement types such as debris avalanches and debris flows.

Care must be taken when interpreting rafted blocks in slide deposit-covered areas since deeply rooted structures might have a similar seafloor expression. This has been clearly demonstrated in the Canary Slide where some formerly presumed rafted blocks had to be later reinterpreted (Masson et al., 1993; Urgeles et al., 1997; Masson et al., 1998). The area covered by rafted blocks may vary substantially from one slide to another. BIG'95 probably is the COSTA slide where rafted blocks cover the largest percentage of the affected area. The blocks concentrate in the so-called "blocky intermediate depositional area" which occupies about 40% of the overall seafloor area affected by the slide (Lastras et al., 2002) (Fig. 3A). The BIG'95 Slide has been divided into (i) source area, (ii) a block-free proximal depositional area below the main headwall, where maximum thicknesses have been found, (iii) the blocky intermediate depositional area and (iv) a distal depositional area reached only by the most mobile components of the slide matrix. These subdivisions can probably be applied to other submarine slides. For example, distinct block-covered areas are known within the Storegga and Finneidfjord Slides while small clusters and isolated blocks also appear in the Afen and Canary Slides. The Gebra Slide forms a massive, single body where no individual blocks could be distinguished (see Section 8 below).

In the Traenadjupet Slide, downslope-oriented 3.5-kHz profiles reveal an uneven seafloor morphology. The downslope termination of the slide deposits (slide toe) is defined by a break in slope and a more gentle seafloor relief with several subbottom reflections further downslope. The hummocky relief of the distal slide deposits may indicate that both unconsolidated sediments and more coherent sediment blocks accumulated in the Lofoten Basin, where the slide deposit

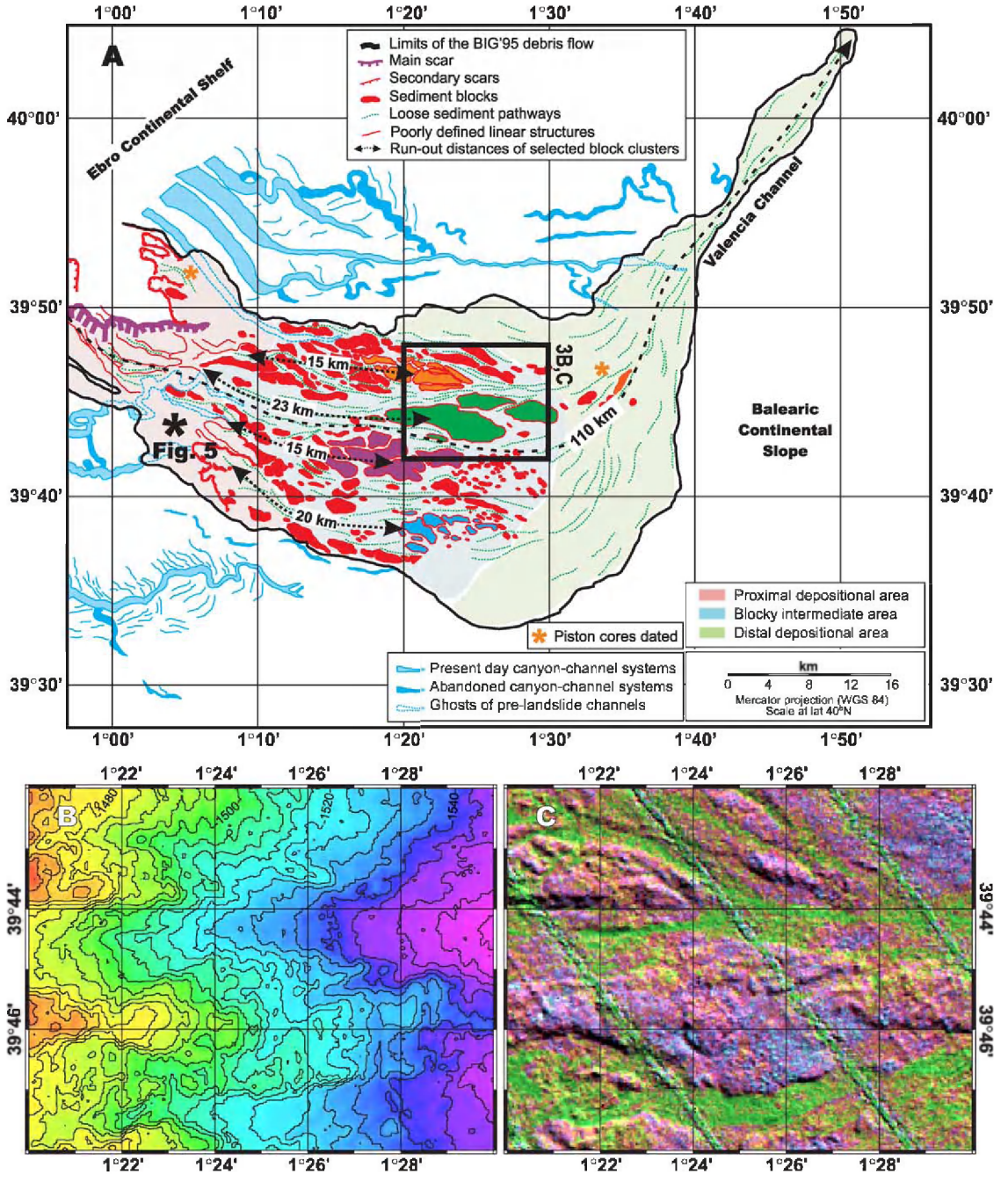

Fig. 3. (A) Interpretation map of the BIG'95 Slide. Limits of debris flow deposit, scars, blocks and looser sediment pathways are shown. Block clusters are indicated in different colors. Run-out distances of some of the block clusters and total run-out of looser sediment are also shown. Block clusters are defined by relocating individual blocks that previously fit together. Box shows location of B and C. The location of the sediment core in Fig. 5 is also indicated (modified from Lastras et al., 2002). (B) Detailed multibeam bathymetry map of part of the "blocky intermediate area" from BIG'95 Slide. See location in A. (C) Backscatter image of the same part of the "blocky intermediate area" from BIG'95 Slide shown in B. Highest backscatter in green, lowest backscatter in purple and blue. Note that the blocks are better seen on the backscatter image than in the detailed bathymetry. See location in A. Refer to main text for detailed explanations. (For interpretation of the references to colour in this figure legend, the reader is referred to the web version of this article.)

ends. Smaller and larger blocks may have been floating in a low viscosity matrix derived from less consolidated sediments, in a similar way to that observed and modelled for the BIG'95 Slide (Lastras et al., submitted for publication).

Where present, blocks vary greatly in size and shape, from rounded to elongated. The largest block in the BIG'95 Slide is 10 km long, a size that is similar to that observed for the blocks in the Canary Slide (Masson et al., 1998). Block heights can be tens and even hundreds of meters above the surrounding seafloor (Lastras et al., 2002). Often, they can be better identified in backscatter images than in detailed swath bathymetry maps (Fig. 3B,C). This is because backscatter expresses variations in the acoustical properties of seafloor materials and slope gradients while bathymetry only expresses height differences. Blocks in the Finneidfjord (Fig. 4A) and Afen Slide deposits are two orders of magnitude smaller than those in the BIG'95 and Canary Slides (see also Section 8 below).

Outrunner blocks constitute a well known feature of translational slides and flows and, within the COSTA sites, about 10 of them have been observed in the Finneidfjord Slide, with run-out distances of up to 3 km and sizes of up to 100×50×1 m (Fig. 4A). Other COSTA slides such as Storegga and Traenadjupet may have outrunner blocks but they have not been completely imaged. Outrunner blocks can be also identified well below the seafloor using 3D seismic data, as illustrated in Fig. 4B.

Plastic flows resulting from the movement of underconsolidated masses of sediments involve, according to Mulder and Cochonat (1999), three kinds of mechanisms: debris flow, fluidized flow and liquefied flow. While motion is supported by matrix strength in debris flows, it is supported by fluid escape in fluidized and liquefied flows. For that reason, most of the previous authors do not include fluidized and liquefied flows within the group of plastic flows. A *debris flow* is "a mass movement involving rapid flowage of debris of various kinds under various conditions; specifically a high-density mudflow containing abundant coarse-grained materials" (Bates and Jackson, 1987). According to Riba et

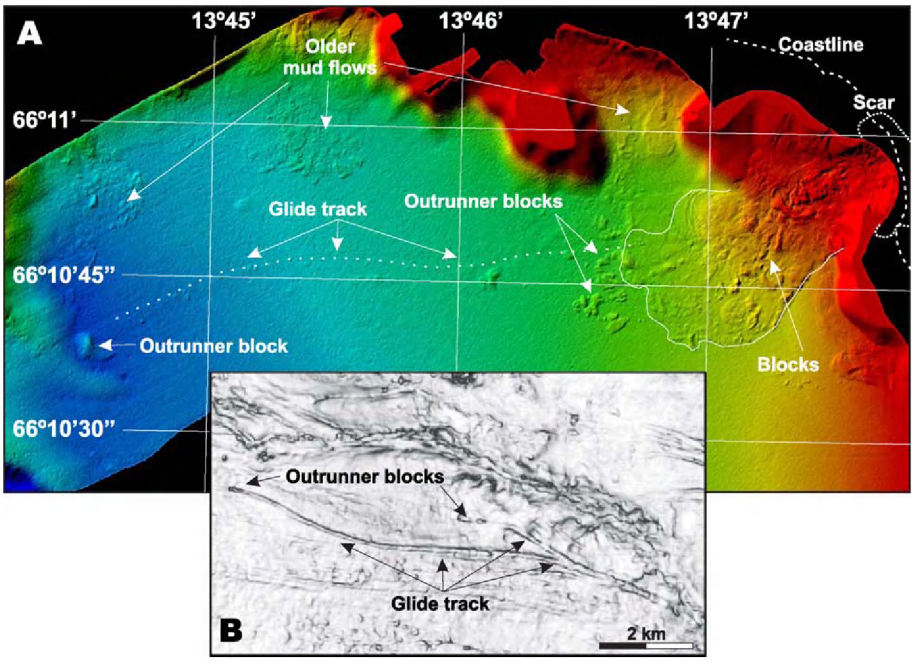

Fig. 4. (A) Shaded bathymetry of Finneidfjord Slide showing its blocky nature and illustrating the presence of some outrunners. (B) 144 ms below the seafloor coherency slice extracted from a 3D seismic coherency volume from the Nigerian continental slope illustrating outrunner blocks and an associated branching, 12 km long glide track. The uneven area above the glide tracks corresponds to a debris flow deposit (courtesy of S.E. Nissen; see also Nissen et al., 1999). (For colour see web version of this article.)

al. (1997), what differentiates debris flows from mud flows is the proportion of granulometric elements from the block, gravel and sand classes, which in debris flows is higher than 50%. Submarine debris flows are usually seen as downslope moving laminar flows of agglomerated particles held together by a cohesive sediment matrix mainly made of silt, clay, and water (Elverhoi et al., 2000). Clay contents as low as 5% could be enough to induce cohesive behavior (Hampton, 1972; Rodine and Johnson, 1976). The matrix, whose strength is the main sediment support mechanism, can easily support clasts of various sizes and blocks of consolidated material that are thus transported as partially buoyant rafted blocks.

Debris flows may move at very different speeds. The flow freezes and deposition occurs when downslope stress is lower than its yield strength. It could also stop by frictional freezing if the matrix is relatively coarse and has limited cohesion. Debris flow deposits consist of breccias and conglomerates with mud clasts and contorted laminations (Fig. 5). Boulder sorting and inverse grading are common in many debris flow deposits. The usual strong cohesion of the matrix makes it difficult to transform into a turbidity current, regardless of seafloor slope and volume of mobilised sediment. However, there are well known cases of correlated turbidites and debris flows such as "b" turbidite in the Madeira Abyssal Plain and the Canary Slide (mostly a debris flow) (Masson, 1994). Debris flows could trigger failures on the sidewalls of the flow path and at its base by spontaneous liquefaction and bearing loading (Mulder and Cochonat, 1996).

Debris flows are well represented within the COSTA sites by the Storegga, Traenadjupet, BIG'95, Finneidfjord, Canary and Gebra landslides (Fig. 5). Differentiating debris flows from debris avalanches is not always easy, especially because some landslides are at the boundary between these two types of mass movements. Some criteria extracted from work in the Canary Islands, where the two types of mass movements exist, are presented in Table 4.

Mud flows belong to the category of plastic flows. They are flowing masses of predominantly fine-grained sediment possessing a high degree of fluidity during movement. They could be considered a variant of debris flows where the coarse debris content is lower than 50%. This is in agreement with Bates and Jackson (1987), who, quoting Sharp and Nobles (1953) and Varnes (1958), wrote "if more than half of the solid fraction consists of material larger than sand size, the term debris flow is preferable". In practice, and in submarine settings, this is quite difficult to determine. A single mass movement might have portions that could be qualified as debris flows while others would be ascribed to mud flows. Within the COSTA sites, this is well illustrated by Finneidfjord Slide (Fig. 4A) and Afen Slide (Fig. 6A,B), which overall is the best representative of mud flows amongst the studied instabilities.

Mud flows, as with debris flows, are members of a gradational series of processes characterized by varying proportions of water, clay and rock debris. The water content of mud flows can range up to 60% of total weight as determined by clay content and mineralogy. The water bonding critically affects the viscosity of the matrix and the velocity and morphology of the flow and the resulting deposit. In mud flows, the viscosity of the flow and its yield resistance are the main parameters controlling the initiation of movement. In mud flows, yield strength equals or almost equals the residual shear strength. We suspect that for high water contents mud flows could grade to liquefied and fluidized flows.

With the exception of, perhaps, the Canary Slide, all of the COSTA landslides are retrogressive and multi-staged (Fig. 6C), likely including the partly surveyed Traenadjupet Slide. The Canary Slide is unique in having its headwall scar mostly buried under the deposits of the El Golfo Debris Avalanche that overloaded the lower northwestern flank of the island of El Hierro thus triggering the debris flow (Urgeles et al., 1997; Masson et al., 1998; see Section 9 below). The persistent pre-, syn- and post-failure burial of most of the headwall scar probably prevented the development of extensive retrogressive failure. However, small faults disrupting the seafloor have been observed on TOBI sonographs adjacent to the margin of the upper part of the debris flow area thus suggesting underlying incipient failure, possibly of a retrogressive nature.

The presence of several scars on the headwall area is an indication of multiple instability phases, although the time lapse between each of them can vary largely, from minutes (i.e., Finneidfjord Slide according to Longva et al., 2003) to millennia (i.e., Storegga Slide according to various papers starting with Bugge et al., 1987 and ending with Bryn et al., 2003b).

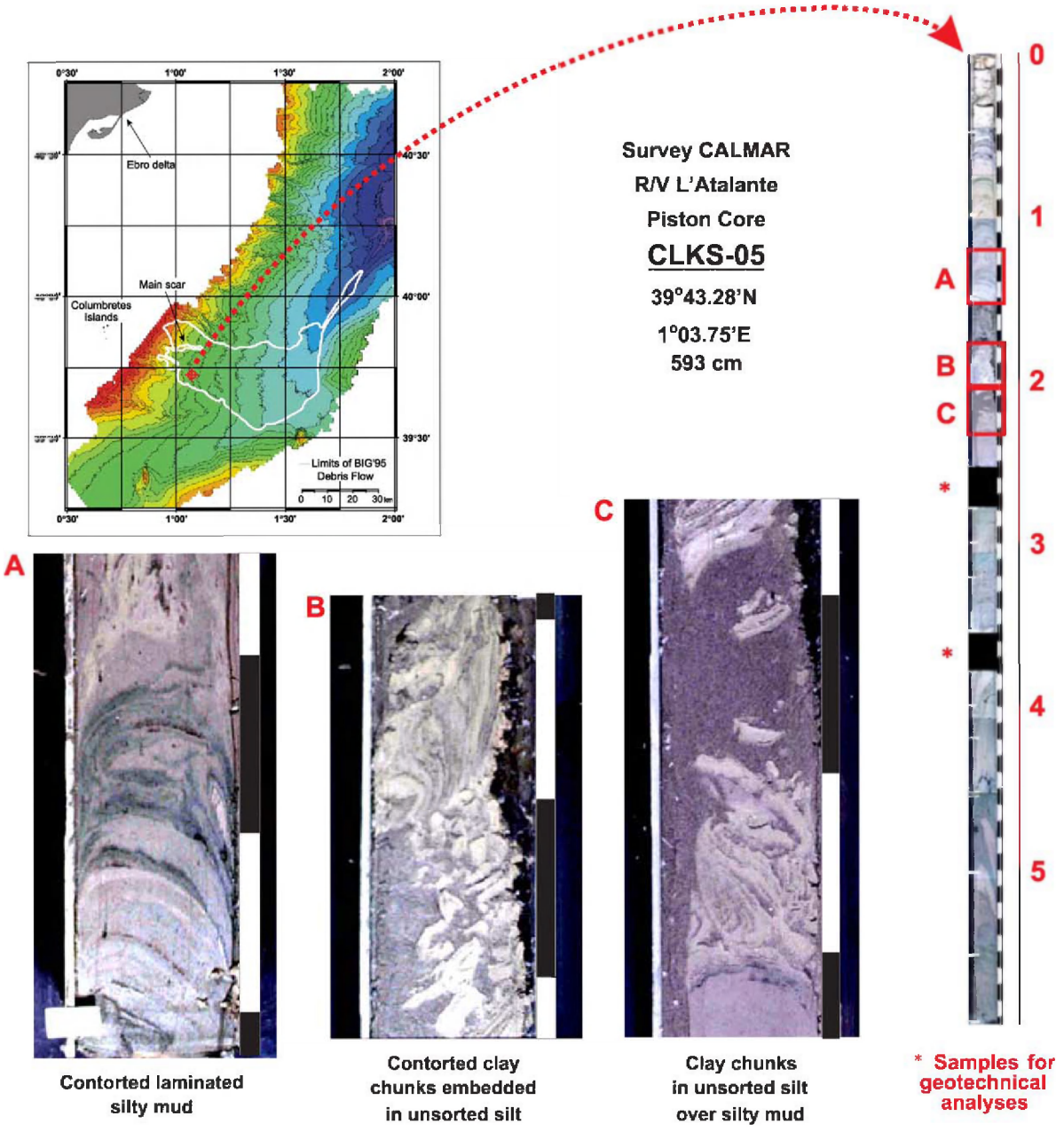

Fig. 5. General and detailed (A, B and C) pictures from a sediment core taken on the BIG'95 debris flow deposit. Location of the core is also shown in Fig. 3. (For colour see web version of this article.)

The Storegga Slide is in fact a set or complex of slides of varying sizes that occurred during at least the last 0.5 Ma, with the latest major event (also known as the Holocene Storegga Slide) dating from about 8.15 calendar ka BP (7.30–7.35 ^{14}C ka BP). While geomorphic and seismic stratigraphic criteria could be useful to identify slide phases which could result in distinct morphologies and sediment facies, dating becomes essential when a precise time frame is required (see Section 10

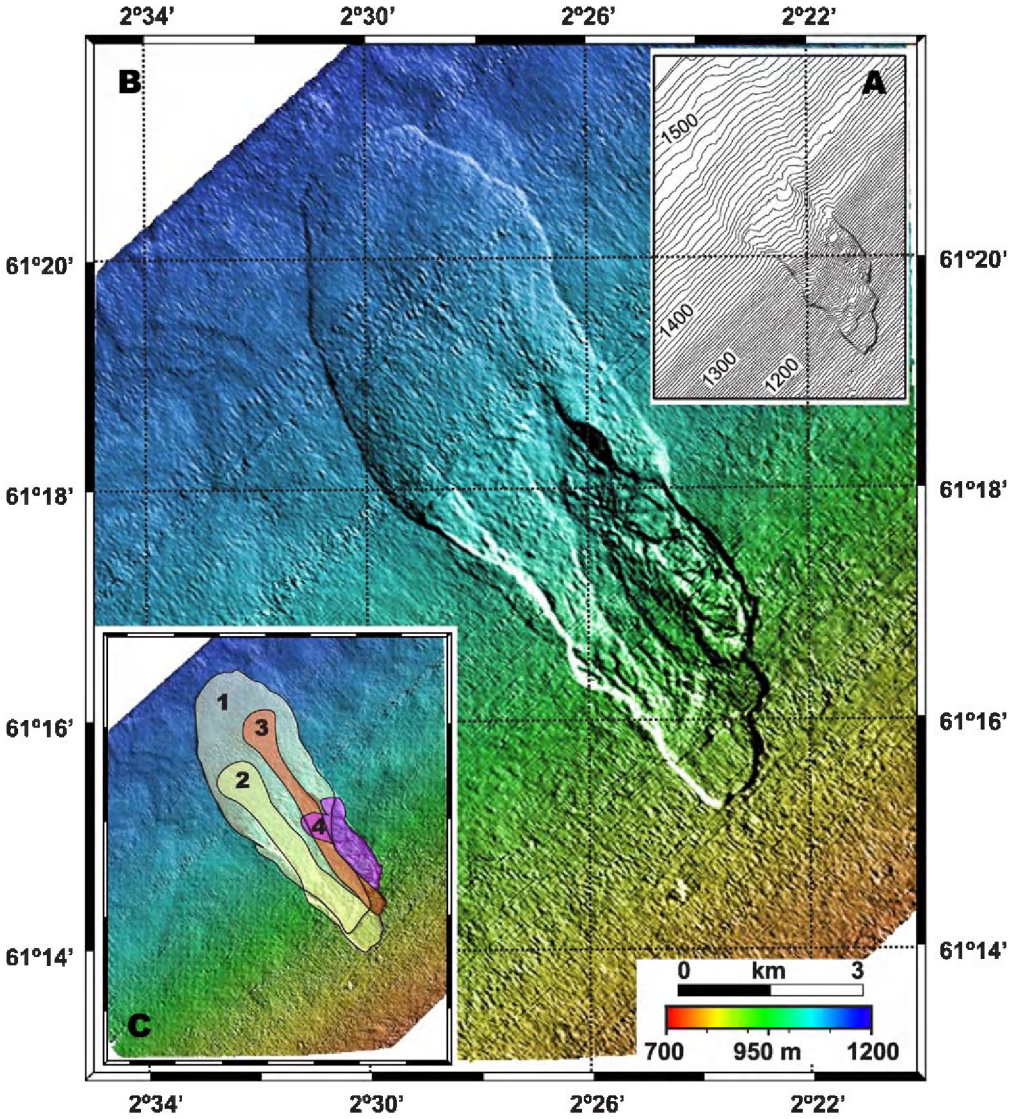

Fig. 6. (A) Detailed bathymetry of the Afen Slide extracted from commercial 3D seismic data assuming a sound speed of 1500 m s^{-1} in water. Note that the morphological expression of the main depositional lobe on the seafloor is very low (cf. Table 4). (B) Acoustic image of Afen Slide extracted from commercial 3D seismic data using the Bulk Line Shift method (for details, see Bulat, 2003 and references therein). Note the small blocky area at the foot of the last failure phase depositional unit (cf. C) (modified from Bulat, 2003). (C) Interpretation of Afen Slide failure phases (1 is oldest, 4 is youngest). Image extracted from seabed picks of commercial 3D seismic data (modified from Wilson et al., 2003b).

below). In Storegga, because of the implications for the oil industry (see Section 2 above), this becomes even more crucial. The recentmost results obtained within the COSTA project show five partially superimposed debris flow lobes in Storegga, numbered from 1 to 5 in Fig. 7. Lobe 1 is associated with a megaturbidite that accumulated in the southern Lofoten Basin. All the lobes correspond to the latest major event. A late minor slide along the northern escarpment of the Storegga Slide dated ca. 5000 ^{14}C yr BP has been reported too. This implies that previously defined slide events (Bugge et al., 1987) are actually erosion boundaries within the same slide failure event.

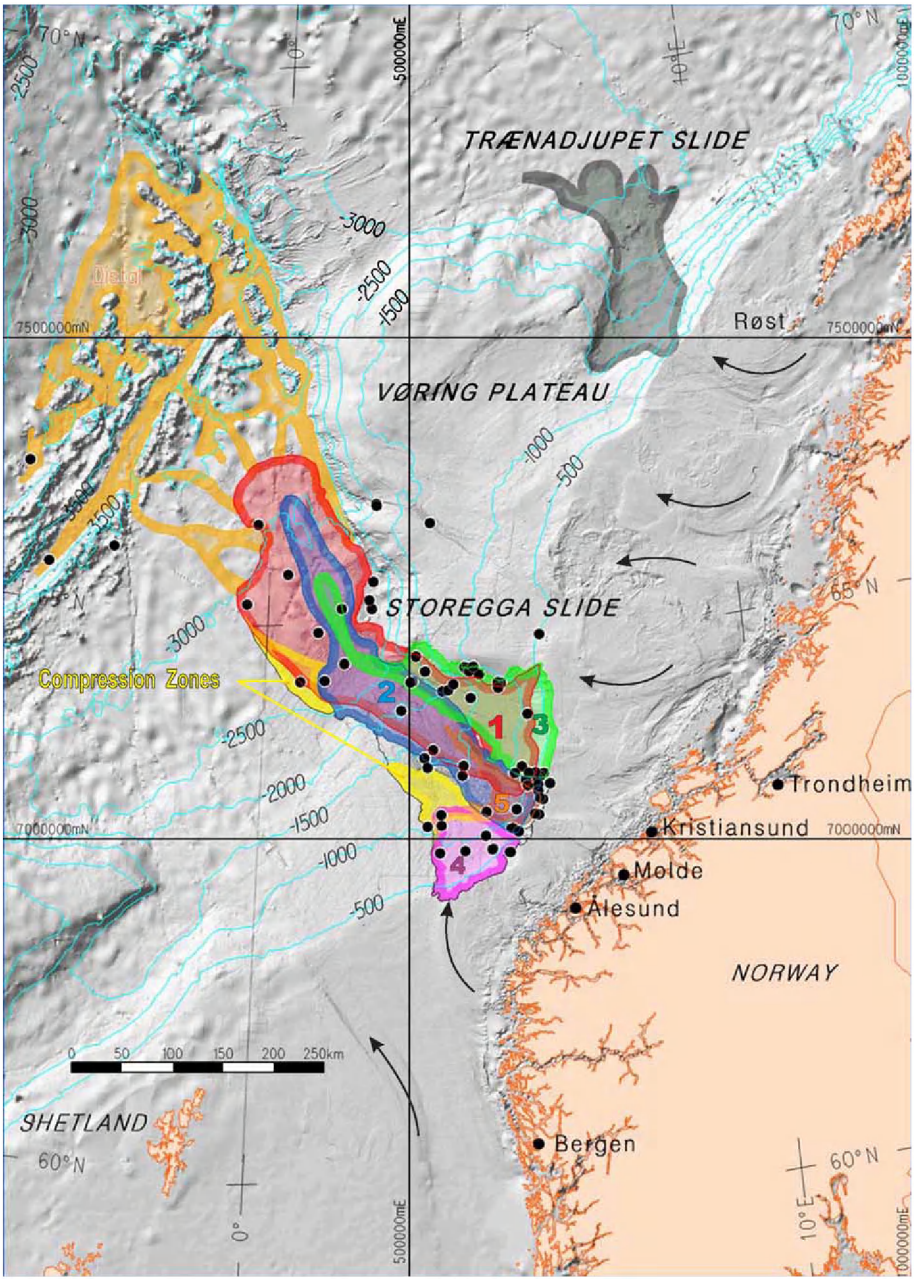

Fig. 7. Shaded bathymetry map of the southern Norwegian Sea showing the Storegga and Traenadjupet Slides. The main depositional lobes of the Holocene Storegga Slide are shown and numbered in stratigraphical order from 1 (oldest) to 5 (youngest) using different colors. The megaturbidite associated to lobe 1 is outlined in orange. Black dots show locations of sediment cores used to date the Storegga Slide within the COSTA project. Also note the glacial troughs (arrows) and megascale streamlined lineations on the continental shelf revealing the location of former ice streams (modified from Haflidason et al., 2003d). (For interpretation of the references to colour in this figure legend, the reader is referred to the web version of this article.)

5. Slide dimensions

The slides studied within the COSTA project are variable in size, from the giant Storegga Slide to the comparatively tiny Finneidfjord Slide (Fig. 8 and Table 5). The largest slides (Storegga, Canary and Traenadjupet) develop off open slopes, while those on the margins of semi-enclosed basins are smaller and show changes in direction reflecting topographic control on sediment flow (BIG'95 and Gebra Slides) (Fig. 8). Whereas calculating the approximate area of the landslides (scar and depositional sections) is relatively easy, calculating the volume of sediment remobilised is more difficult. Four main approaches could be applied. The first is calculating the volume of sediment missing in the headwall scar area, which requires assuming a pre-slide seafloor topography. For this method to be applied, it is necessary to have a well-defined headwall scar, which is not always the case. The Canary Slide illustrates a poorly defined main scar that is partially buried by the El Golfo Debris Avalanche (Masson et al., 1998).

The second approach is calculating the volume of sediment accumulated in the downslope depositional section, which implies knowing how deep below the seafloor the base of the slide deposit lies. The better the basal slide deposit topography is constrained, the more precise the volume calculation can be. This approach also requires attributing to the slide deposit an appropriate P wave speed. However, calculations are often hampered because: (1) the base of the slide deposit is poorly imaged or not imaged at all so that the basal topography is not well defined and (2) the P wave velocity is just assumed.

The third approach is considering pre-deposit seafloor topography and then calculating the volume accumulated on top of such assumed topography (Urgeles et al., 1999). The limitation of this procedure is that the pre-deposit topography is, in most cases, an

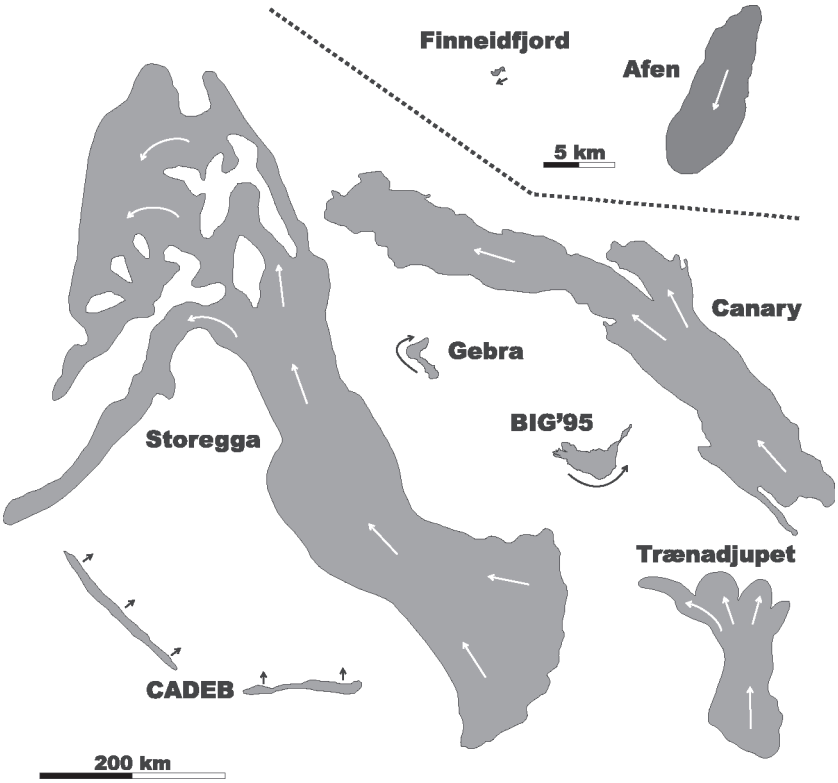

Fig. 8. Comparison of shape and area of the instabilites studied within the COSTA project. Note that Afen and Finneidfjord slides are referred to a smaller scale bar than the rest of the slides.

Table 5
Dimensions of the submarine instabilities studied within the COSTA project including additional information on the methods applied to calculate slide volumes, and on general shape and direction of downslope movement

Instability	Total area[a] (km^2)	Total WDR[b] (m)	Height drop[c] (m)	WDR[b] of deposit (m)	Length× width (km)	Max/ average thickness (m)	Deposit-covered area[e] (km^2)	Volume (km^3)	Volume calculation method	General shape of deposit	General direction of movement	Segments within slide deposit
Storegga	90,000	130/3850	3720	290/3850	~770×115[d]	200/60	85,000 (94%)	≤3000	Comparison of pre-slide assumed bathymetry and post-slide bathymetry, with support from seismic reflection profiles	Fan-like coalescing debris lobes	SE to NW	Composite slide. Up to 70 debris flow units have been identified based on a range of acoustic data. Five lobes resulting from the main Holocene event
Canary	40,000	3900/5400	1500	4300/5400	600×60–90	20/10	35,000 (87.5%)	400	Average thickness of deposit from high resolution seismic reflection profiles multiplied by the area	Strongly elongated with braided appearance on sidescan imagery made up of several debris flow channels flanked by thicker levees of debris. Some lobate tongues diverge from main flow pathway	ESE to WNW	No segments distinguished
Traenadjupet	14,100	400/3000	2600	2400/3000	200×≤70	150/100	9100 (65%)	900	Measurements on multichannel seismic reflection profiles at ~2700 and ~3000 m of water depth taking Vp=2000 m s^{-1}. The average thickness has been then multiplied by the area	Four prominent sediment lobes terminating in the southern Lofoten Basin	S to N and NNW	Available data do not allow distinguishing segments
CADEB	2200	30/110	80	30/110	250×7–15	35/35	2200 (100%)	38.5	CADEB consists of seafloor and sub-seafloor crenulations that could be attributed to creeping. No actual failure has occurred	Elongated deformation belt roughly parallel to the isobaths	SW and S to NE and N	No segments distinguished

BIG'95	>2000	<600/2000	>1400	650/2000	110×<30	135/16	2000 (>95%)	26	Measurements on very high resolution seismic reflection profiles taking V_p=1600 m s^{-1}. The average thickness has been then multiplied by the area	Overall horsetail shape with the apex of the tail being at its distalmost tip. The northern Balearic slope forced the moving sediment mass to turn	NW to SE turning SW to NE	Source area and upper depositional section without blocks; intermediate depositional area with blocks; and distal depositional area devoid of blocks
Gebra	515	900/1950	1050	1650/1950	35×25	135/135	315 (61%)	21	Average thickness of deposit from high resolution seismic reflection profiles multiplied by the area checked against height by area of the main scar	Topographically constrained, lens-shaped body filling the floor of King George Basin	SE to NW turning SW to NE	Two erosional segments in the source area plus a depositional lower segment have been identified
Afen	40	825/1120	295	1005/1120	13×3	20/10	20 (50%)	0.2	Average thickness of deposit from 2D high resolution seismic reflection profiles multiplied by the area calculated from seabed image derived from 3D exploration seismics	Lobate shape though evidence of erosion at upslope end by a subsequent debris lobe which over-rides the first debris lobe	SE to NW	Three, step-bounded segments increasing in width downslope are distinguished in the source area
Finneidfjord	1	<0/62	>62	22/62	1×0.5	10/2	0.4 (40%)	0.001	Comparison of pre- and post-slide event bathymetric and topographic maps	Fan of coalescing debris lobes in outskirts of deposits, outrunner blocks beyond an hummocky terrain closer to back wall where rocks from land make the slide surface	NE to SW	Upper, intermediate and lower segments with distinct features distinguished

The rightmost column on "segments" refers to reaches along the seafloor area affected by the slide showing distinct morphological and depositional features, such as in BIG'95 slide where in addition to the source area, a block-free proximal depositional reach below the main headwall, a blocky intermediate depositional reach, and a distal depositional reach are distinguished (see Fig. 3). Note that most of the figures have been rounded and should be taken as best estimates. Thicknesses (maximum and average) are cumulative and could integrate deposits from various phases.

[a] Total area affected, including both erosional (scar-bounded) and depositional areas.

[b] Water depth range.

[c] Total height from headwall to toe, except for CADEB, where no headwall can be identified.

[d] Length×width of debris only covered area is 450×115 km.

[e] Includes both debris flows and turbidites.

unknown, requiring the pre-deposit assumed surface to be flat, an overly simplistic approximation.

Volume values obtained using these three methods sometimes match while sometimes they do not. Discrepancies can imply both additional sources of sediment that add to the volume released from the headwall scar, or "lost" sediment as more or less dilute flows escape from the area where the main pile of sediment accumulates. The causal relationship between turbidites and debris flow deposits is well known in several places, including Hawaii, Storegga and the Canaries (Jansen et al., 1987; Garcia and Hull, 1994; Masson, 1994, 1996). Addition of sediment to a downslope moving mass could occur by basal dragging, as convincingly shown by Lastras et al. (2004). Disturbed sediments usually show a distinct acoustic facies relative to the surrounding sediments. However, sediment disturbance by basal dragging does not necessarily involve significant displacement. In such a situation, the problem is whether to ascribe the sediment volume affected by the dragging process to the volume of sliding sediment. The concept of movement or displacement is implicit in the sliding concept, and in this situation there is no appreciable displacement. This could turn into an actual difficulty, both conceptual and practical, to identify the basal surface of the slide deposit.

The fourth method consists of comparing pre-slide and post-slide topographies. This method, which is highly reliable, could be applied only in places where reasonably precise maps existed before the slide event. Because precise seafloor mapping is a relatively recent development, this method is restricted to very young events, such as Finneidfjord.

Following a survey of experts on the various slides considered within the COSTA project, we found that the second method (volume of deposit) is, despite of its limitations, the most widely applied. Thicknesses estimated from seismic reflection profiles are commonly the key parameter taken to calculate the volume of the slide deposit (Table 5).

The Storegga Slide is by far the largest of the studied slides covering an area of 90,000 km^2, of which the slide scar is 27,000 km^2. The back wall runs along the outer shelf and slope for about 300 km. Estimates of the overall volume of the Holocene Storegga Slide have changed with time following different authors. This is partly due to the enormous size of the slide, which still contains poorly surveyed sections. Early estimates (i.e., Jansen et al., 1987) were merely approximations from a time when the slide was divided into three phases thought to succeed each other over a long period of time. More recently, Bryn et al. (2003b) reported a value of about 3500 km^3. The most recent data gathered within the COSTA project yields an estimated slide volume of 3000 km^3 as a maximum and probably close to 2500 km^3. The Holocene Storegga Slide is pre-dated by seven slides varying in area from 2400 to 27,100 km^2. Five of them partly underlie the Holocene Storegga Slide, indicating that this is a margin segment prone to long-term failure (Bryn et al., 2003b). Despite the high interest in Storegga Slide, there is no isopach map of the slide deposit available.

The second and third largest slides within the COSTA project in terms of total area are the Canary and Traenadjupet Slides. While the first yields a relatively thin deposit (10 m average thickness), the second is much thicker (100 m average thickness), which results in the second largest volume (900 km^3) after the Storegga Slide. However, caution must be taken when considering figures about the Traenadjupet Slide since large parts of it are still poorly surveyed or not surveyed at all. The rest of the slides considered are one or more orders of magnitude smaller in terms of volume. Caution must be taken since in most of the cases the volume does not result simply from multiplying the total area by the average thickness as shown in Table 5. The complex geometries, often with several debris lobes and blocks, make volume calculation a rather difficult exercise.

The plot in Fig. 9A relates total length, mean width and area of the eight instabilities studied within the COSTA project. The distribution of the dots representing the various instabilities is self-explanatory with the Storegga and Canary Slides separated from the rest in the upper part of the plot, and CADEB isolated in the lowermost right part of the plot. This illustrates the "exceptional" character of these three instabilities. The Storegga and Canary Slides are noteworthy because of their large downslope development (expressed as "total length" in Fig. 9A) and areal extent. In contrast, CADEB has a very limited downslope development but a noticeable alongslope development (expressed as "mean width" in Fig. 9A) as it would correspond to a deformation belt roughly parallel to the isobaths. The

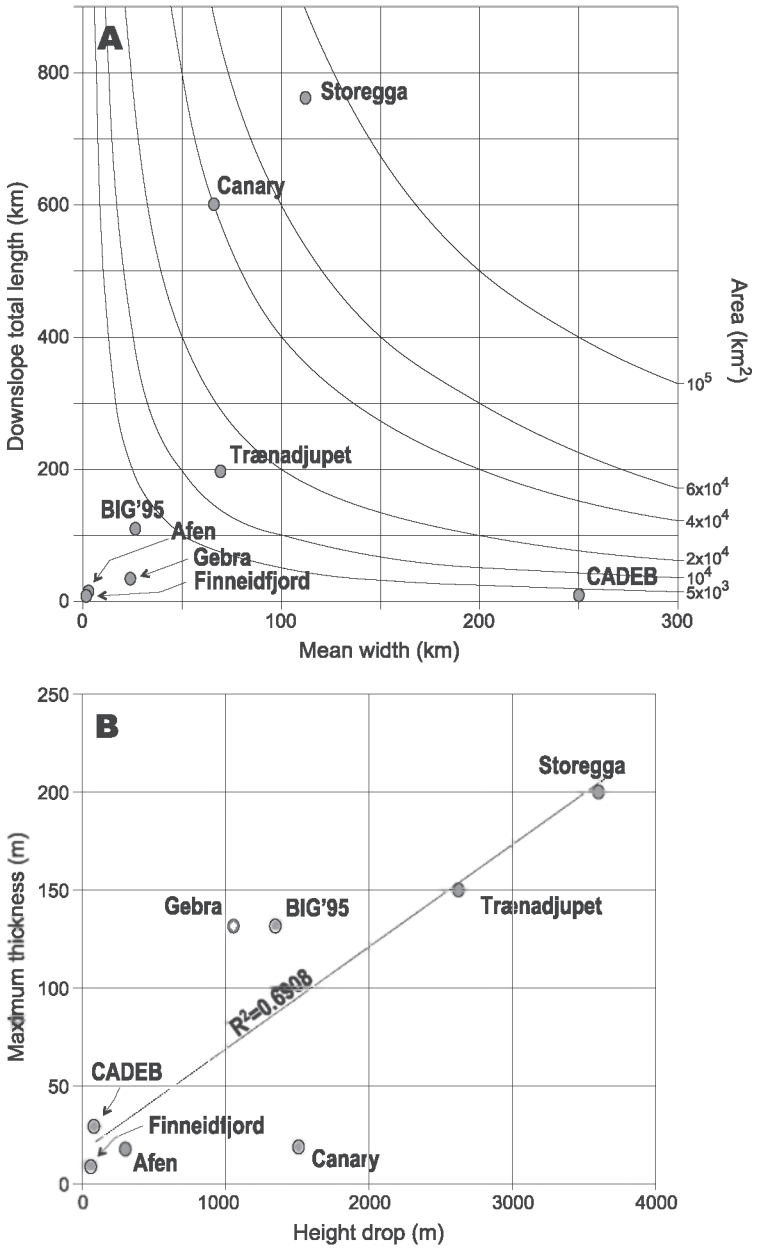

Fig. 9. (A) Downslope total length vs. mean width and area plot for the instabilities studied within the COSTA project. (B) Maximum thickness vs. height drop for the instabilities studied within the COSTA project. A regression line is shown illustrating the direct relation between these two parameters.

downslope "total length" in Fig 9A shows a correlation with the "height drop" column in Table 5. The rest of the instabilities form a cluster grouping relatively small slides close to the lower left corner of the plot with the Traenadjupet Slide in a somewhat transitional position in between that cluster and the largest-in-area Canary and Storegga Slides.

As far as thickness of deposit is concerned, the COSTA sites combine slide deposits with maximum thicknesses in excess of 100 m both in glacial-

dominated (Storegga, Traenadjupet and Gebra Slides) and river-dominated (BIG'95 Slide) settings, with slides resulting in deposits having maximum thicknesses of a few tens of meters (Canary and Afen) to few meters (Finneidfjord) (Table 5). Average thicknesses are very close or even equal to maximum thicknesses for homogeneously thick slides such as Gebra Slide (135 m). Maximum and average thicknesses do not necessarily relate to the overall volume of a given slide. This is clearly illustrated by the Canary Slide, which is third in terms of volume in Table 5 while it displays some of the thinnest maximum and average thicknesses. Excluding Gebra Slide, amongst the COSTA study cases, the largest estimated average thicknesses correspond to Traenadjupet (100 m) and Storegga (60 m). Since the thickness of slide deposit may vary significantly over short distances, the average thickness is a parameter that must be taken with care (see below). Both maximum and average thicknesses relate to the nature and behavior of the sliding materials, together with pre-slide topography.

The largest height drop of slide-affected areas, from the headwall upper rim to the distalmost depositional area or slide toe, is of 3720 m for the Storegga Slide. Height drops in excess of 1000 m are measured in the Canary, BIG'95 and Gebra Slides, the last two being located in semi-enclosed basins. The total height of slides relates to the overall physiography of the margins where they are located and, thus, to the geodynamical history of the margin. Within the COSTA sites, there are slides released form the shelf edge and uppermost slope (Storegga and Traenadjupet), mid-slope (BIG'95, Gebra and Afen) and lower slope (Canary). This is probably related to triggering mechanisms also (see Section 9 below). CADEB and Finneidfjord are extremely shallow-seated instabilities.

Fig. 9B suggests a direct relationship between height drop and maximum thickness, with the Canary Slide as a special case because of its limited maximum thickness (20 m) with respect to its height drop (1500 m) if compared to other slides. The observed correlation could be explained not only because larger height drops would imply bigger sediment volumes and thus greater thicknesses, but also because thick piles of destabilised sediment would be more resistant to disintegration and flattening during downslope transport. BIG'95 and Gebra are markedly above the regression line in Fig. 9B probably because the semi-enclosed character of the basins where they occurred prevented their alongslope development and associated thinning of the resulting deposits. The toes of the Balearic and South Shetland Islands slopes avoided further straight run-out of the flows, resulting in somewhat thicker maximum thicknesses than would occur if the failed sediment was not required to turn.

Slide deposits start to accumulate just below the headwall in most of the cases, although maximum thicknesses are most often found in the upper and intermediate depositional reaches. Nevertheless, large variations in thickness are rather common mostly depending on the pre-slide seafloor topography, the presence of blocks and the basal erosional power of the flow. This is well illustrated by the BIG'95 isobath and isopach maps (see Figs. 13 and 14 in Lastras et al., 2004c). However, isopach maps of the slide deposits are still lacking for most of the COSTA slides. This is due to insufficient seismic reflection coverage that fully penetrates the slide deposits, and also to focusing on specific sections of large slides (i.e., the Ormen Lange area in Storegga). This situation reflects a weakness that should be overcome in the future years, at least for a selected group of slides representing the main types of seafloor instabilities.

It is to be noted that the deposit-covered area usually represents large percentages of the total area affected by a slide. In other words, headwall scars from which large volumes of sediment are released might cover only small parts of the total seafloor area disturbed by an instability event, as observed in the BIG'95 (<5%), Storegga (6%) and Canary (12.5%) slides. There are, however, instabilities where the ratio between the deposit-covered area and the upper erosional area is more balanced, as illustrated by the Traenadjupet (65% of the affected area is deposit-covered), Gebra (61%), Afen (50%) and Finneidfjord (only 40%) slides (Table 5).

6. Scars and slip planes

Scars are perhaps the most critical area to be investigated within submarine instabilities since they represent the source area and allow comparison with nearby non-failed areas. To a large extent, scar location, morphology and size, jointly with the nature of the failed material and the triggering mechanism, influence

the type of mass movement, its dynamics and the volume of the resulting deposit. Of paramount importance are also the seafloor dip and the inclination of slip planes at and beyond the headwall. A slip plane is simply defined as a planar slip surface which itself is defined as "a landslide displacement surface, often slickensided, striated, and subplanar; it is best exhibited in argillaceous materials and in those materials which are highly susceptible to clay alteration when granulated" (Bates and Jackson, 1987). "Landslide shear surface" and "gliding surface" are considered as synonymous of "slip surface" in the same way than "glide plane" is synonymous of "slip plane". The marine geoscientific community tends to preferentially use "slip plane" and "glide plane" although it would be more appropriate using "slip surface". The concept of slip plane as used in the literature is often unclear since it can refer to the stratigraphically or mechanically distinct plane constituting the base of a pile of sediment failed or prone to failure, but also the former seafloor over which the flow of sediment has been moving and on which the slide deposit lies. In the current overview paper, the first meaning is used.

Scars can be from tens of kilometers to tens of meters long and scar height can vary substantially along their length from hundreds to tens of meters or even less, possibly related to irregular thicknesses of the sedimentary units later involved in failure processes (i.e., Traenadjupet Slide). Scars on the upper slope can control the nature and location of the shelf break.

A systematic analysis of the key parameters referred to as landslide scars and slip planes has been undertaken for the set of instabilities studied within the COSTA project (Table 6). Amongst these instabilities, low mean seafloor slope angles (<2°) characterize all the margin segments where failures have occurred with the only exception of the very recent, small Finneidfjord Slide where pre-failure slope angles up to 20° are reported. The average slope of the slip planes beyond headwall escarpments is also low, most usually between 1° and almost 0°. These observations prove that steep seafloor pre-failure and potential slip plane angles are not a requirement for small, medium and megaslide events to occur. In complex slides, where several scars and sliding phases have occurred, it is rather common that more than one slip plane exists, although the various slip planes could be very similar in origin and nature. Layer-parallel slip surfaces, and jumps between slip surfaces located in different stratigraphic levels, have been observed, for example, in the Storegga Slide headwall area (Bryn et al., 2003b). However, it has been also observed that one single layer could behave as the only slip plane for several nearby slides, as it is the case of a set of small slides in the Eivissa Channel, Western Mediterranean (Lastras et al., 2004a).

Precise identification of the nature of slip planes relies on the availability of sediment cores or drillings from which samples could be obtained. Such availability is rather uncommon since corers commonly used in academia cannot reach slip planes except where they crop out or lie at very shallow sub-seafloor depths. In a few cases, specially where there is oil industry interest, such as in Storegga, not only cores but samples from drills and downhole logs are available, thus allowing a precise characterization of the materials forming the slip plane. Three main sediment types are known in the Storegga region: pre-glacial biogenic oozes, glacial tills and debris flow deposits, and distal glacial-marine to marine clays. Most of these materials classify as clays according to geotechnical tests (see summary of geotechnical properties in Bryn et al., 2003b). Slip planes in Storegga are developed in marine clays, which are geotechnically weaker and have higher sensitivities than glacial clays, and show contractive behavior upon loading (Kvalstad et al., 2002). However, the loading of interlayered biogenic oozes could have facilitated initial sliding. Individual weak layers, representing dramatic changes in environmental conditions and sedimentation rates, have been identified on the Storegga Slide escarpment (i.e., Haflidason et al., 2003c). Glacial/interglacial stratigraphic boundaries, also from the Ormen Lange area, are potentially efficient slip planes inside the Storegga Slide. The modern Storegga headwall is made of stable over-consolidated glacial clays and current-controlled infill of the slide scar by soft marine clays is going on.

In contrast, source areas (headwall escarpments) show great slope variability, from >20° (Storegga, Afen and Finneidfjord slides) to less than 1° (Canary Slide and CADEB). BIG'95 (10°), Traenadjupet (2°) and Gebra (1.5°) slides display intermediate values. Slope angles at the toe of the depositional section are <1° in all cases. It is common for headwall areas to present more than one scar. When the landsliding

Table 6
Slope, scar and slip plane data for small-, medium- and megaslide events investigated within the COSTA project

Landslide	Max/min slope angle[a]	Source area/ deposit toe slopes	Number of scars WDR[b] (m)	Main scar		Upslope climbing of deposits[c] (Y/N)	Max/min slope of basal slip plane[d]
				WDR[b] (m)	Shape/height (m)[e]/slope angle/burial situation		
Storegga	1.5°/1°	23°/0.1°	Many 130/530	130/530	A composite set of irregular scars with varying orientations, heights and slope angles rather than a single main scar form the slide headwall/some are partially buried	Y	2°/1°
Canary	0.15°	1°/~0°[f]	Not known[g] 3900/4300	Not known[g]	Not known[g]	Y	0.35°
Traenadjupet	~2°	2°/~0°	≥2, 400/650	400–550	Straight, parallel to the shelf edge/up to 150/~20°/not buried	N	Not known
CADEB	0.55°/0.15°	0.55°/0.15°	No scars	–	No main scar	N	0.2°/0.1°
BIG'95	2°/1°	10°/<1°	>3, 600–1200	800–1200	Complex, horseshoe shaped sinuous geometry/up to 200/ 17°/locally buried by materials from upslope secondary scars and from degradation of the slide scar itself	Y[h]	~1°
Gebra	0.4°	1.5°/~0°	2 sets, 900–1950	950–1500	Elongated brick-shaped depression, with local amphitheatres, and overall flower-like geometry/up to 160 m/up to 30°/not buried, fresh	N	1.5°/~0°
Afen	~1.5°	2.2°/0.6°	3 825/1045	825–1000	Outermost scar cutting down from undisturbed seabed. Straight downslope sidewall scar on the southwestern side. The northeastern side is sidestepped (retrogressive failure)/up to 10/5°/partially buried in the lower parts of the slide	N	~1°
Finneidfjord	20°/<5°	20°/1°	1, <0/40	<0/20	Bowl shaped/up to 20/25° to 5°/not buried	N	5°/1°

[a] Mean seafloor slope angle of the margin segment where failure occurred.
[b] Water depth range.
[c] Evidence of local upslope climbing by landslide deposit.
[d] The base of landslide deposit is taken as basal slip plane.
[e] Note that most often the scar height is not the difference between the shallowest and the deepest water depths expressed in the WDR column since the scar upper and lower boundaries may change water depth while displaying a given height, which is usually smaller than or, as a maximum, equal to, the WDR.
[f] The deposit toe lies at the edge of the Madeira Abyssal Plain.
[g] Main scar partially buried by debris avalanche deposits from farther upslope.
[h] Upslope climbing observed at the base of the slope opposite the source area.

history at a given site is particularly complex, identifying the main scar can be far from obvious. Complex slides, with multiple slide phases, have composite sets of scars located at water depths sometimes hundreds of meters apart, representing successions of major and minor, often retrogressive, events. The best example of this situation is the Storegga Slide, with BIG'95, Gebra and Afen

providing good examples too, although less complex than Storegga (Table 5 and Fig. 6).

Amphitheatres and sinuous shapes are common both in main scars and secondary scars, although rectilinear shapes have been equally observed, for example, in Traenadjupet and parts of the Storegga and Gebra slides. Good examples of the morphological variability of headwall scars of the Storegga and BIG'95 slides have been published recently by Haflidason et al. (2003c) and Lastras et al. (2003), respectively. Such morphological variability allows interpretation of the processes involved in the triggering of main events and further evolution of scar areas. Partial burial of scars could occur as a result of upslope retrogressive failure and subsequent sediment release, as best illustrated by the BIG'95 Slide (Lastras et al., 2002). The most extreme case is the headwall scar of the Canary Slide, which is almost entirely buried under deposits released by an earlier upslope event (Masson et al., 1998).

Deep-towed side scan sonar sonographs have provided self-explanatory images illustrating the progressive degradation and leveling of headwall escarpments. Arcuate secondary scars where sediments have started to move downslope, forming well-defined subparallel ridge systems probably related to detachment processes have been identified on TOBI sonographs both in the northern Storegga Slide escarpment and in the BIG'95 horseshoe-shaped headwall (Fig. 10). Open linear to arcuate creep-like fold crests, crown cracks and staircase successions of low to intermediate relief steps are also common in headwall escarpments, thus indicating they are prone to, or have experienced further destabilisation and leveling following main events. The total height jump of the headwall scar could be locally resolved by sets of steps of lower height.

The study of secondary scars is at least of the same importance as investigating main scars since secondary scars have the potential to provide clues to better understand failure mechanisms and evolution of the instabilities. Secondary scars have been identified in the Traenadjupet (one secondary scar, 100 m high), BIG'95 (two, up to 100 m and about 50 m high, both with 6–9° of slope angle), Gebra (one set with up to 130 m of total height) and Afen (two less than 10 m high, with 2° of slope angle) slides. Though most secondary scars are found upslope from the main scar and/or cutting and degrading it, often due to retrogression, they have also been observed downslope of the main scar, such as in BIG'95. Upslope retrogression could end by final headwall leveling or specific geological conditions, such as in the Storegga Slide where it stopped when the flat lying, overconsolidated glacial deposits of the continental shelf were reached (Bryn et al., 2003b). Downslope secondary scars could form during or shortly after the passage of destabilised sediment masses released upslope. Both sudden loading and basal dragging have been invoked to explain the formation of this kind of secondary scars (Lastras et al., 2002; Masson et al., 1998).

Amongst the seafloor instabilities studied within the COSTA project, the Storegga and Gebra slides present, with independence of their size and the number of events involved, noticeable setting and morphological similarities (Fig. 11). The Storegga Slide rear edge is about 300 km long and 250 km wide while the Gebra Slide scar is only about 30 km in length and up to 12 km wide. Both slides are located offshore continental shelves which had grounded ice on their edges during glacial maxima. Also, the headwalls of the two slides lie at relatively short distances from paleo-ice stream ends. However, while the headwall upper rim forms the current shelf edge in the Storegga Slide, the two main sets of scarps bounding the Gebra Slide are located, respectively, on the lower part of a steep upper slope and on a gentle lower slope (Bryn et al., 2003b; Imbo et al., 2003) (Table 6). Since the succession of slides in the Storegga area is believed to have started on the mid- to lower slope and then developed retrogressively (Bryn et al., 2003b), the Gebra Slide could represent an earlier stage of the Storegga Slide.

Both the Storegga and Gebra Slides display a cauliflower-like, wide, roughly semi-circular uppermost scar area followed downslope by a sort of narrower corridor bounded by relatively steep flanks (Figs. 8 and 11A,B). These corridors open to low relief broader depositional areas (Lofoten Basin for Storegga Slide and King George Basin for Gebra Slide) where the distalmost products of each of the events have been deposited.

Headwall areas often include detached blocks, both rotated and rafted, blocks that have remained in situ and other elements leading to rough terrains where highs and lows succeed each other. This is perfectly

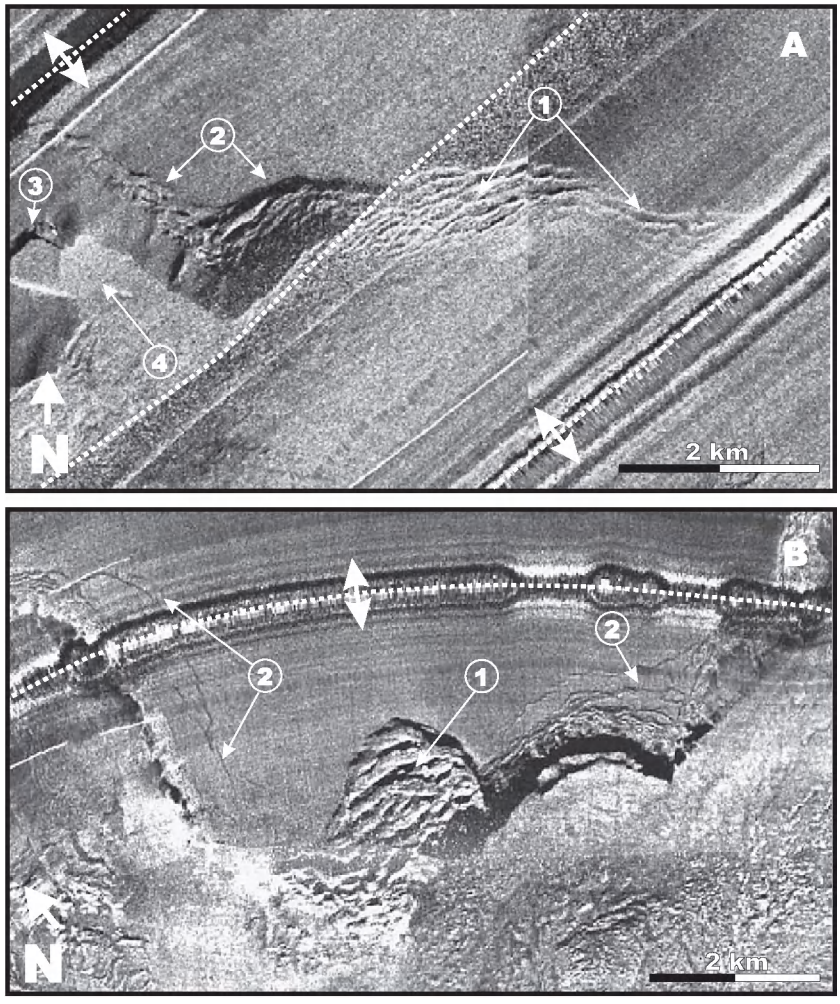

Fig. 10. (A) TOBI composite sonograph from the deepest section of BIG'95 Slide headwall showing ridge systems and staircase morphologies (1) attributed to creeping and indicative of retrogression and leveling. A step (2) reshaped by small retrogressive slides is also observed. A minor secondary scar (3) and a debris tongue (4) onlaping it are seen too. Double arrows show ensonification direction and dashed lines indicate where this direction changes. A processing artifact appearing as a tiny vertical cut crosses the image at about the position of number 1 within a circle (modified from Lastras et al., 2003). (B) TOBI sonograph of a 90–100 m jump on the northern Storegga Slide escarpment showing subparallel ridge systems (1) probably related to creeping processes and open crown cracks (2) suggesting further failure. An arcuate secondary slide scar embraces the subparallel ridge systems. Double arrows show ensonification direction (modified from Haflidason et al., 2003c). Note the resemblance between the two images suggesting that about the same processes occurred in the two slides despite their strikingly different settings. Also note that the scales are very close.

illustrated by the 3D view in Fig. 11D, which corresponds to a zoom of a small part of the Ormen Lange zone from the Storegga Slide headwall. In some places, compressional zones, pressure ridges, debris lobes and fluid escape structures are observed on or at the foot of headwall scarps (Fig. 10A). A looser matrix may occupy the spaces between the elements keeping part or most of their original coherency (Lastras et al., 2002). Also, seafloor and sub-seafloor polygonal faults have been reported in headwall areas as related to gas hydrate BSRs and sediment destabilisation (Bünz et al., 2003; Berndt et al., 2003).

On the headwall foot, the most common situation is for most of the failed sediment to be evacuated from

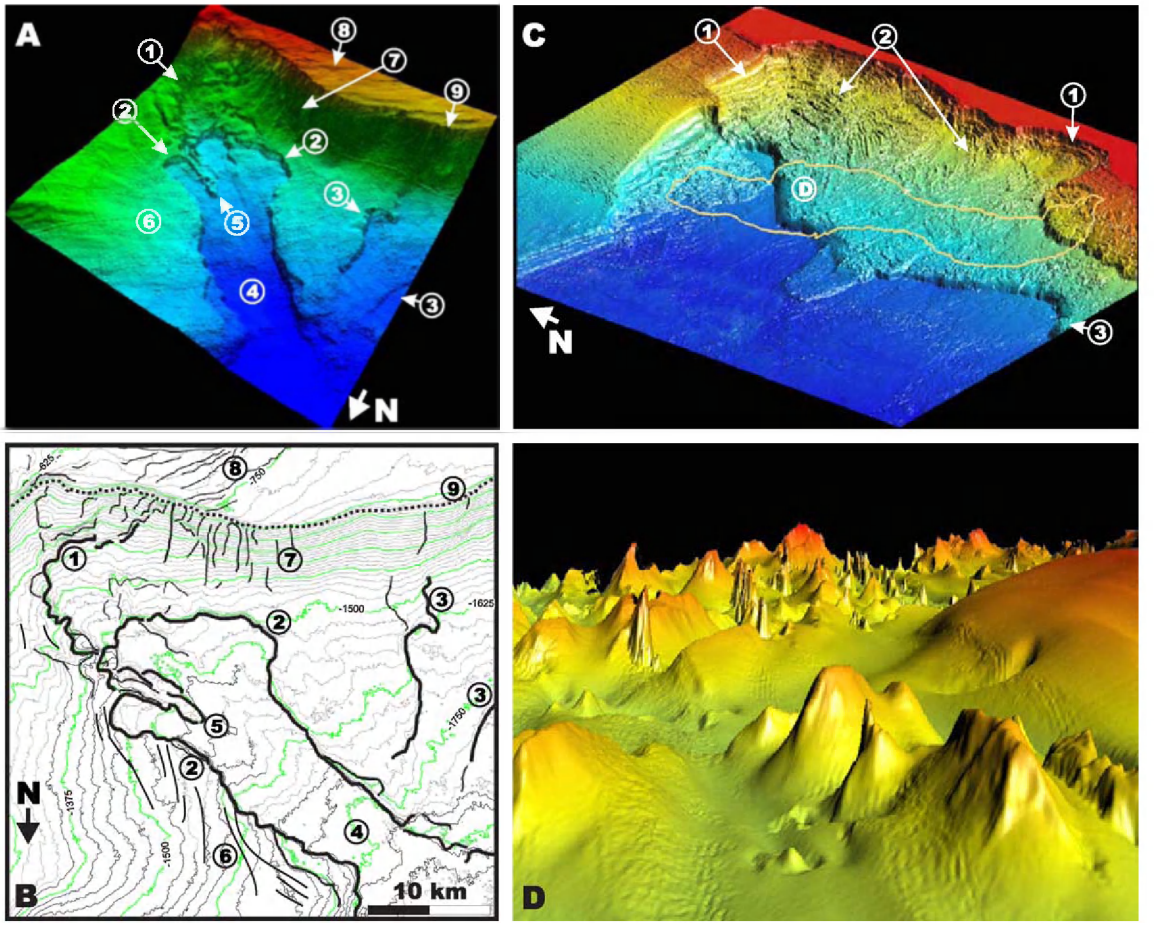

Fig. 11. Views of Gebra and Storegga slides at various scales for ease of comparison and interpretative sketch of Gebra Slide. (A) Frontal aerial oblique view of Gebra Slide source area derived from swath bathymetry data showing the upper scarp (1), the lower main scarp (2), other nearby scarps (3), a debris corridor (4) bounded by the intermediate and lower scarp, a stable block area (5), sets of slope gullies (7), megascale glacial lineations on the continental shelf (8) and 800–1000 m deep shelf edge (9). Note the overall physiographic setting of the slide area. (B) Bathymetric map and overlapping interpretative drawing of Gebra Slide source area and surroundings. Numbers refer to the same elements than in frame A except for (6), which corresponds to alignments of creep-like fold crests seen on seismic reflection profiles but not on the 3D view in A. Note the location of the upper, and perhaps younger scarp and that of the lower, and possibly somewhat older main scarp on the lowermost continental slope. (C) Frontal aerial oblique view of the Ormen Lange gas field section of the Storegga Slide headwall (1) and upper scar displaying alignments of detached blocks (2) and secondary scarps (3). The section illustrated in C could be considered equivalent to one of the arcuate zones delineated by the bathymetrically lower, Gebra Slide main headwall scarp on A although with a higher resolution. The yellow line corresponds to the outer limit of the Ormen Lange gas field. (D) 3D view of seabed topography from the Ormen Lange section between the upper and lower headwall of the Storegga Slide main scar where slide blocks jutting 30–60 m up from the seabed and an Holocene clay infill could be observed on AUV swath bathymetry data (modified from Totland, 2001). (For interpretation of the references to colour in this figure legend, the reader is referred to the web version of this article.)

intermediate to lower scar areas, where often only a relatively thin layer of failed sediments is left. Such a situation is perfectly illustrated by the Gebra Slide where a <35-m-thick debris flow deposit floors the mid-lower slide scar which itself is about 160 m high and 7.5 km wide at the crossing with the airgun seismic reflection profile shown in Fig. 12A. Whether the debris layer left in the Gebra Slide scar and the main deposit infilling King George Basin correspond to the same or to two different events is a matter of

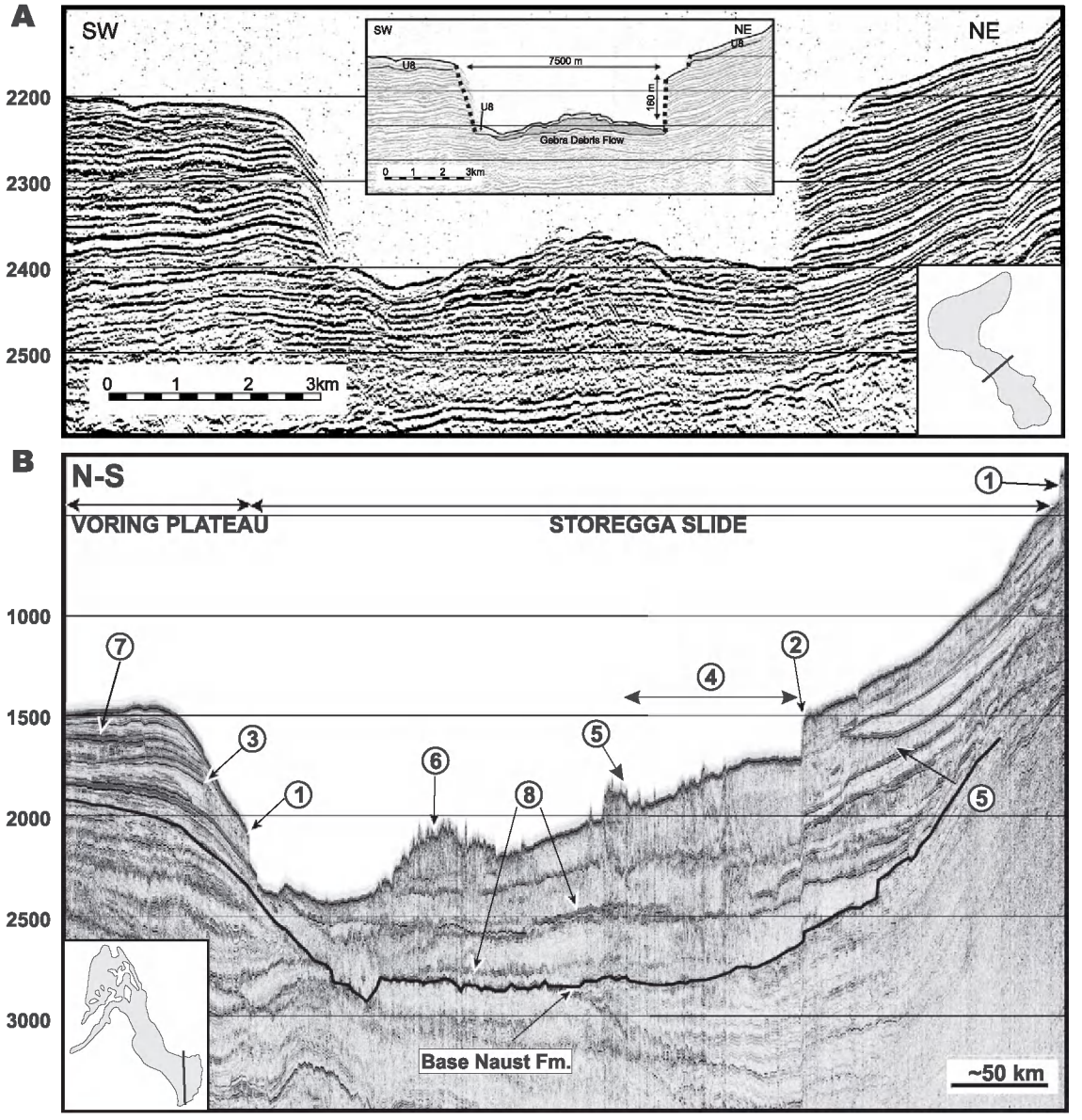

Fig. 12. (A) Airgun seismic reflection profile and interpretative line drawing across the intermediate scar area of Gebra Slide. Note the relatively thin debris flow deposit left inside the scar (grey pattern), which is capped by a thin veneer of post-slide sediment, and the overall dimensions of the scar section. See location on lower right inset. Vertical scale in ms TWTT. (B) Seismic reflection profile across the Storegga Slide scar showing the slide escarpment (1), an inner slide escarpment (2), an older slide escarpment (3), a compressional zone (4), material from Tampen Slide (an informal name given to one of the slides pre-dating the Holocene Storegga Slide) (5), additional slide material (6), hemipelagic glacimarine sediments (7) and disturbed glacigenic sediments (8). The base of Naust Formation, the uppermost seismostratigraphic unit defined on the mid-Norwegian margin, is also shown (continuous bold line). According to Haflidason et al. (2003c), the so-called Intra Naust A reflector is associated with one of the most pronounced failure planes identified in the upper Storegga Slide area. See location on lower left inset. Vertical scale in ms TWTT.

debate (Imbo et al., 2003). Two main escarpments (or even more), such as are observed for the Gebra Slide, could have been generated both from one single event, as interpreted for the Grand Banks Slide (Piper et al., 1999), or from a succession of upslope backstepping events as postulated for the Traenadjupet Slide (Laberg et al., 2002). Cross sections similar to that on Fig. 12A have been obtained from the intermediate and lower Storegga Slide scar, although there the overall stratigraphy inside the scar is somewhat more complex, with disturbed glacigenic units underlying sedimentary units resulting from failure (Fig. 12B).

Upslope climbing sediment failure within the source area has been interpreted to occur locally in the Storegga, Canary and BIG'95 slides, either from detailed swath bathymetry maps (BIG'95), deep-towed side scan sonographs (Storegga and Canary) or high resolution seismic reflection profiles (BIG'95). In BIG'95, such behavior has been deduced from climbing onlaps of debris units on both the flanks of nearby channel-levee complexes of the Ebro margin and the lowermost slope opposite to the slide source area (Canals et al., 2000c). The fact that part of the sediment released from slide escarpments accumulates on previous seafloor surfaces inclined against the direction of the flow paths implies very dynamic and energetic behavior. Reflecting turbidites have been hypothesized by some authors to refer to turbiditic events experiencing rebounds from one side of a basin, sub-basin or depression to another until final settling of the particles. This could result in climbing and hanging turbidite deposits in and around the basin floor. Such events would occur in enclosed and semi-enclosed basins.

Despite the gross relation between height drop and maximum thickness of resulting deposit illustrated by the regression line in Fig. 9B, a word of caution is required about automatically relating scar heights and debris deposit thicknesses. These two parameters do not necessarily have a direct correspondence (note that deviation from the regression line on Fig. 9B could be significant), which implies that special attention has to be paid when trying to reconstruct failed sediment volumes solely from the scar height. Also, in any volumetric reconstruction, it is fundamental to know the thickness of the remobilised sediment and whether different remobilisation distances involve different sedimentary units (see Section 8 below).

7. Run-out distances

Run-out could be defined as the horizontal distance between the upper edge of the slide headwall and the distalmost point reached by sediments mobilised during a slide event. In multi-staged slides, run-out tends to increase with time because of upslope retrogression, continued transport and downslope extension of the released sediments. Different slide phases usually have different run-outs, with the largest failures in terms of volume having in general the largest run-outs. Often, secondary slides involving relatively small volumes of sediment have run-outs that are largely contained within the areas defined by the largest failures. In this situation, even if there is some upslope retrogression involved, secondary failures do not increase substantially or at all the run-out of the whole multi-staged set of slides they belong to. Identifying the run-out from different events in a multi-staged slide requires locating the source area and differentiating the deposits resulting from each of the events, a task which often is far from easy.

In addition, Lastras et al. (2004a) have shown an interesting case in the Eivissa Channel, Western Mediterranean, where four slides display modest sediment movement accompanied by remarkable downslope propagation of deformation that extensively remolds the slope sediment without necessarily translating it very far downslope, thus resulting in a very limited run-out. The above examples illustrate that run-out and length of slide are not necessarily equivalent concepts.

The run-out distance of a debris flow depends on its effective yield strength and viscosity. Following Johnson (1970), the yield strength, κ, of a viscoplastic material equals the basal shear stress, τ_β, when the flow comes to its stop

$$\kappa = \tau_\beta = \rho' g h_p \sin\alpha \quad (1)$$

where ρ' is the average submerged density of a plug, g is the acceleration due to gravity, h_p is both plug and deposit thickness and α is the slope angle at the location where the flow stops. For the expression above, it is assumed that the flow behaves as a Bingham material, consisting of two zones, an upper plug zone in which the yield stress is not exceeded and an underlying lower plug shearing zone where the

shear stress exceeds the yield stress (Norem et al., 1990; Jiang and LeBlond, 1993). The plug concept involves assuming the flow moves donwslope without significant internal deformation, i.e., as a block or plug. In practice, plugs are assimilated into debris lobes, which could be distinguished in high resolution seismic reflection profiles from their acoustically homogeneous composition, usually made of transparent or opaque facies (Table 4).

Elverhoi et al. (1997) applied Johnson's (1970) expression to submarine slides on deep-sea fans along the Norwegian–Barents Sea continental margin and found that the characteristic yield strength κ varied almost one order of magnitude between Isfjorden debris lobes (κ=9000 Pa) and Bear Island lobes (κ=1100 Pa). While relatively high yield strengths correspond to short run-out distances, it has been hypothesized that the differences in yield strengths relate to variations in the physical properties of the source materials. The acoustical properties of the deposits could be diagnostic in that respect, since opaque facies would correspond to shorter run-outs and transparent facies to larger run-outs (Elverhoi et al., 1997). Minor changes (2–4%) in sediment concentration, expressed as bulk density, could account both for yield strength and acoustic properties variations (Major and Pierson, 1992).

There are, however, debris flows where different elements have different run-outs. This situation is well illustrated by the BIG'95 Slide where blocks released from the main scar and secondary scars have a few tens of kilometers of run-out whereas a looser matrix has more than 100 km of run-out (Fig. 3 and Table 7). A similar situation occurs in other slides studied within the COSTA project, including Storegga, Afen, Canary and, most probably, Traenadjupet. With the exception of outrunners, relatively large blocks derived from headwall and upper parts of failed seafloor areas tend to accumulate at short distances from source areas if compared with total run-out (Figs. 3, 4, 6 and 11D). It is also well known that, when there is reduced yield strength and viscosity after slide failure, the flow pattern is characterized by velocity gradients normal to the bed producing a segregation of the particles wherein larger particles become concentrated in the top (Edgers and Karlsrud, 1981; Savage, 1987).

Transformations experienced during downslope transport largely determine total run-out. In particular, transformation into fluid-rich, reduced density flows and turbidity currents greatly helps in achieving larger run-outs. Turbidity currents resulting in extended run-outs added 500 km to the total run-out of the Storegga Slide, which is slightly less than 800 km (Bugge et al., 1987 and Table 7). Also, the so-called "turbidite b" in the Madeira Abyssal Plain adds some hundred of kilometers to the total run-out of the Canary Slide (Weaver et al., 1992; Masson, 1996). Indications exist that the BIG'95 and Traenadjupet Slides could have generated turbidites extending their total run-out.

In a more mechanical approach, Locat and Lee (2002) divided the flowing material in two components: dense flow (a debris avalanche, debris flow or mud flow) and suspension flow. Drag forces acting on the upper surface of the dense flow sustain the suspension flow and will transform it into a turbidity current once the dense flow moves slower than the suspension flow or stops. Slopes as low as 0.1° (compare with slope angles in Table 6) could be enough for this phenomenon to take place (Schwab et al., 1996). In addition, once a critical velocity around 5–6 m s^{-1} is reached, hydroplanning could reinforce mobility by reducing the shearing strength at the base of the moving mass (Mohrig et al., 1999; Elverhoi et al., 2000).

A geometrical description of run-out where two components are considered, the run-out distance sensu stricto (L) and the upslope extended run-out distance or retrogression (R), is presented in Fig. 13. Total height drop (Table 5 and Fig. 9B) vs. total run-out distance (H/L', where $L'=L+R$) is an easy to use ratio to characterize the mobility of a submarine landslide in terms of the geometry of the deposits before and after the slide event. However, using solely the H/L' ratio may provide oversimplified views of the actual, more complex situations (see first paragraph, this section). H/L' represents in fact the angle of the line joining the slide headwall to the farthest point reached by the resulting deposit ($H/L'=\tan\alpha$). Such a slope angle could be assumed to equal the apparent friction angle ϕ (Table 6). In addition, according to Scheidegger (1973), the friction coefficient would decrease substantially for volumes of sediment larger than 0.0001 km^3 (100,000 m^3), which is the case for all the COSTA slides, including the smaller ones. R has been related both to the $Cu/\gamma' H$ ratio, where Cu is the undrained shear strength and γ' the submerged unit weight, and to

Table 7
Run-out distances and associated parameters for the set of submarine landslides investigated within the COSTA project

Landslide	Run-out distances (km)			Flow pathways visible on the seafloor		Rafted blocks					High/low backscatter zones (HBZ/LBZ)
	Total	Block clusters	Individual blocks	Y/N	Location within slided mass	Y/N	Total number	Max. size (m)	Max. height (m)	Location within slided mass	
Storegga	770	Up to 450	NF	Y	All along the slided masses	Y	Not known	1800×200	70	Middle segment	HBZ corresponding to disrupted blocks interpreted as sediment failure area. LBZ corresponding to fine-grained sediment interpreted as turbiditic pathways
Canary	600	NR	NF	Y	Best developed in middle part of slide	Y	Many	300×300	Slightly elevated above general slide surface	Best developed in middle segment	NR
Traenadjupet	200	NR	NR	Y	Slide scar (only area covered by TOBI data)	NR	–	–	–	–	NR
BIG'95	110	15–23	55	Y	All along the slided mass, and specially in the middle depositional area in between rafted blocks	Y	~200	12,500×3000	~20	Middle segment	HBZ forming a network of elongated depressions partially filled by loose matrix containing topographically elevated (blocks) LBZ
Gebra	70	NR	NR	N (buried if any)	–	NR	–	–	–	–	NR (buried)
Afen	7.35	–	3	Y	Middle segment	Y	5	500×500	6	Middle segment	LBZ noted alongslope at the level of the headwall interpreted as sorted silt / very fine sand-dominated contourites
Finneidfjord	1	0.2–1	3	Y	All along the slided mass	Y	~20	60×30	1	Middle and lower segments	No backscatter data

CADEB is excluded since it has no run-out. NR: not recognized (insufficient surveying). NF: not found.

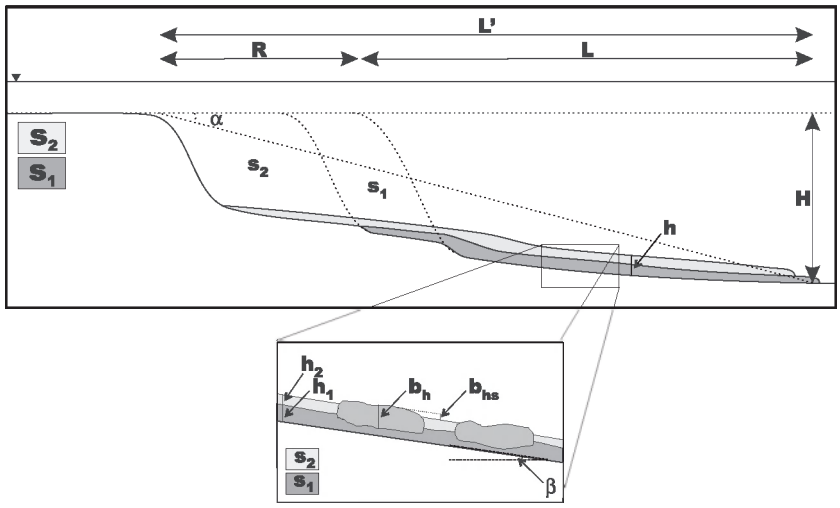

Fig. 13. Geometrical description of mobility. L: run-out distance sensu stricto, R: retrogression distance, L': total run-out distance ($L+R$), H: total height drop, α: mean slope angle, h: total deposit thickness, S_1: slide phase 1, S_2: slide phase 2, h_1: height of slide phase 1 deposit, H_2: height of slide phase 2 deposit, b_h: rafted block height, b_{hs}: rafted block height over the surrounding seafloor, β: basal angle.

the liquidity index (I_L) (Mitchell and Markell, 1974; Lebuis et al., 1983; Locat and Lee, 2002).

In their paper on submarine landslides, Hampton et al. (1996) provide numerous quantitative data on the mobility of submarine mass movements collected from the literature (see their Table 1 and references therein). With the exception of the Storegga Slide, for which they use L'=160 km only (770 km according to COSTA results), none of the slides studied during the last years within the COSTA and precursor projects was considered by those authors. Because of that, and also given the scope of the current overview paper and the large number of new data available, the COSTA selected slides have been highlighted in Fig. 14. The values of H/L' ratio plotted by Hampton et al. (1996) as a function of volume have been drawn in our Fig. 14 from where it is inferred that submarine landslides are much more mobile and tend to involve larger volumes than subaerial landslides, and that volcano-related submarine landslides can have extreme run-out distances. To account for the very low remoulded shear strength required for the observed mobility (up to 770 km for Storegga in Fig. 14), Locat et al. (1996) invoked a significant loss in strength of the soil mass in the starting zone (see also the paragraph above on "transformations", this section).

Fig. 14 shows, however, considerable scatter in the data points as it could be expected considering the diversity of environmental conditions under which submarine mass movements occur. Run-out could be both enhanced or limited because of specific seafloor features such as channels and obstacles and, in general, because of the overall physiography of the transport and depositional areas, as nicely illustrated by the BIG'95 and Gebra Slides.

The parameters and observations more directly related to run-out for the submarine landslides studied within the COSTA project are summarized in Table 7. The largest total run-outs by far, in excess of 500 km, correspond to the Storegga and Canary Slides, while Traenadjupet, BIG'95 and Gebra Slides form an intermediate group with total run-outs in between 70 and 200 km. The smaller Afen and Finneidfjord Slides have total run-outs of less than 10 km. Finally, CADEB has no run-out since, although deformed, sediments still are in place. For this reason, CADEB has been excluded from Table 7. Joint analysis of Tables 5 and 7 shows a direct correspondence between area, volume and run-out. The fact that block clusters and blocks (with the exception of outrunner blocks as in the Finneidfjord Slide, see Section 5 above and Fig. 4) have shorter run-outs is also illustrated by Table 7. The general relations between geometrical descriptors of mobility, and thus run-out, and slide volume are depicted in Fig. 14.

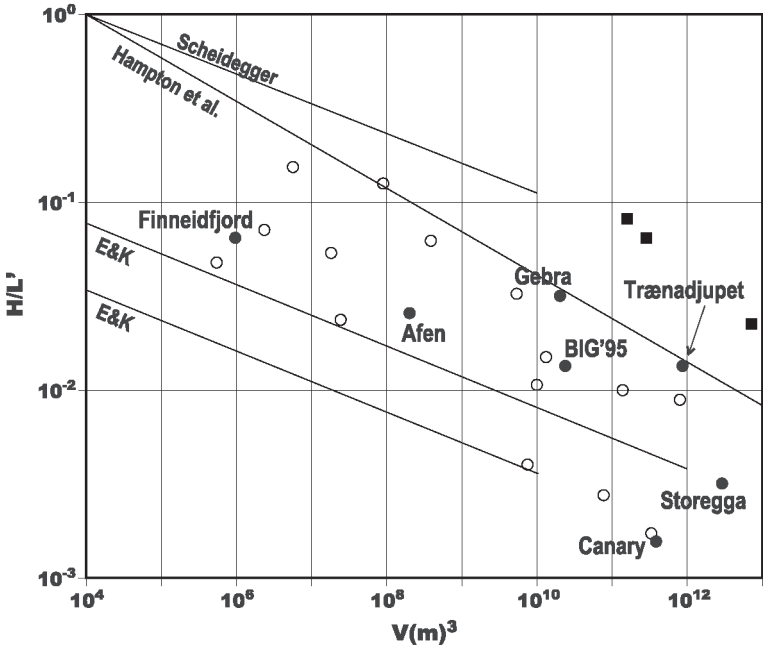

Fig. 14. Mobility of submarine mass movements as a function of the H/L' ratio (see main text) versus volume of failed mass applied to the slides studied within the COSTA project (black dots). Height, length (considered equivalent to total run-out distance for the purpose of this table) and volume data for the COSTA slides can be found in Table 5. Edgers and Karlsrud (1982) proposed lower bound values for submarine landslides (E&K upper line) and subaerial quick clay slides (E&K lower line). The average values for subaerial landslides proposed by Scheidegger (1973) and Hampton et al. (1996) proposed upper bound for submarine landslides are also included. Note that all the COSTA slides except Storegga and Canary slides fit within the limits defined by E&K upper line and Hampton et al. line for submarine landslides. This highlights the exceptional character of Storegga and Canary slides in terms of both large run-out compared to height drop, and large volume. Open circles and black squares correspond to non-volcanic and volcanic slides as originally plotted by Hampton et al. (1996).

Flow lines and pathways, seen either on side scan sonographs or in multibeam backscatter images, or in both, are a common feature of the studied slides, specially in the intermediate segments. Overall, it appears that mass movement in the headwall and upper segment is complex and poorly organized. Farther along the pathways, the flow tends to become more organized to finally become more uniform towards the distal parts, which are only reached by the most mobile materials. Streamlining is with little doubt related to shear planes within the sediment mass and, at least in some cases, with segregation of particles during shearing. Such behavior, which is best illustrated by the BIG'95 Slide (Fig. 15), would be independent of flow size. There are, however, slides where streamlining is observed along most of their length, for example, the Storegga and Finneidfjord slides (Table 7).

Rafted blocks varying in number from a few to hundreds have been identified in all COSTA slides except Traenadjupet, which is insufficiently surveyed, and Gebra, which is buried under >75 m of post-slide material. The size of rafted blocks is from hundreds to even thousands of meters across, although this could be biased by the resolution of the acoustic imaging systems, which could keep smaller blocks unresolved. An exception to this is the small Finneidfjord Slide whose biggest blocks are only 60×30 m (Fig. 4A and Table 7). Note, however, that this is a shallow slide that has been surveyed with the highest resolution swath mapping system (EM100) used in all the COSTA slides. The largest size of rafted blocks is unrelated to the overall dimensions of the slide. The maximum size of rafted blocks in the huge, 90,000 km^2 and <3000 km^3 Storegga Slide is 1800×200 m, whereas in the ~2000 km^2 and 26 km^3 BIG'95 Slide blocks as large as 12,500×3000 m have been measured (Tables 5 and 7). The term "outsized rafted blocks" seems appropriate for those cases. The maximum height of the rafted blocks above

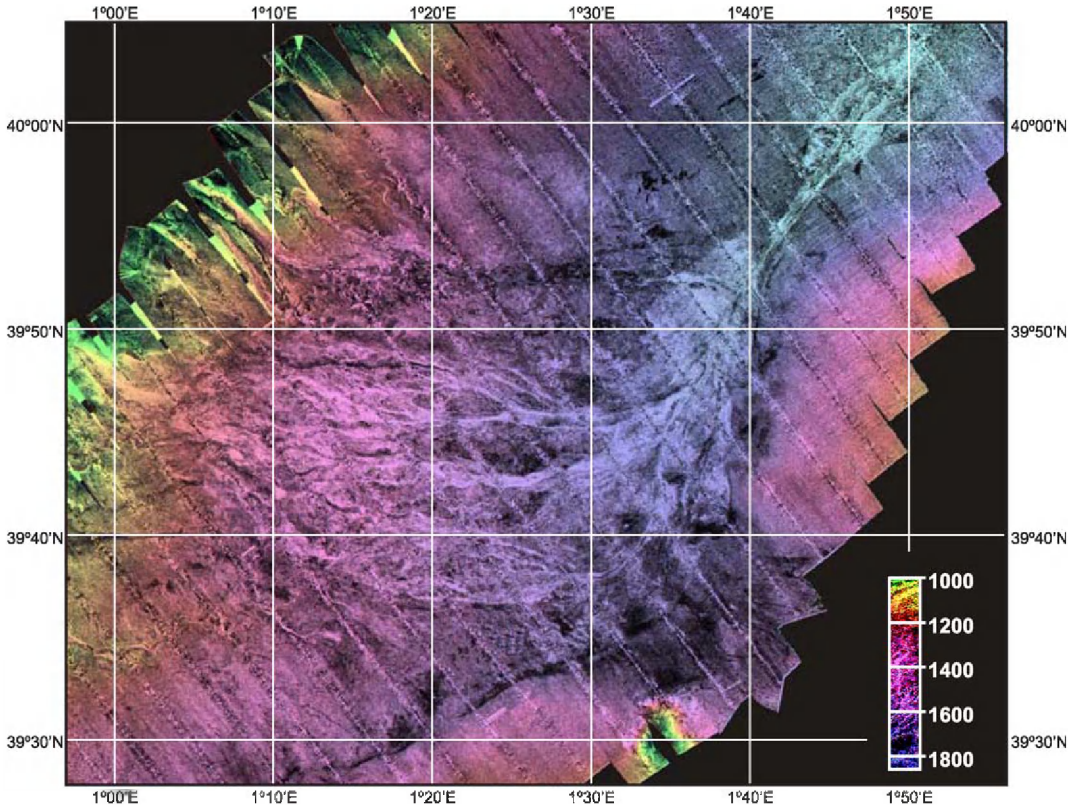

Fig. 15. Combined backscatter (darker: lower backscatter, lighter: higher backscatter) and water depth (see color bar) image of the BIG'95 Slide. Note low backscatter rafted blocks and high backscatter horse tail-like lineations corresponding to shallow elongated depressions containing loose sandy sediments. Original data from Simrad EM-12S multibeam bathymetry system collected onboard R/V *Hesperides*. (For colour please see web version of this article.)

the surrounding seafloor ranges from several tens of meters (70 m in Storegga Slide) to a few meters or even less (1 m at Finneidfjord is the smallest maximum height measured for the COSTA slides). Data in Table 7 seem to indicate that, in opposition to rafted block sizes, there is a direct relation between block height and dimensions of the overall slide. Notwithstanding, a word of caution is again required since the number of slides analyzed within the COSTA project is limited, and there could be exceptions to the hypothesized general rule, such it appears to be the Canary Slide.

As observed for flow lines, rafted blocks occur most often in the intermediate segments of submarine slides, as if it were a physical threshold preventing their evacuation farther downslope (Figs. 3 and 6). An association between rafted blocks and flow lines is thus unveiled, which can be used as a search criterion for one of these two features once the first one has been identified. It has to be noted, however, that, in some cases, such as once more the Canary Slide, blocks previously interpreted as rafted blocks have been later reinterpreted as in situ blocks that have not been swept away by the downslope moving mass of sediment (Masson et al., 1998). Imaging high and low backscatter zones within the sliding mass could provide further clues to interpret the sediment dynamics of specific events, although the meaning of high and low backscatter patterns may vary largely from one slide to another. As an example, blocks can lead both to relatively high and low backscatter patterns depending on the characteristic of the surrounding seafloor. In the BIG'95 Slide, rafted blocks show low backscatter while the elongated depressions between blocks display high backscatter (Fig. 15).

8. Triggering mechanisms

A triggering mechanism, or a combination of triggering mechanisms is required to destabilise sedimentary packages already prone to failure because of a set of preconditioning factors. Failure occurs when the downslope oriented shear stress (driving shear stress) exceeds the shear strength (resisting stress) of the material forming the slope, as expressed by the well known Mohr–Coulomb failure criterion:

$$\tau_f = c' + (\sigma - u)\tan \phi' \quad (2)$$

where τ_f is the shear strength (equivalent to the shear stress at failure), c' is the effective cohesion, ϕ' is the friction angle, σ is the total stress acting normal to the failure surface and u is the pore water pressure. The term $(\sigma - u)$ is the effective normal stress, σ'. Generically speaking, processes that reduce the strength include earthquakes, tidal changes and sedimentation as the most important, but also wave loading, weathering and presence of gas. Those that increase the stress are wave loading, earthquakes, tidal changes, diapirism, sedimentation and erosion (Hampton et al., 1996). The equilibrium of a slope will finally depend on the relation between resisting forces and driving forces. For most sediment, the effective cohesion is low or even negligible and the friction angle generally is about 20–45° depending on compositional variations. More significantly, expression (2) shows a linear relation between shear strength and effective stress, i.e., a reduction in the effective stress leads to an equivalent reduction of the shear strength.

Gravity, seismically induced stress and storm-wave induced stress are considered the most significant downslope driving stresses with respect to submarine landslides. Mechanically, a landslide occurs when the downslope driving stresses, nearly always involving gravity and other factors, exceed the resisting strength of the slope-forming material. While many studies of limiting equilibrium of submarine slopes have been conducted, it is beyond the scope of this paper entering into detailed descriptions on that subject. A good summary could be found in Hampton et al. (1996), which also includes relevant references. The same authors identify five submarine environments where slope failure is most common since they often match the necessary conditions for landsliding to occur, such as rapid accumulation of thick sedimentary deposits, sloping seafloor, and other types of high environmental stresses. The environments that could be designated as "submarine landslide territory" are: (1) fjords, (2) active river prodeltas, (3) submarine canyon-fan systems, (4) the open continental slope and (5) oceanic volcanic islands and ridges. The COSTA project includes representatives of all but one (the submarine canyon-fan systems) of these environments: Finneidfjord (fjords), CADEB (active river prodeltas), Storegga, Traenadjupet, BIG'95, Gebra and Afen (open continental slope), and Canary (oceanic volcanic islands).

A substantial number of factors that could explain large scale slope instabilities along continental margins can be found in the literature. They would include (1) high sedimentation rates leading to build-up of excess pore pressure (overpressurized layers) and underconsolidation (weak layers), (2) loading and crust flexing by a static weight such as a grounded ice sheet, (3) fast loading by a dynamic weight such as a landslide mass released from upslope, (4) destabilization of gas hydrates, (5) fluid seepage including seepage of shallow methane gas, (6) bubble-phase gas charging, (7) presence of diagenetic fronts, (8) oversteepening of the margin, (9) erosion at the base of the slope, (10) seismic loading due to earthquakes, (11) low tides, (12) storm-wave loading, (13) sea-level change, (14) volcanic growth and dyke injection, (15) faulting, (16) tectonic compression, (17) diapir and mound formation, (18) biologic processes and (19) human activities on or affecting the seafloor. Canals (1985) grouped the triggers into external (i.e., seismic loading or storm-wave loading) and internal (i.e., weak layers or diagenetic fronts). Locat and Lee (2002) report several case studies illustrating how most of the factors listed above favored or directly triggered submarine landslides. When interpreting past submarine landslides, combinations of some of the triggers listed above are often invoked. It is worth mentioning that, though seismic loading and oversteepening have been considered as triggers since the early work of Morgenstern (1967), it has been also demonstrated that repeated seismic shaking could lead to "seismic strengthening" of the sediments if drainage is allowed between successive events (Boulanger et al., 1998; Boulanger, 2000).

Because of their varied settings, the submarine landslides studied within the COSTA project illustrate how different pre-conditioning factors and triggers could interact to finally lead to sediment failure at

Table 8
Pre-conditioning factors and likely/proven final triggers for the submarine landslides studied within the COSTA project

Landslide	Margin type	Seismic activity	Volcanism		Presence of gas and diagenetic fronts
			Recent activity, dyking	Volcanic structures nearby	
Storegga	Passive	Intermediate	Lacking	Ocean basalt/continental margin boundary under the intermediate slide segment	Gas hydrates confined to a small zone along the northern flank of the slide and the slide area itself. BSR present
Canary	Ocean island flank	Low, related to volcanism	Last, 37 ky old volcanic edifice still growing	Flank of volcanic island less than 1.12 My old	Not known
Traenadjupet	Passive	Intermediate	Lacking	Lacking	BSR detected
CADEB	Active	High ($M \leq 6.6$)	Lacking	Lacking	Presence of shallow gas
BIG'95	Passive	Low to intermediate ($M \leq 4.9$)	Fluid escape likely detected from the feet of seamounts in the Valencia Trough	Volcanic dome beneath the scar area, Columbretes Islets volcanic archipelago upslope the scar, and several seamounts nearby	Likely presence of shallow gas in former prodeltaic sediments on the shelf edge and upper slope
Gebra	Passive (back-arc basin)	Intermediate to high ($M \leq 6.7$)	Subrecent to modern volcanic activity both submarine and subaerial (Deception Island mostly), associated with seismicity	Young volcanic lineaments along basin axis. Incipient seafloor spreading	Gas hydrates known in nearby areas (South Shetland Islands margin). Diagenetic fronts also known in the region
Afen	Passive	Low ($M \leq 2.9$)	Lacking	Lacking	Distinct BSR close to the area representing a diagenetic front associated with opal-A/opal-C transition
Finneidfjord	Passive	Intermediate ($M \leq 5.8$)	Lacking	Lacking	Presence of biogenic gas

Sedimentary conditions			Other factors	Final triggering [a] mechanisms
Sedimentation rates (cm ky^{-1})	Main sources of sediment	Distance to main source[b] (km)		
150/200 during LGM and deglaciation, and 2/10 during interglacial and interstadials (northern slide escarpment area)	Active ice streams during glacial periods. Ocean current influence mostly during interglacials (erosive on the upper margin, winnowing in connection with sea level changes)	0,1/30 from LGM[c] grounding line	Rapid loading of fine-grained hemipelagic deposits and oozes by fast glacial deposition during glaciation peaks	Earthquake activity associated with postglacial isostatic rebound
Not available	Volcanic ejecta and pelagic settling	30 to El Hierro Island shore	–	Loading of the sedimented slope by a debris avalanche
Up to 100. Up to 80 m of LGM[c] glacigenic sediment deposited over some few thousand years, prior to sediment failure	Active ice streams during glacial periods. Hemipelagic settling and bottom currents during interstadials and interglacials	Very short. Sediments delivered to sliding area during LGM[c]	Deposition of contourite drifts with high sedimentation rate (~100 cm ky^{-1}) in which the basal slip plane developed on the upper slope	Earthquake activity associated with postglacial isostatic rebound or decomposition of gas hydrates, or a combination of the two
1000/10000, with 636 averaged maximum over the last 5.5 ky. 400/1600 for the last 100 years	Po River and the eastern Apennine rivers load of siliciclastic mud and coarse sediment	~350 to Po River mouth, few tens to eastern Apennine rivers	Possible presence of overpressurized layers	Loading by earthquakes and tsunamis, with presumed increase of excess pore pressure in basal weak layer
8.5/12.4 in the mid–lower slope, and <3 at the base of the slope during the Holocene. Might have been much larger during sea level lowstands, when the Ebro River opened directly to the upper slope	Ebro River load of siliciclastic sands, silts and clays. Presumed shelf-edge spillover during lowstands.	~80 (present and probably early Holocene)	Past depocenters off the Ebro River mouth located on the outer shelf and upper slope above the main scar. Sea level rise after LGM[c]	Earthquake activity likely, but greatly preconditioned by a complex combination of factors
High variability depending on time interval and location. LGM[c] rates estimated at ≤ 3400. Post-slide rates around 240	Active ice streams during glacial periods. Hemipelagic settling, turbidity current and, perhaps, bottom currents during warmer intervals	15 from LGM[c] grounding line	Semi-graben edge below main headwall (tectonic control)	Earthquake activity associated with tectonic setting, possibly enhanced by postglacial isostatic rebound
11, averaged over the Quaternary	Grounded ice edge during glacial periods, and current-transported material during interglacials and interstadials	~40 km	Slide headwall located within a contourite drift deposit	Earthquake activity
150/250	River sources eroding into glacimarine sediments	2	Quick clay layers. Anthropogenic actions	Excess pore pressure from a combination of climatic and anthropogenic factors

various time and size scales. In Table 8, we summarize preconditioning factors and final triggers of the instabilities investigated within our project. While five of them, including the largest and the smallest of the slides studied (Storegga, Traenadjupet, BIG'95, Afen and Finneidfjord slides), occurred on passive margins, there are also representatives of ocean island flanks (Canary Slide), back arc basins (Gebra Slide) and active margins (CADEB). Curiously, CADEB, the instability from the active West Adriatic margin is the only one dominated by plastic deformation with no disintegration nor flow of the sediment mass.

The Storegga Slide, the largest of the studied instabilities, is according to the latest interpretations based on a wealth of data partially from the oil industry (Table 2), the last of a series of slides occurring in the same area during the last 500 ka. Such a succession of relatively similar events follows a repeated cycle of climatically controlled sedimentary processes leading every time to about the same result. The cycle starts with the deposition of fine-grained marine clays on the slope and outer shelf during interglacials and transitions. These clays accumulate under the influence of energetic currents. Contourite drifts reaching more than 100 m of thickness developed during these periods of reduced or non-existing grounded ice on the continental shelf. Contourite sediment may partly fill in old slide scars and other sea floor depressions. Afterwards, as glaciation progresses, the sedimentary regime changes dramatically. Subglacial bulldozing-like transport is greatly enhanced, especially under ice streams whose imprint is still clearly visible on the modern mid-Norwegian continental shelf as glacial troughs and megascale streamlined structures (Fig. 7 and Canals et al., 2000a, 2003). During glacial maxima, the grounding line is pushed forward to the edge of the continental shelf and fast flowing ice streams actively carry deformable subglacial till which is quickly deposited on the outer margin and subsequently transported downslope as glacial debris flows to form glacial fan systems as the North Sea Fan and Skjoldryggen glacial depocenter (Dowdeswell et al., 1996; Vorren et al., 1998; Solheim et al., 1998; Dimakis et al., 2000; Bryn et al., 2003b; Dahlgren and Vorren, 2003). A main depocenter of glacial clays has been proposed for the area now occupied by the upper Storegga Slide scar, close to the North Sea Fan (Bryn et al., 2003b, their Fig. 2). Under such a situation, excess pore pressure tends to rise. In turn, effective strength of sediments barely increases with sediment burial, being thus lower than expected. Clayey units deposited during interglacials and transitions have then a great potential to behave as slip planes or weak layers. As Bryn et al. (2003b) point out, in these circumstances, permeability is a key factor in trapping excess pore pressure and also in transferring excess pore pressure laterally to areas with less overburden, reducing the strength where slopes are in addition steeper because of the lack of smoothening by fast sediment accumulation. It must be noted that the Storegga Slide is located in the reentrant between the North Sea Fan and Skjoldryggen outer margin glacial depocenters, in a situation which is similar to that observed for the Gebra Slide and along the Pacific margin of the Northern Antarctic Peninsula (Canals et al., 2002; Imbo et al., 2003; Amblas et al., submitted for publication). Reentrants in between shelf edge glacial lobes and outer margin depocenters would then behave as instability corridors because of lateral transfer of excess pore pressure generated beneath thick nearby sediment piles but also because of the weight of grounded ice. Thicker ice occurs in the main ice streams, thus reinforcing the excess pore pressure effect, while ice is thinner in smaller ice streams and intervening areas where slide headwalls would tend to locate.

A final external trigger is, however, required. For the Storegga Slide and its cousin Gebra Slide, this external trigger was likely earthquake activity, a hypothesis that seems to be confirmed by modelling and reports on seismic activity (Bryn et al., 2003b; Imbo et al., 2003). Note that failure of the Storegga and Gebra Slides did not necessarily occur synchronously with glaciation maxima. In fact, enhanced seismicity during initial deglaciation because of glacioisostatic rebound may well be the required final trigger, as strongly suggested by the ages of both Storegga and Gebra Slides (see Section 10 below). Earthquake swarms may progressively prepare the

Notes to Table 8:

[a] For landslides whose occurrence has not been observed, this column refers to the most likely final triggers.

[b] Refers to distance from headwall upper edge.

[c] Last Glacial Maximum.

sediment pile for sliding through the formation of creep structures, open cracks and initial block detachment until final and major failure occurs. The Gebra Slide in particular lies in a highly seismically active area where earthquakes with a magnitude of up to 6.7 have been measured recently (Pelayo and Wiens, 1989; Ibanez et al., 1997; Jin et al., 1998). In addition, young volcanic edifices and lineaments with associated hydrothermal activity occur nearby (Suess et al., 1987; Schlosser et al., 1988; Klinkhammer et al., 1995; Gracia et al., 1996a,b; Bohrmann et al., 1999). The possibility that layers of volcanic ash behaved as weak layers and developed into slip planes in the Northern Antarctic Peninsula region and for the Gebra Slide in particular has been suggested by Imbo et al. (2003). These layers would add to marine clays and oozes as potential mechanical discontinuities favoring landsliding.

The Traenadjupet Slide lies 300 km north of the Storegga Slide and the general setting and boundary conditions are very similar. The shallowest part of the Traenadjupet Slide headwall is just in front of the mouth of a former ice stream whose path is observed on the modern continental shelf (Fig. 7). This location determined the formation of a main depocenter of glacial clays on the area presently occupied by the upper slide scar and likely resulted in the generation of excess pore pressure during glacial times. Glacial and early deglacial high sedimentation rates on the slope promoted instability but, most important, prevented fluid escape from the relatively thin layers (<10 m) of interglacial and interstadial sediments due to the low permeability of the glacigenic clays (Table 8). Layers made of interglacial and interstadial sediments would then behave as weak layers and slip planes. The Traenadjupet Slide could differ from the Storegga and Gebra slides in that the initial failure might be located near the present headwall, although there is also the possibility for it to have occurred downslope from a large escarpment now lying at 1800 m of water depth (Laberg and Vorren, 2000). A second major difference is that Traenadjupet Slide occurred several thousand years after the withdrawal of the ice sheet from mid-Norway, whereas Storegga and Gebra took place at earlier times (see Section 10 below).

The Afen Slide occurred in a low seismicity region and, as with the BIG'95 Slide, similar size and shape slides are buried less than 100 ms below it, thus indicating a recurrence of failures. The Afen Slide headwall and the headwalls of older slides buried beneath are located within a contourite drift deposit comprising very well sorted, low cohesion silty sand. Sub-horizontal slip planes also show evidence of contourite activity and represent similar previous deposits. Sandy contourites are less cohesive than clayey sediments and are also susceptible to liquefaction under dynamic loading, thus having the potential for raising the pore pressure of the surrounding cohesive sediments (Wilson et al., 2003a,b). Contourite units are, therefore, of particular relevance since they have acted as slip planes not only in Afen Slide but also along the North Atlantic margin of Europe, as illustrated by Traenadjupet and probably some of the Storegga phases. Sedimentation rates are, however, very low in the Faeroe-Shetland Channel, where the Afen Slide is, with less than 200 m of Quaternary deposits (Long et al., 2003b). This implies the lowest sedimentation rates amongst all the instability areas studied within the COSTA project, jointly with those from the BIG'95 Slide (Table 8).

Vertical faults occasionally reaching the seafloor, with offsets of several meters, have been identified on high resolution seismic reflection profiles from the Afen Slide area. There is a set of faults with traces that mimic the edges of the slide scar 100 ms below the seafloor. The COSTA project has shown that a distinct BSR has been identified in the Afen Slide area but geophysical evidences and cuttings from an exploration well drilled through it indicate that the reflector represents a diagenetic front associated with opal-A to opal-C transformation (Table 8). In addition to the above-described preconditioning factors, an external localized trigger is required to explain the Afen Slide. Indirect evidence from several authors show that seismicity in the Afen area might have been enhanced because of post-glacial isostatic rebound, as it has likely been the case for the Storegga and Traenadjupet Slides (Muir-Wood, 2000; Stewart et al., 2000). Since the Victory Transfer Zone passes directly beneath the Afen Slide, renewed activity along such a transfer zone could have triggered slope failure (Rumph et al., 1993; Wilson et al., 2003a,b). Nevertheless, historical data and five years of active seismic monitoring with detection capabilities of magnitude 2 have shown that seismicity is negligible in the entire Faeroe-Shetland Channel (Musson, 1998; Ford et al., 2002). Therefore,

it can be concluded that the area of the Afen Slide is presently stable in the short term (Hobbs et al., 1997).

The Canary Slide is one of the world's best studied debris flows affecting the flanks of an oceanic island. The overall morphology of the failure area suggests removal of a slab-like sediment body that started to disintegrate almost simultaneously with the onset of downslope transport. According to Masson et al. (1998), failure was triggered by sudden loading of the lower island slope by a debris avalanche deposit, known as El Golfo Debris Avalanche that removed part of the island and upper slope. The upper part of the 4700 m high scar left by the debris avalanche is perfectly visible nowadays and forms the 1500 m high El Golfo cliff inshore, one of the most spectacular slide headwalls in the world. The two events, debris avalanche and debris flow, must have been about synchronous because the avalanche fills and disguises the seafloor expression of the Canary Slide headwall, which implies the avalanche deposits were still mobile enough when the debris flow was triggered. Roberts and Cramp (1996) considered both the effects of ground accelerations related to earthquakes and of loading by the debris avalanche, and concluded that the loading mechanism was more likely to trigger a disintegrative failure leading to a debris flow. The avalanche itself would likely have been triggered during an eruptive phase, or shield phase, when the development of the volcanic rift zones on the three-arm shaped El Hierro Island was at a maximum. Tensional stresses accumulate in rift zones during shield building and, when acting on oversteepened piles of recently formed volcanic material, can suddenly lead to large landslides (Urgeles et al., 1997). Sea level changes could also have contributed to triggering instabilities on El Hierro Island (Weaver and Kuijpers, 1983; Masson et al., 1993).

The BIG'95 Slide is the best representative COSTA project landslide occurring in river-fed, siliciclastic, progradational continental slopes. It most likely occurred because of a combination of external and internal factors and a final trigger (Table 8). Such a combination would include enhanced local sedimentation on the upper and mid-slope in association with depocenters from the paleo-Ebro River during lowstands, differential compaction of sediments as related to a volcanic dome beneath the main scar, oversteepening of the margin due to dome intrusion and lowstand presumed high sedimentation, low-to-moderate seismic activity and postglacial sea level rise (Farran and Maldonado, 1990; Grünthal et al., 1999). Gas hydrates are not known in the Ebro margin, but gassy sediments exist in the modern Ebro prodelta and could have existed in former outer shelf and upper slope depocenters. That the BIG'95 area is prone to failure is demonstrated by the vertical stacking of several acoustically transparent, lens-shaped bodies separated by stratified intervals observed in mid penetration high resolution seismic reflection profiles (Lastras et al., 2004c). The final trigger for the main event might have been an earthquake because one earthquake of magnitude 4 to 5 occurs statistically every 5 years, according to the USGS/NEC PDE instrumental records for the last 30 years. Larger earthquakes in the mid and northern Mediterranean Iberian margin are also known from historical pre-instrumental reports and eyewitnesses. The largest earthquake measured in the instrumental (M_{wa}=4.6) epoch took place offshore in May 15, 1995, several miles north of BIG'95 and had the potential to induce significant ground motions. However, except for perhaps fluid escape features, no other newly formed structures or remobilisation events were observed at that time, thus evidencing that the slope is now stable at least for seismic events of that magnitude.

As previously stated, the CADEB mostly represents a pre-failure state where sediment is deformed but not failed yet (Fig. 2A). CADEB is situated in the foredeep/foreland basin of the Apennines and is affected by frequent seismic activity and associated tsunamis (Ciabatti et al., 1987; Royden et al., 1987). The maximum historical shock took place on the July 30th, 1627 in the Gargano Promontory, with an intensity-derived magnitude of 6.1. Recurrence times of 84 and 228 years have been found for both tsunamis of any size and for large events produced by earthquakes of magnitude >6.6, respectively, after simulations (Tinti et al., 1995 and references therein). The active tectonics of the area is also expressed by the Quaternary uplift of older rocks forming structural highs. Accumulation rates for the late Holocene are the highest (1000–10,000 cm ka^{-1} with 636 cm ka^{-1} as averaged maximum) amongst all the study areas and, as a result, a 35-m-thick mud wedge formed over the last 5.5 ka during the present sea level highstand (Correggiari et al., 2001 and Table 8). This 5.5 ka to

present mud wedge, on top of the seaward-dipping downlap surface (maximum flooding surface) acting as weak layer and slip plane, in between Ortona and Gargano, constitutes, strictly speaking, the CADEB. However, sediment accumulation rates have not been linear and noticeable variations have occurred during the late Holocene both in time and space. The main sources of sediment are the Po River and the eastern Apennine rivers with modern discharges of 15×10^6 and 32×10^6 t yr^{-1}, respectively (Frignani and Langone, 1991; Cattaneo et al., 2003b).

The geostrophic circulation in the western Adriatic Sea favors mud accumulation south of riverine sources parallel to the coast of the Italian Peninsula thus resulting in a shore-parallel depocenter which overall displays crenulations over as much as 40% of its extent. Shearing planes characterize the shallower head region, whereas compressional pressure ridges and mud diapirs become dominant in the toe region, expressing the downward push of the entire muddy wedge. However, nowhere has deformation evolved into disintegration and flow, which could be at least partially attributed to the plasticity of the sediment that can thus accommodate deformation without evolving into failure. The extremely low slope angles (less than a half degree, Table 6) and the presumed escape of fluids, which relieves excess pore pressure generated by the very high sedimentation rates could have played an additional role in preventing disintegration. In addition to gas at very shallow levels, which hardly could have played a role in the deformation processes, gas venting and gas-charged sediments have been reported from other shallow stratigraphic units beneath the late Holocene mud wedge (Conti et al., 2002). A lowering in sedimentation rates for the last century measured from ^{210}Pb activity offshore Ortona opens the question as to whether the CADEB deformations are relict, slowed down or still active. Comprehensive descriptions and discussions of CADEB and nearby late Holocene muddy prodeltas in the western Adriatic Sea can be found in Correggiari et al. (2001) and Cattaneo et al. (2003a,b).

The small Finneidfjord Slide is the best known of the COSTA slides in terms of preconditioning factors and triggering mechanisms since it occurred in 1996 as previously stated, over an area previously affected by an older slide. That Finneidfjord is prone to sliding is proven by the eight slides known along its shores, which occurred during the last 2000 years. The Finneidfjord area displays intermediate seismic activity with a 5.8 estimated magnitude maximum historical shock dated for the 31st of August 1819. Glacio-isostatic rebound, which has been related to an enhancement of the seismic activity in Northern Europe, is estimated at 3.5 cm yr^{-1}. Biogenic gas is known to occur within the sediment, where a stratigraphic unit including a weak layer often caps it. Sedimentation rates are rather high, from 150 to 250 cm ka^{-1}. Initial sliding is thought to start at half tide by hydrostatic overpressure along a weak layer. The slide punctured quick clay pockets in the shore ramp and developed as a quick clay slide (Table 3). Changes in groundwater flow were registered some time before the slide event. The spring before the slide was particularly wet and led to high hydrostatic pressure (excess pore pressure) in ground previous to the event. Anthropogenic factors include a nearby main road with heavy traffic causing tremors over the onshore part of the slided area, construction of a tunnel with many detonations close to the slide area, and rock debris dumped on shore next to the slide scar which could contribute to changing groundwater flow. The initial slide started below sea level at the steepest part of the fjord slope, about 50–70 m from a highway running parallel to the shore. Afterwards, the slide developed retrogressively landwards and in less than 5 min took away successively the beach below the road, 250 m of the road, one car and a nearby house that sank into the sea. Four people died. Several minor mass movements occurred afterwards but 1 h later everything was quiet again (Janbu, 1996; Longva et al., 2003). The pre-slide beach slope already had a low safety margin, possibly less than 10%, which was easily exceeded because of the combination of natural, and anthropogenic causative factors.

From the detailed descriptions above and from the summary in Table 8, a picture of the preconditioning factors and final triggers for the COSTA instabilities appears with clarity. To what extent these findings can be extrapolated to other failures that will eventually be investigated with the same degree of detail is something that will be unveiled in the near future. Seismic activity is an important factor, even in areas such as passive margins where seismic quietness can be expected. Activation of seismicity because of post-glacial isostatic rebound is a major, widespread

process in high latitude margins. However, there are slides in low seismicity areas too, such as Canary, Afen and to a lesser extent BIG'95. Volcanic activity and volcanic structures could also be relevant, since they may lead to oversteepening during growing phases, induce seismicity, generate ash-rich weak layers, induce excess pore pressures, create mechanical discontinuities and cause slope changes either because of volcano growth or crustal overloading.

Gas, and especially gas hydrates and their dissociation, have often been associated with slope instability (Hampton et al., 1996). It must be possible, however, that silica and other diagenetic fronts, still poorly known, could also play a significant role in slope destabilisation. BSRs could both be caused by gas hydrate and diagenetic front boundaries. An important quality of gas is that its absence nowadays does not imply at all that amounts of it were not present when destabilisation occurred, as hypothesized for the source area of the BIG'95 Slide. Shallow gas, essentially of biogenic origin, is common in shallow unstable areas fed by rivers such as CADEB and Finneidfjord. The relationship between pockmarks and other gas escape features and sliding is controversial. While fluid venting would relax excess pore pressure and thus diminish the risk of failure, it could also be an indication that overpressures exist and this would favor failure. It should be also expected that after unloading of part of a slope because of a large landslide, fluid escape should reactivate since the overburden pressure has been dramatically reduced. A similar phenomenon has been hypothesized for the reactivation of volcanic emissions following giant landslides in ocean islands. In fact, active pockmarks are thought to be very rare.

Sedimentation rates and the nature of the sediments are of crucial importance since they determine not only the rate of generation of excess pore pressure, but also their eventual relaxation as a function of the permeability of the sedimentary strata. The "sedimentation factor" plays, in addition, a role over the development of mechanical discontinuities and weak layers. To that respect, climatically controlled strong bottom currents, forming contourite drifts and layers, hold a great potential to behave as slip planes and have been of enormous relevance in some ocean margins such as the eastern North Atlantic. It is important to consider the sources of sediment and the distance of the failed zone from the point or line sources since both parameters control the development of properties that directly relate to instability. In the same way sedimentation is climatically driven, instability also responds to climatic cycles as demonstrated by the repeated occurrence of sliding events at about the same place once a specific set of sedimentary conditions is achieved. This is particularly true for instabilities in glaciated margins, where slide occurrence is controlled by the location of the grounding line and ice streams carrying basal lodgment till to the upper slope. The more we could learn about how climate influences slope failure, the better we will be able to perform sound slide forecasting.

Finally, after the cumulative effect of preconditioning factors, a final, most often external, trigger is required for failure to occur. Earthquake activity is by far the most common external trigger invoked to account for the COSTA slides.

9. Ages of slide events

The available information about the ages of the submarine landslides studied within the COSTA project is summarized in Table 8, where information about dating techniques, number of datings, sedimentary units dated and, in some cases, recurrence intervals is provided too. It is best reading Table 8 jointly with Tables 2 and 3 where information on the number and type of sediment cores, and on the retrogressive and/or multi-staged character for each of the landslides can be found. In any case, dates in Table 8 refer to main failure events unless otherwise indicated.

Due to its complexity and significance, dating of the Storegga Slide has been a major task within the COSTA project. Over 100 cores of various types have been collected to date within both major and minor sliding events (Table 2). Dating proceeded in various steps including lithological analyses and detailed stratigraphy of selected sediment cores, handpicking of the foraminifer *N. pachyderma* at key intervals and age analyses by ^{14}C AMS complemented by tephrochronology, magnetic susceptibility and gamma density. According to the latest results, the main Holocene Storegga Slide occurred approximately at 7300 ^{14}C yr BP or 8200 calendar years BP, and is the last of a series of giant slides which succeeded each other at semi-regular intervals during the last 500 ka

in the same area (Bryn et al., 2003b; Haflidason et al., 2004). In the Ormen Lange gas field area, dating results of the many identified minor debris lobes gave the same age as the large Holocene Storegga Slide. Notwithstanding, in some cores from the distal slide area, the base of post-slide sediments appears to be slightly younger, 6600–6900 ^{14}C yr BP, which is attributed to low sedimentation rates and microfossil concentrations, which could induce dating biases since each sample averages a much longer time interval than samples from the high sedimentation areas on the upper and mid slide. The recentmost, minor sediment failure, dated at ca. 5000±500 yr BP occured along the northern Storegga escarpment (Haflidason et al., 2003b).

Traenadjupet is the closest large slide to the Storegga Slide. However, its study is much less advanced and the information available is still limited. As for Storegga, ^{14}C AMS dating has been performed on *N. pachyderma* specimens mostly from post-slide sediments recovered in 18 gravity cores, 10 of which are from the slided area and 8 from nearby areas. ^{14}C AMS ages indicate that post-slide sedimentation occurred within the Traenadjupet area after about 4000 ^{14}C yr BP, which suggests that the slide event took place shortly prior to that age. Dating results can be found in Laberg et al. (2002).

The Afen Slide is representative of small slides from the eastern North Atlantic, within previously glaciated margins. Only five samples from one core have been ^{14}C AMS dated, which allowing placement of the final phases of movement after 5800±60 yr BP (Holmes et al., 1997) (see Section 5 above and Fig. 6). The recurrence interval is on the order of 250 ka, based on seismostratigraphic criteria including identification of buried slides beneath Afen Slide (Holmes et al., 1997).

The Gebra Slide is the fourth representative of slides on glaciated margins, although it is located in the southern hemisphere west of the northern tip of the Antarctic Peninsula (Fig. 1). The age estimate of the Gebra Slide is based on seismostratigraphic criteria, inferences from sedimentation rates and deglaciation history of the North Antarctic Peninsula, indicating that it occurred some time during the transition from the Last Glacial Maximum to the current interglacial, 13,500–6500 yr BP (Harden et al., 1992; Pudsey et al., 1994; Banfield and Anderson, 1995; Prieto et al., 1999; Canals et al., 2002). Coring and dating of sediments just above the slide deposit are required to better constrain the age of the Gebra Slide.

The Canary Slide resulted not only in a debris flow deposit but also in a turbidite, the "b" turbidite accumulated on the Madeira Abyssal Plain. This allowed using turbidite stratigraphy and biostratigraphy tied to the oxygen isotope timescale calibrated with ^{14}C AMS dates. It was found an age estimate of 17–13 ka BP for this event (Weaver et al., 1994; Masson, 1996). The "b" turbidite is the youngest volcaniclastic turbidite in the Madeira Abyssal Plain and early studies recognized that it had been deposited at the transition between isotope stages 1 and 2, and had a probable age of 15±2 ka (Weaver et al., 1992). Provenance of the "b" turbidite from the flanks of the westernmost Canary Islands is supported by geochemical evidence (Pearce and Jarvis, 1995). Interfingerings between sands, silts and muds of the "b" turbidite and debris flow layers at the edge of the abyssal plain unequivocally show that the "b" turbidite and the Canary Slide were deposited simultaneously and that they were generated by a single slope failure event (Weaver et al., 1994; Masson et al., 1997). Dates from turbidite sequences are compatible with K/Ar dates from pre- and post-landslide volcanic events on El Hierro Island (Guillou et al., 1995). A recurrence interval of <75,000 years has been estimated for the western Canary Islands of Tenerife, La Palma and El Hierro (Canals et al., 2000b; Masson et al., 2002).

The BIG'95 Slide is the most recent major instability event affecting the Ebro margin and the floor of the Valencia Trough, as demonstrated by its seismostratigraphic position on the very top of the mostly stratified Quaternary sedimentary sequence (Lastras et al., 2002, 2004c; Urgeles et al., 2003). ^{14}C AMS analyses on four *G. ruber* and one *G. bulloides* samples from two piston cores gave very consistent results, allowing us to date the event at between 10,490 and 10,190 years BP (11,647–11,129 cal years BP). Datings were performed on a thin hemipelagic layer, barely visible on the highest resolution seismic reflection records, draping the slide deposit. One buried debris flow deposit below BIG'95 and just on top of the regional G reflector separating Pliocene and Quaternary sequences allows estimating a recurrence interval of about 800 ka, although a higher frequency cannot be

ruled out. Further seismic imaging and coring/drilling, also in the distal Valencia Fan turbiditic units originated from the Ebro margin would be required to better establish the frequency of mass wasting events in that area. Early studies suggested that repeated instabilities could occur in various places and at different times along the Ebro margin (Maldonado et al., 1985; Alonso and Maldonado, 1990; Alonso et al., 1990; Field and Gardner, 1990; Canals et al., 2000c).

The age of the materials involved in the CADEB deformation belt is well time constrained, between the 5.5 ka BP maximum flooding surface acting as slip plane and the modern seafloor. Numerous dates from ^{14}C AMS, short-lived radionuclides, tephrochronology, biostratigraphy and seismostratigraphy methods are available from the various units in the CADEB area (Asioli et al., 1999; Langone et al., 1996; Trincardi et al., 1996; Calanchi et al., 1996, 1998; Oldfield et al., 2003). Geochronological data indicate that a basal highstand systems tract, a seismically transparent unit up to 1.5 m thick above the maximum flooding surface, represents an interval of condensed deposition between 5.5 and 3.7 ka BP (Correggiari et al., 2001; Oldfield et al., 2003; Cattaneo et al., 2003b). Since deformation could not start before a minimum thickness of prodeltaic muds was reached (i.e., about 700 years would be required to reach 10 m of thickness at a sedimentation rate of 1.5 cm yr^{-1} as given by Cattaneo et al., 2003a), it is likely that CADEB deformation initiated sometime after 3.7 ka BP, possibly around 3 ka BP. Very high resolution seismic reflection profiles show that an uppermost weakly reflective unit was likely emplaced after the formation of the creep-like features in the prodelta wedge. The base of this unit, which postdates the main phase of deformation, has been dated at year 1630 (Correggiari et al., 2001). Assuming that CADEB features are now relict, a total time span of about 2600 years would be encompassed for their formation. If considering they are still active, the total time span would be about 3000 years.

Dating of the Finneidfjord Slide does not pose any difficulty since it was observed to happen the 20th of June 1996 in about 1 h of time (see description of events in Section 9 above). The recurrence interval for the whole 7 km^2 fjord is 250 years based on identification of older slide deposits on seismic reflection profiles. Deposits from ca. 9000 years old slide have been identified directly below the 1996 deposit.

The set of submarine landslides investigated within the COSTA project corresponds to a rather narrow age range from an estimated maximum of 17,000 for the Canary Slide to a minimum of 4000 for the Traenadjupet Slide, CADEB and Finneidfjord Slide excluded. The major sliding phases along the eastern North Atlantic margins are limited to an even narrower time window of less than 4000 years, from 8200 to 4000

Table 9
Age dating results and recurrence intervals for the submarine landslides studied within the COSTA project

Landslide	Main dating technique	Number of datings	Age of main event (cal yr BP or date)	Sedimentary units dated	Recurrence interval (years)
Storegga	^{14}C AMS	~80	8200 latest failure ca. 5000	Pre-, slide and post-slide	Not known. Large events likely follow climatic cyclicity
Canary	Oxygen isotopes Turbidite stratigr. ^{14}C AMS	Several tens	17,000/13,000	Pre-, slide and post-slide	<75,000 (in Western Canaries)
Traenadjupet	^{14}C AMS	22	~4000	Mostly post-slide. Four from slide sediments	Insufficient data
CADEB	^{14}C AMS Tephrochronology	~130	~3000/1630 AD (total ≈ 2600 y)	Pre-, syn- and post-deforming sediments	Not applicable
BIG'95	^{14}C AMS	5	11,647–11,129	Post-slide	≤800,000
Gebra	Seismostratigraphy	–	13,500/6500	Post-slide	Not known
Afen	^{14}C AMS	5	5800	Post- and slide	250,000
Finneidfjord	Observed to happen	Not required	June 20th, 1996	Observed to happen	250 (in fjord)

The calibration program used for ^{14}C AMS is Calib. 4 (Stuiver et al., 1998). Data from various sources (see main text).

years BP. The Gebra Slide, in the southern hemisphere, might be a few thousand years older, but it could also fit within the 8200/4000 years BP time window (Table 9). This reinforces the view that larger scale failures in glaciated margins tend to occur after glaciation peaks, i.e. during initial and advanced deglaciation phases and shortly after modern oceanographic conditions have been established. It has been hypothesized that the change in ice loading rather than high sedimentation rates is the dominant mechanism for large-scale instability events on glacial margins (Mulder and Moran, 1995; see Section 9 above). Modern and submodern instabilities and deformations have impacted or, at least, have the potential to impact infrastructures, as represented by Finneidfjord Slide and CADEB. The tsunamigenic capacity of some of the slides studied within the COSTA project is either proved (Storegga, Canary) or highly probable (Traenadjupet, BIG'95). Assessment of tsunamigenic risk requires knowing the recurrence intervals of failures, which in general has proven difficult to achieve either because data are insufficient or not precise enough, or simply because the investigated instabilities have a unique character. Calculation of recurrence intervals is more meaningful when applied to an area larger than the one directly affected by each individual event, either a long margin segment, a set of neighbor ocean island flanks or a fjord in its entirety (e.g., Goldfinger and Nelson, 1999).

10. Concluding remarks

The COSTA project has provided a unique opportunity to investigate a variety of geologically recent submarine instabilities along the northern and southern continental margins of Europe. The effort performed and the results achieved make clear that a combination of regional scale studies with thorough analyses of individual instabilities from various points of view is essential to progress towards a comprehensive understanding of mass wasting events at a global scale. As important as these phenomena are, submarine landslides will gain further priority in the joint industry-academia research agenda with the increase in the need for safe exploration and exploitation of deep-sea energy resources to meet the demands of our society. In addition, a new generation of detailed regional and local geohazard maps of continental margins, including submarine instabilities, is anticipated for the near future. Not only the offshore industry but also tsunami and slide-threatened coastal communities and facilities will enormously benefit from the results of research projects like COSTA.

In this overview paper we have described and assessed eight submarine instabilities, of which all but one are within the Economic Exclusive Zone of European nations. We have used both original results generated within the COSTA project during the last three years and previously published data included in papers authored to a large extent by scientists belonging to or closely related to the formal COSTA team. This paper focuses on the seafloor and shallow sub-seafloor expression of sedimentary instabilities using some of the best imaging techniques available, from full coverage swath mapping and deep-towed side scan sonar to very high resolution seismics, 3D seismics and coring, with the final aim of gaining insight into slope failure dynamics and impacts. In particular we have examined, and compared wherever appropriate, the settings and the types of mass movements involved in the studied slides, their dimensions and the characteristics of scar and slip planes, run-out distances, triggering mechanisms and ages. Implicit within this context is the sediment failure architecture.

A summary list of the main results includes, amongst many others, the following:

- Holocene to modern day submarine instabilities are common all around Europe, both in glacial and river-dominated settings, although the largest failures such as the gigantic Storegga Slide tend to be early to mid-Holocene in age. There are no Holocene slides known on the flanks of the Canary Islands, a mid-ocean island setting that differs from mainland Europe glacial and river-influenced settings.
- Young submarine landslides on deep continental margins usually have a complex, multi-staged, retrogressive behavior. Quite frequently, one single event evolves into different mass movement types both in space and time. "Pure" behaviors are rare. Since current classifications of submarine mass movements are essentially taken from subaerial mass movement classifications, an in-

depth revision in the light of data provided by new imaging tools would be very convenient, including the use of new criteria.

- The deposit-covered area usually represents more than 50% of the total seafloor area disturbed by an instability event. Scar areas with no or very reduced sliding sediment cover may represent less than 15% of the affected area. The relation between the two areas depends on the volume of sediment released, the headwall height drop, and the disintegrative and flowing behavior of the remobilised mass. At least for the COSTA slides, maximum thicknesses and height drop are directly related.
- Submarine failures of various sizes usually occur under $<2^{\circ}$ pre-slide slope angles, with slip planes inclined generally between 1° and almost 0°. As previous studies have stated, particularly steep slopes are not a requirement for failure to occur. To the contrary, "weak layers" of various natures are a *sine qua non* requirement for sliding to occur.
- Scar areas greatly differ both in shape and size. Their analysis is crucial to learn about preconditioning factors and final triggers leading to destabilisation. The scar evacuation efficiency is a parameter to be taken into account when investigating the dynamics of slope failures. Although usually there is only one single main scar, multiple sets of secondary scars involving relatively minor amounts of sediment are common and contribute to the progressive levelling of headwall escarpments. Commonly, debris lobes from those secondary events accumulate within the boundaries defined by the largest event.
- Calculation of the volume of remobilised sediment solely from headwall scar height and area might be inaccurate since additional volumes of sediment can be involved in the mass movement during downslope transport. On occasion, sediment below the sliding mass is remoulded without significant downslope displacement.
- Features related to slow downslope flowage (i.e., creeping and pressure ridges), crack opening and block detachment may anticipate (but also postdate) fast-occurring mass movements. Identification of such precursory features is fundamental for slide assessment in areas prone to failure.
- Distinct run-outs have been identified for the various components (i.e., blocks and looser matrix) of a sliding mass. While the looser elements could extend several times the total run-out, bulkier and more cohesive elements tend to present much shorter run-outs. Retrogressive events and the resulting sedimentary products do not contribute much in extending the total run-out.
- Gebra Slide, off the northern Antarctic Peninsula, could be considered as an analogue for the initial phases of the Storegga instabilities, since both lie in similar settings and started on the mid to lower slope of a glaciated margin. In addition, they share several geomorphic features such as scar shape, retrogressive headwalls, stable blocks and distal flattened deposits.
- Of the various pre-conditioning factors or environmental stresses reported in the literature, those having played a major role in COSTA landslides are sedimentation effects, a seismically active tectonic setting, presence of gas and diagenetic fronts, and volcanic processes, the later even in passive margins. Sedimentation effects refer mostly, although not necessarily, to relatively high sedimentation rates able to generate excess pore pressures. They also refer to climatically driven or local processes able to form "weak layers" such as contourites and other kinds of poor permeability marine clays.
- Loading by earthquakes, either of "pure" tectonic nature or related to volcanism or post-glacial isostatic rebound, is thought to be by far the most common final trigger accounting for COSTA slide events. Intermediate seismic activity, with an intermediate seismic shock is generally more than enough to induce landsliding if pre-conditioning factors occur. Nevertheless, specific slides may have been caused by peculiar triggers, as illustrated by the Canary Slide, which was triggered by loading of a sedimented slope by a debris avalanche coming from upslope.
- The relation between ice stream mouths and slope instability in high latitude areas is unclear. The hypothesis of lateral transfer of excess pore pressure to the sides of the ice stream where there is less sediment overburden and steeper gradients because of the lack of smoothening by sediment directly contributed by the ice-stream, deserves further attention.

Of course, not every type of instability has been considered within COSTA, mostly because of the limited resources and time available to perform the committed researches. While deep glaciated margin settings have been reasonably well covered (five case studies out of eight), in connection with the oil industry interest, river-dominated settings have been insufficiently investigated, and carbonate-dominated settings have not been addressed at all. Other than CADEB, which is not a unique but a rather specific case of muddy detached prodeltaic system, studies of instabilities in shallow prodeltas and delta fronts have not been performed within COSTA. Failure events affecting the levees of deep-sea fans and channel-levee complexes, and those destabilising inner canyon and channel walls in slope settings, which could result in sediment plugs favoring avulsions and formation of neochannels and lobes, wait to be investigated using a common, integrated approach. The well developed carbonate margin segments common in the Mediterranean hold a wide spectrum of mass movement types about which, in addition to their location and general features, little is known.

We intend for the present paper to be not a final ending but an intermediate stage contributing toward bringing consistency and solving some of the key questions formulated during the last 10 years around the topic of submarine landsliding. If this paper helps in clarifying some concepts, in opening new questions and in promoting novel research approaches, the many scientists co-authoring it will feel their task accomplished.

Acknowledgements

This study was supported by "Continental Slope Stability" (COSTA, ref. EVK3-1999-00028) project, with contributions from the following EU and Spanish research projects: "European Deep Ocean Margins" Research Training Network (EURODOM, ref. RTN2-2001-00281), "European margin strata formation" (EUROSTRATAFORM, ref. EVK3-2001-00200), "Procesos de inestabilidad sedimentaria en márgenes continentales e insulares españoles: los megadeslizamientos del Ebro y de Canarias" (GRANDES, ref. MAR98-0347), "Corrientes de hielo y sistemas sedimentarios glacio-marinos del margen pacífico de la Península Antártica" (COHIMAR, ref. REN2000-0896/ANT). Contribution from Generalitat de Catalunya to the "Barcelona Consortium on Marine Geosciences" thematic network and to CRG on Marine Geosciences is equally acknowledged. Officers, crews, technicians and students involved in sea-going work have provided essential help during data acquisition and when doing laboratory work. Many colleagues have contributed with useful comments, punctual information and in data treatment. Their list would be simply too long. Fellowship holders acknowledge their funding agencies. The reviewers are thanked for their constructive and helpful comments. Last but not least, Gilles Ollier, scientific officer of the COSTA project in Brussels, provided during the whole life of the project clever advice and invaluable support.

References

Alibes, B., Rothwell, R.G., Canals, M., Weaver, P.P.E., Alonso, B., 1999. Determination of sediment volumes, accumulation rates and turbidite emplacement frequencies on the Madeira Abyssal Plain (NE Atlantic): a correlation between seismic and borehole data. Mar. Geol. 160, 225–250.

Alonso, B., Maldonado, A., 1990. Late Quaternary sedimentation patterns of the Ebro turbidite systems (Northwestern Mediterranean): two styles of deep-sea deposition. Mar. Geol. 95, 353–377.

Alonso, B., Field, M.E., Gardner, J.V., Maldonado, A., 1990. Sedimentary evolution of the Pliocene and Pleistocene Ebro margin, northeastern Spain. Mar. Geol. 95, 313–331.

Amblas, D., Urgeles, R., Canals, M., Calafat, A.M., Rebesco, M., Camerlenghi, A., Estrada, F., Hughes-Clarke, J.E., De Batist, M., 2004. Continental shelf glacial troughs and continental rise development off the North Antarctic Peninsula. Quat. Sci. Rev. (submitted for publication).

Aparicio, A., Metafile, J.M., Araña, V., Villa, I.M., 1991. La edad del volcanismo de las islas Columbrete Grande y Alborán (Mediterráneo occidental). Bol. Geol. Min. 102, 562–570.

Argnani, A., Favali, P., Frugoni, F., Gasperini, M., Ligi, M., Marani, M., Mattietti, G., Mele, G., 1993. Foreland deformational pattern in the southern Adriatic Sea. Ann. Geofis. 36, 229–247.

Asioli, A., Trincardi, F., Lowe, J.J., Oldfield, F., 1999. Short-term climate changes during the Last Glacial–Holocene transition: comparison between Mediterranean records and the GRIP event stratigraphy. J. Quat. Sci. 14, 373–381.

Badley, M.E., 1985. Practical Seismic Interpretation. Int. Human Res. Dev., Boston, MA. 266 pp.

Banfield, L.A., Anderson, J.B., 1995. Seismic facies investigation of the late Quaternary glacial history of Bransfield Basin. In: Cooper, A.K., Barker, P.F., Brancolini, G. (Eds.), Geology and Seismic Stratigraphy of the Antarctic Margin, AGU Ant. Res. Ser., vol. 68, pp. 123–140.

Baptista, M.A., Miranda, P.M.A., Miranda, J.M., Mendes Victor, L., 1998. Constrains on the source of the 1755 Lisbon tsunami inferred from numerical modelling of historical data. J. Geodyn. 25 (2), 159–174.

Barcena, M.A., Gersonde, R., Ledesma, S., Fabres, J., Calafat, A.M., Canals, M., Sierro, F.J., Flores, J.A., 1998. Record of Holocene glacial oscillations in Bransfield Basin as revealed by microfossil assemblages. Antarct. Sci. 10 (3), 269–285.

Barley, B., 1999. Deepwater problems around the world. Lead. Edge 18 (4), 488–494.

Bartolini, C., Caputo, R., Pieri, M., 1996. Pliocene–Quaternary sedimentation in the Northern Apennine Foredeep and related denudation. Geol. Mag. 133, 244–273.

Bates, R.L., Jackson, J.A., 1987. Glossary of Geology. Amer. Geol. Inst., Alexandria, USA. 788 pp.

Berndt, C., Bünz, S., Mienert, J., 2003. Polygonal fault systems on the mid-Norwegian margin: a long-term source for fluid flow. In: van Rensbergen, P., Morley, C. (Eds.), Subsurface Sediment Mobilization, Geol. Soc. London Spec. Publ. 216, pp. 283–290.

Best, A.I., Clayton, C.R.I., Longva, O., Szuman, M., 2003. The role of free gas in the activation of submarine slides in Finneidfjord. In: Locat, J., Mienert, J. (Eds.), Submarine Mass Movements and Their Consequences. Kluwer Acad. Publ., Dordrecth, The Netherlands, pp. 491–498.

Blondel, P., Murton, B.J., 1997. Handbook of Seafloor Sonar Imagery, Wiley-Praxis Ser. in Remote Sensing. John Wiley & Sons, Chichester, UK, 314 pp.

Bondevik, S., Svendsen, J.I., 1994. Annales Geophysicae, European Geophys. Soc.: 1. Solid Earth Geophysics and Natural Hazards, Suppl. 1 vol. 12, pp. C207.

Bondevik, S., Svendsen, J.I., 1995. Paleotsunamis in the Norwegian and North Seas. Rep. Univ. Bergen (unpubl.).

Bondevik, S., Svendsen, J.I., Johnsen, G., Mangerud, J., Kaland, P.E., 1997. The Storegga tsunami along the Norwegian coast, its age and runup. Boreas 26, 29–53.

Bohrmann, G., Chin, C., Petersen, S., Sahlig, H., Schwarz-Schampera, U., Greinert, J., Lammers, S., Rehder, G., Daehlmann, A., Wallmann, K., Dijkstra, S., Schenke, H.W., 1999. Hydrothermal activity at Hook Ridge in the Central Bransfield Basin, Antarctica. Geo Mar. Lett. 18, 277–284.

Bosman, A., Chiocci, F.L., Romagnoli, C., Tommasi, P., 2004. Fast evolution of a submarine volcanic flank experiencing a large-scale landslide: the case of Stromboli, Aeolian Islands. Rapp. Comm. Int. Mer. Médit. 37, 10.

Boulanger, E., 2000. Comportement cyclique des sédiments de la marge continentale de la rivière Eel: une explication possible pour le peu de glissements sous-marins superficiels dans cette région, M. Sc. Thesis, Dept. Geology and Geol. Eng., Laval Univ., Sainte-Foy, Quebec.

Boulanger, E., Konrad, J.M., Locat, J., Lee, H.J., 1998. Cyclic behavior of Eel River sediments: a possible explanation for the paucity of submarine landslide features. AGU, EOS Abstr. 79, 254.

Bouriak, S., Vanneste, M., Saoutkine, A., 2000. Inferred gas hydrates and clay diapirs near the Storegga Slide on the southern edge of the Voring Plateau, offshore Norway. Mar. Geol. 163, 125–148.

Bryn, P., Berg, K., Lien, R., Solheim, A., Forsberg, K.F., 2003a. How we conclude on the Storegga Slide risk, COSTA. Continental Slope Stability Workshop 4, 10–13 Febr. 2003, Bologna, Italy, Abstr. Vol. 4 pp.

Bryn, P., Solheim, A., Berg, K., Lien, R., Forsberg, C.F., Haflidason, H., Ottesen, D., Rise, L., 2003b. The Storegga Slide Complex: repeated large scale sliding in response to climatic cyclicity. In: Locat, J., Mienert, J. (Eds.), Submarine Mass Movements and Their Consequences. Kluwer Acad. Publ., Dordrecth, The Netherlands, pp. 215–222.

Bugge, T., 1983. Submarine slides on the Norwegian continental margin, with special emphasis on the Storegga area. Publ. Cont. Shelf Inst. 110 (152 pp.).

Bugge, T., Befring, S., Belderson, R.H., Eidvin, T., Jansen, E., Kenyons, N.H., Holtedahl, H., Sejrup, H.P., 1987. A giant three-stage submarine slide off Norway. Geo Mar. Lett. 7, 191–198.

Bugge, T., Belderson, R.H., Kenyon, N.H., 1988. The storegga slide. Philos. Trans. R. Soc. London Ser. A: Math. Phys. Sci. 325, 357–388.

Bulat, J., 2003. Imaging the Afen Slide from commercial 3D seismic—methodology and comparison with high-resolution data. In: Locat, J., Mienert, J. (Eds.), Submarine Mass Movements and Their Consequences. Kluwer Acad. Publ., Dordrecht, The Netherlands, pp. 205–213.

Bulat, J., Long, D., 2001. Images of the seabed in the Faeroe-Shetland Channel from commercial 3D seismic data. Mar. Geophys. Res. 22, 345–367.

Bünz, S., Mienert, J., Berndt, C., 2003. Geological controls on the Storegga gas-hydrate system of the mid-Norwegian continental margin. Earth Planet. Sci. Lett. 209, 291–307.

Calanchi, N., Cattaneo, A., Dinelli, E., Gasparotto, G., Lucchini, F., 1998. Tephra layers in late Quaternary sediments of the central Adriatic Sea. Mar. Geol. 149, 191–209.

Campbell, K.J., 1999. Deepwater geohazards: how significant are they? Lead. Edge 18 (4), 514–519.

Canals, M., 1985. Estructura sedimentaria y evolución morfológica del talud y el glacis continentales del Golfo de León: fenómenos de desestabilización de la cobertera sedimentaria plio-cuaternaria, PhD thesis, Univ. Barcelona, Spain, 618 pp.

Canals, M., Acosta, J., Baraza, J., Bart, P., Calafat, A.M., Casamor, J.L., De Batist, M., Ercilla, G., Farran, M., Frances, G., Gracia, E., Ramos, E., Sanz, J.L., Sorribas, J., Tassone, A., 1993. Evolución geológica de la Cuenca de Bransfield y de la Dorsal Sur del Mar de Scotia, Campaña GEBRA'93. Informe de campaña, Univ. Barcelona, 147 pp. (unpubl.).

Canals, M., Acosta, J., Baraza, J., Bart, P., Calafat, A.M., Casamor, J.L., De Batist, M., Ercilla, G., Farran, M., Frances, G., Gracia, E., Ramos, E., Sanz, J.L., Sorribas, J., Tassone, A., 1994. La Cuenca Central de Bransfield (NW de la Península Antártica): primeros resultados de la campaña GEBRA-93. Geogaceta 16, 132–135.

Canals, M., Urgeles, R., Calafat, A.M., 2000a. Deep sea-floor evidence of past ice streams off the Antarctic Peninsula. Geology 28 (1), 31–34.

Canals, M., Urgeles, R., Masson, D.G., Casamor, J.L., 2000b. Los deslizamientos submarinos de las Islas Canarias. Makaronesia 2, 57–69.

Canals, M., Casamor, J.L., Urgeles, R., Lastras, G., Masson, D., Berne, S., Alonso, B., De Batist, M., 2000c. The Ebro continental margin, Western Mediterranean Sea: interplay between canyon-channel systems and mass wasting processes. In: Weimer, P., Nelson, H. (Eds.), Deep-Water Reservoirs of the World (CD). Gulf Coast Section SEPM Foundation, Houston, Texas (USA), pp. 152–174.

Canals, M., Casamor, J.L., Urgeles, R., Calafat, A.M., Domack, E.W., Baraza, J., Farran, M., De Batist, M., 2002. A subglacial sedimentary system off the northern Antarctic Peninsula from seafloor evidence. Geology 30 (7), 603–606.

Canals, M., Calafat, A., Camerlenghi, A., De Batist, M., Urgeles, R., Farran, M., Geletti, R., Versteeg, W., Amblas, D., Rebesco, M., Casamor, J.L., Sanchez, A., Willmott, V., Lastras, G., Imbo, Y., 2003. Uncovering the footprint of former ice streams off Antarctica, EOS, Trans. AGU, 84 (11): 97, 102–103.

Cantagrel, J.M., Arnaud, N.O., Ancochea, E., Fuster, J.M., Huertas, M.J., 1999. Repeated debris avalanches on Tenerife and genesis of Las Canadas caldera wall (Canary Islands). Geology 27, 739–742.

Carracedo, J.C., Day, S., 2002. Canary Islands, Classic Geology in Europe 4. Terra Publ., Harpenden, UK. 294 pp.

Carracedo, J.C., Guillou, H., Laj, J., Kissel, K., Perez Torrado, J.F., Rodriguez Badiola, E., 1995. Volcanic history of the island of El Hierro, Canarian Archipelago. EGU 8th Meeting, Strasbourg, France, Terra Nova (abstr. suppl.), vol. 7, pp. 162.

Carter, R.M., 1975. A discussion and classification of subaqueous mass-transport with particular application to grain flow and fluxoturbidites. Earth-Sci. Rev. 11, 145–177.

Cattaneo, A., Trincardi, F., 1999. The late Quaternary transgressive record in the Adriatic epicontinental sea: basin widening and facies partitioning. In: Bergman, K., Snedden, J. (Eds.), Isolated Shallow Marine Sand Bodies: Sequence Stratigraphic Analysis and Sedimentologic Interpretation, Spec. Publ. SEPM 64, pp. 1–20.

Cattaneo, A., Corregiari, A., Penitenti, D., Trincardi, F., 2003a. Morphobathymetry of small-scale mud reliefs on the Adriatic shelf. In: Locat, J., Mienert, J. (Eds.), Submarine Mass Movements and Their Consequences. Kluwer Acad. Publ., Dordrecht, The Netherlands, pp. 401–408.

Cattaneo, A., Correggiari, A., Langone, L., Trincardi, F., 2003b. The late Holocene Gargano subaqueous delta, Adriatic shelf: sediment pathways and supply fluctuations. Mar. Geol. 193 (1–2), 61–91.

Ciabatti, M., Curzi, P.V., Ricci Lucchi, F., 1987. Quaternary sedimentation in the central Adriatic Sea. G. Geol. 49, 113–125.

Clavell, E., Berastegui, X., 1991. Petroleum geology of the Gulf of Valencia. In: Spencer, A.M. (Ed.), Generation, Accumulation and Production of Europe's Hydrocarbons, Sp. Publ. Eur. Assoc. Petr. Geosc., vol. 1, pp. 355–368.

Cochonat, P., Bourillet, J.F., Savoye, B., Dodd, L., 1993. Geotechnical characteristics and instability of submarine slope sediments, the Nice slope (N–W Mediterranean Sea). Mar. Georesour. Geotechnol. 11, 131–151.

Conti, A., Stefanon, A., Zuppi, G.M., 2002. Gas seeps and rock formation in the northern Adriatic Sea. Cont. Shelf Res. 22, 2333–2344.

Cook, H.E., Mullins, H.T., 1983. Basin margin environment. AAPG Mem. 33, 540–617.

Correggiari, A., Roveri, M., Trincardi, F., 1992. Regressioni "forzate", regressioni "deposizionali" e fenomeni din instabilitá in unitá progradazionali tardo-quaternarie (Adriatico centrale). G. Geol. 54, 19–36.

Correggiari, A., Roveri, M., Trincardi, F., 1996. Late Pleistocene and Holocene evolution on the north Adriatic Sea. Quaternario., Ital. J. Quat. Sci. 9, 697–704.

Correggiari, A., Trincardi, F., Langone, L., Roveri, M., 2001. Styles of failure in late Holocene highstand and prodelta wedges on the Adriatic shelf. J. Sediment. Res. 71 (2), 218–236.

Dahlgren, T., Vorren, T.O., 2003. Sedimentary environment and glacial history during the last 40 ka of the Voring continental margin, mid-Norway. Mar. Geol. 193, 93–127.

Damuth, J.E., 1978. Echo character of the Norwegian–Greenland Sea: relationship to Quaternary sedimentation. Mar. Geol. 28, 1–36.

Dawson, A.G., Long, D., Smith, D.E., 1988. The Storegga Slides: evidence from eastern Scotland for a possible tsunami. Mar. Geol. 82, 271–276.

Dawson, A.G., Long, D., Smith, D.E., Shi, S., Foster, I.D.L., 1993. Tsunamis in the Norwegian Sea caused by the Storegga submarine landslides. In: Tinti, S. (Ed.), Tsunamis in the World. Kluwer Acad. Publ., The Netherlands, pp. 31–42.

De Blasio, F.V., Harbitz, C.B., Lien, R., 2004. Flow models of small to medium-scale debris flows originating from compacted clay materials. Mar. Geol. 213. 439–455.

De Moustier, C., 1988. State of the art swath bathymetry survey systems. Int. Hydrogr. Rev., Monaco 65 (2), 25–54.

De Moustier, C., Matsumoto, H., 1993. Seafloor acoustic remote sensing with multi-beam echo-sounders and bathymetric side-scan sonar systems. Mar. Geophys. Res. 15, 27–42.

Dimakis, P., Elverhoi, A., Hoeg, K., Solheim, A., Harbitz, C.B., Laberg, J.S., Vorren, T.O., Marr, J., 2000. Submarine slope stability on high-latitude glaciated Svalbard–Barents Sea margin. Mar. Geol. 162, 303–316.

Dingle, R.V., Morris, P., Lavelle, M., Howe, J., 1998. HILATS rock coring, vibrocoring and seismic surveys on the continental shelf of the northern Antarctic Peninsula (February–March 1998): Cruise JR29, BAS cruise rep. (unpubl.).

Doglioni, C., Mongelli, F., Pieri, P., 1994. The Puglia uplift (SE Italy): an anomaly in the foreland of the Apennine subduction due to buckling of a thick continental lithosphere. Tectonics 13, 1309–1321.

Dott, R.H., 1963. Dynamics of subaqueous gravity depositional processes. AAPG Bull. 47 (1), 104–128.

Dowdeswell, J.A., Kenyon, K.H., Elverhoi, A., Laberg, J.S., Hollender, F.J., Mienert, J., Siegert, M., 1996. Large-scale sedimentation on the glacier influenced Polar North Atlantic

margins: long-range side-scan sonar evidence. Geophys. Res. Lett. 23, 3535–3538.

Duin, E.J.T., Mesdag, C.S., Kok, P.T.J., 1984. Faulting in the Madeira Abyssal Plain sediments. Mar. Geol. 56, 299–308.

Edgers, L., Karlsrud, K., 1981. Viscous analysis of submarine flows. Publ.-Norw. Geotech. Inst. 143, 1–10.

Edgers, L., Karlsrud, K., 1982. Soil flows generated by submarine slides: case studies and consequences. In: Chrysostomomidis, C., Connor, J.J. (Eds.), Proc. 3rd Int. Conf. Behavior of Offshore Structures, vol. 2. Hemisphere Publ., Bristol, Pa., USA, pp. 425–437.

Eidvin, T., Jansen, E., Rundberg, Y., Brekke, H., Grogan, P., 2000. The upper Cainozoic of the Norwegian continental shelf correlated with the deep sea record of the Norwegian Sea and the North Atlantic. Mar. Pet. Geol. 17, 579–600.

Elverhoi, A., Norem, H., Andersen, E.S., Dowdeswell, J.A., Fossen, I., Haflidason, H., Kenyon, N.H., Laberg, J.S., King, E.L., Sejrup, H.P., Solheim, A., Vorren, T., 1997. On the origin and flow behavior of submarine slides on deep-sea fans along the Norwegian–Barents Sea continental margin. Geo Mar. Lett. 17, 119–125.

Elverhoi, A., Harbitz, C.B., Dimakis, P., Mohring, D., Marr, J., Parker, G., 2000. On the dynamics of subaqueous debris flows. Oceanography 13 (3), 109–117.

Embley, R.W., 1976. New evidence for occurrence of debris flow deposits in the deep sea. Geology 4, 371–374.

Escutia, C., Maldonado, A., 1992. Paleoceanographic implications of the Messinian surface in the Valencia Trough, northwestern Mediterranean Sea. In: Banda, E., Santanach, P. (Eds.), Geology and Geophysics of the Valencia Trough, Western Mediterranean, Tectonophysics, vol. 203, pp. 263–284.

Evans, D., King, E.L., Kenyon, N.H., Brett, C., Wallis, D., 1996. Evidence for long-term instability in the Storegga Slide region off western Norway. Mar. Geol. 130, 281–292.

Evans, D., McGiveron, M., Harrison, Z., Bryn, P., Berg, K., 2004. Along-slope variation in the late Neogene evolution of the mid-Norwegian margin in response to uplift and tectonism, In: Dore, A.G., Cartwright, J., Stoker, M.S., Turner, J.P., White, N. (Eds.), Exhumation of the North Atlantic margin: timing, mechanisms and implications for petroleum exploration, Spec. Publ. Geol. Soc. London 196, 139–151.

Fabres, J., Calafat, A., Canals, M., Barcena, M.A., Flores, J.A., 2000. Bransfield Basin fine-grained sediments: late-Holocene sedimentary processes and Antarctic oceanographic conditions. Holocene 10 (6), 703–718.

Farran, M., Maldonado, A., 1990. The Ebro continental shelf: Quaternary seismic stratigraphy and growth patterns. Mar. Geol. 95, 289–312.

Fernandez, M., Foucher, J.P., Jurado, M.J., 1995. Evidence for the multi-stage formation of the southwestern Valencia Trough. Mar. Pet. Geol. 12, 101–109.

Field, M.E., Gardner, J.V., 1990. Pliocene–Pleistocene growth of the Río Ebro margin, northeast Spain: a prograding-slope model. Geol. Soc. Amer. Bull. 102, 721–733.

Ford, G., Simpson, B., Ottemoller, L., 2002. NW Scotland offshore seismicity: sixth annual report to 30 September 2002, British Geol. Survey Tech. Rep. CR/02/285.

Frignani, M., Langone, L., 1991. Accumulation rates and ^{137}Cs distribution in sediments off the Po River delta and the Emilia-Romagna coast (nothwestern Adriatic Sea, Italy). Cont. Shelf Res. 11, 525–542.

Frignani, M., Langone, L., Pacelli, M., Ravaioli, M., 1992. Input distribution and accumulation of dolomite in sediments of the middle Adriatic Sea. Rapp. CIESM 33, 324.

Garcia, M.O., Hull, D.M., 1994. Turbidites from giant Hawaiian landslides: results from Ocean Drilling Site 842. Geology 22, 159–162.

Gennesseaux, M., Mauffret, A., Pautot, G., 1980. Les glissements sous-marins de la pente continentales niçoise et la rupture de cables en mer Ligure (Méditerranée occidentale). C. R. Acad. Sci., Paris 290 (D), 959–962.

Geyer, R.A. (Ed.), CRC Handbook of Geophysical Exploration at Sea. CRC Press, Boca Raton, FLA, 445 pp.

Goldfinger, C., Nelson, H., 1999. Holocene recurrence rate of Cascadia great earthquakes based on turbidite event record. AGU, EOS Abstr. 80, 1024.

Gracia, E., Dañobeitia, J.J., PARSIFAL Team, 2003. Mapping active faults offshore Portugal (36°N–38°N): implications for seismic hazard assessment along the southwest Iberian margin. Geology 31 (1), 83–86.

Gracia, E., Canals, M., Farran, M., Sorribas, J., Pallas, R., 1996a. Central and Eastern Bransfield basins (Antarctica) from high-resolution swath-bathymetry data. Antarct. Sci. 9 (2), 168–180.

Gracia, E., Canals, M., Farran, M., Prieto, M.J., GEBRA Team, 1996b. Morphostructure and recent evolution of the Bransfield back-arc basin (NW Antarctic Peninsula). Mar. Geophys. Res. 18 (1–3), 429–448.

Grant, J.A., Schreiber, R., 1990. Modern swathe sounding and sub-bottom profiling technology for research applications: the Atlas Hydrosweep and Parasound systems. In: Hailwood, E.A., Kidd, R.B. (Eds.), Marine Geological Surveying and Sampling. Kluwer Acad. Publ., Dordrecht, Holland, pp. 153–168.

Griffiths, G., Thorpe, S.A., 1996. Marine instrumentation. In: Summerhayes, C.P., Thorpe, S.A. (Eds.), Oceanography. An Illustrated Guide. Manson Publ., London, UK, pp. 280–299.

Groupe ESCYANICE, 1982. Recent mass wasting processes on the Provençal margin (Western Mediterranean). In: Saxov, S., Nieuwenhuis, J.K. (Eds.), Marine Slides and Other Mass Movements. Plenum Press, New York, pp. 53–58.

Grünthal, G., Bosse, C., Sellami, S., Mayer-Rosa, D., Giardini, D., 1999. Compilation of the GSHAP regional seismic hazard for Europe, Africa and the Middle East. Ann. Geofis. 42, 1215–1223.

Gueguen, E., Doglioni, C., Fernandez, M., 1998. On the post-25 Ma geodynamic evolution of the Western Mediterranean. Tectonophysics 298, 259–269.

Guillou, H., Carracedo, J.C., Laj, C., Kissel, C., Perez Torrado, J.F., Rodriguez Badiola, E., 1995. K–Ar ages and geomagnetic reversals from lavas of Hierro, Canary Islands. Terra Nova 7 (abstr. Suppl. 1), 163.

Guillou, H., Carracedo, J.C., Perez Torrado, J.F., Rodriguez Badiola, E., 1996. K–Ar dates and magnetic stratigraphy of a hotspot-induced, fast grown oceanic island: El Hierro, Canary Islands. J. Volcanol. Geotherm. Res. 73, 141–155.

Haflidason, H., Gravdal, A., Sejrup, H.P., 2003a. The Northern Storegga Escarpment—Morphology and Features. In: Mienert, J., Weaver, P. (Eds.), European Margin Sediment Dynamics, Side-Scan Sonar and Seismic Images. Springer-Verlag, Berlin, pp. 45–53.

Haflidason, H., Lekens, W., Lien, R., Bryn, P., Sejrup, H.P., 2003b. The dating of the Storegga Slide: precision and problems, COSTA. Continental Slope Stability Workshop 4, 10–13 Febr. 2003, Bologna, Italy, Abstr., Vol., pp. 12.

Haflidason, H., Sejrup, H.P., Berstad, I.M., Nygard, A., Richter, T., Bryn, P., Lien, R., Berg, K., 2003c. A weak layer feature on the Northern Storegga Slide escarpment. In: Mienert, J., Weaver, P. (Eds.), European Margin Sediment Dynamics, Side-Scan Sonar and Seismic Images. Springer-Verlag, Berlin, pp. 55–62.

Haflidason, H., Lekens, W., Allaway, T., Hjonnevag, M., Nygard, A., 2003d. Dating of the Storegga Slide: Final report to Norsk Hydro, Rep. 100-001/03, Dept. Earth Sc. University of Bergen, Norway, 353 pp.

Haflidason, H., Sejrup, H.P., Nygard, A., Bryn, P., Lien, R., Berg, K., Masson, D.G., Forsberg, C.F., 2004. Architecture, geometry and slide development of the Storegga Slide. Mar. Geol. 213. 201–234.

Hampton, M.A., 1972. The role of subaqueous debris flow in generating turbidity currents. J. Sediment. Petrol. 42, 775–793.

Hampton, M.A., Lee, H.J., Locat, J., 1996. Submarine landslides. Rev. Geophys. 34 (1), 33–59.

Harbitz, C.B., 1992. Model simulation of tsunamis generated by the Storegga Slides. Mar. Geol. 105, 1–21.

Harden, S.L., DeMaster, D.J., Nittrouer, C.A., 1992. Developing sediment geochronologies for high-latitude continental shelf deposits: a radiochemical approach. Mar. Geol. 103, 69–97.

Heezen, B.C., Ewing, M., 1952. Turbidity currents and submarine slumps, and the 1929 Grand Banks earthquake. Am. J. Sci. 250, 849–873.

Heezen, B.C., Hollister, C.D., 1971. The Face of the Deep. Oxford Univ. Press, New York, USA. 659 pp.

Hobbs, P.R.N., Long, D., Northmore, K.J., 1997. Modelling slope stability conditions on the West Shetland slope. British Geol. Survey Tech. Rep. WN/97/32C.

Holmes, R., Bulat, J., Gillespie, E.J., Hine, N., Hobbs, P., Jones, S., Riding, J., Sankey, M., Tulloch, G., Wilkinson, I.P., Walker, A., 1997. Geometry, processes of formation and timing of the Afen submarine landslide west of Shetland, British Geol. Survey Tech. Rep. WB/97/33C.

Hovland, M., Curzi, P.V., 1989. Gas seepage and assumed mud diapirism in the Italian central Adriatic Sea. Mar. Pet. Geol. 6, 161–169.

Hughes Clarke, J.E., 1988. The geological record of the 1929 "Grand Banks" earthquake and its relevance to deep-sea clastic sedimentation, PhD thesis, Dalhousie Univ., Halifax, Nova Scotia, Canada.

Hughes Clarke, J.E., Mayer, L.A., Piper, D.J.W., Shor, A.N., 1989. Pisces IV submersible operations in the epicentral region of the 1929 Grand Banks earthquake. Pap.-Geol. Surv. Can. 88-20, 57–69.

Hünerbach, V., Masson, D., et al., 2004. Landslides in the North Atlantic and its adjacent seas: an analysis of their morphology, setting and behaviour. Mar. Geol. 213. 343–362.

Ibanez, J.M., Morales, J., Alguacil, G., Almendros, J., Ortiz, R., Del Pezzo, E., 1997. Intermediate-focus earthquakes under South Shetland Islands (Antarctica). Geophys. Res. Lett. 24, 531–534.

Imbo, Y., De Batist, M., Canals, M., Prieto, M.J., Baraza, J., 2003. The Gebra Slide: a submarine slide on the Trinity Peninsula Margin, Antarctica. Mar. Geol. 193 (3–4), 235–252.

Janbu, N., 1996. En samlet vurdering av forholdene for under og etter skredet I Finneidfjord 20. Juni 1996, Arsaksvurdering, Rapp. 1, rev. 1, 18. Nov. 96.

Jansen, E., Befring, S., Bugge, T., Eidvin, T., Holtedahl, H., Sejrup, H.P., 1987. Large submarine slides on the Norwegian continental margin: sediments, transport and timing. Mar. Geol. 78, 77–107.

Jiang, L., LeBlond, P.H., 1993. Numerical modelling of an underwater Bingham plastic mudslide and the waves it generates. J. Geophys. Res. 98 (C6), 10303–10317.

Jin, Y.K., Lee, D.K., Nam, S.H., Kim, Y., Kim, K.J., 1998. Seismic observation at King Sejong Station, Antarctic Peninsula. Terra Antart. 5, 729–736.

Johnson, A.M., 1970. Physical Processes in Geology. Freeman, Cooper, San Francisco, CA, USA, 557 pp.

Jones, E.J.W., 1999. Marine Geophysics. John Wiley & Sons, Chichester, UK. 466 pp.

Kawata, Y., Benson, B.C., Borrero, J.C., Borrero, J.L., Davies, H.L., de Lange, W.P., Imamura, F., Letz, H., Nott, J., Synolakis, C.E., 1999. Tsunami in Papua New Guinea was as intense as first thought. Eos, 80 (9): 101, 104–105.

Kenyon, N.H., 1986. Evidence from bedforms for a strong poleward current along the upper continental slope of northwest Europe. Mar. Geol. 72, 187–198.

King, L.H., Rokoengen, K., Gunleiksrud, T., 1987. Quaternary seismostratigraphy of the Mid-Norwegian shelf, 65–67 30N—a till tongue stratigraphy. The Cont. Shelf and Petrol. Res. Inst. A/S (IKU) Publ., Trondheim, Norway, vol. 114, 58 pp.

Klaucke, I., Cochonat, P., 1999. Analysis of past seafloor failures on the continental slope off Nice (SE France). Geo Mar. Lett. 19, 245–253.

Klinkhammer, G.P., Chin, C.S., Wilson, C., Rudnicki, M., Keller, R.A., Fisk, M.R., Lawver, L.A., 1995. Results of a search for hydrothermal activity in the Bransfield Strait, Antarctica. EOS Suppl. 7, 710. (Nov.).

Krastel, S., Schminke, H.U., Jacobs, C.L., Rihm, R., Le Bas, T.P., Alibes, B., 2001. Submarine landslides around the Canary Islands. J. Geophys. Res. 106, 3977–3997.

Kuenen, Ph.H., 1937. Experiments in connection with Daly's hypothesis on the formation of submarine canyons. Leidse Geol. Meded. 8, 327–335.

Kuenen, Ph.H., Migliorini, C.I., 1950. Turbidity currents as a cause of graded bedding. J. Geol. 58, 91–127.

Kvalstad, T.J., Gauer, P., Kaynia, A.M., Nadim, F., Bryn, P., 2002. Slope stability at Ormen Lange. Proc. Int. Conf. Offshore Site Investigation and Geotechnics, Sustainability through Diversity, 26–28 Nov. 2002, London.

Laberg, J.S., Vorren, T.O., 2000. The Traenadjupet Slide, offshore Norway—morphology, evacuation and triggering mechanisms. Mar. Geol. 171, 95–114.

Laberg, J.S., Vorren, T.O., Mienert, J., Evans, D., Lindberg, B., Ottesen, D., Kenyon, N.H., Henriksen, S., 2002. Late Quaternary palaeoenvironment and chronology in the Traenadjupet Slide area offshore Norway. Mar. Geol. 188, 35–60.

Langone, L., Asioli, A., Correggiari, A., Trincardi, F., 1996. Age–depth modelling through the late Quaternary deposits of the central Adriatic Basin. Mem. Ist. Ital. Idrobiol. 55, 177–196.

Lastras, G., Canals, M., Hughes-Clarke, J.E., Moreno, A., De Batist, M., Masson, D.G., Cochonat, P., 2002. Seafloor imagery of the BIG'95 debris flow, Western Mediterranean. Geology 30 (10), 871–874.

Lastras, G., Canals, M., Urgeles, R., 2003. Lessons from sea-floor and subsea-floor imagery of the BIG'95 debris flow scar and deposit. In: Locat, J., Mienert, J. (Eds.), Submarine Mass Movements and Their Consequences. Kluwer Acad. Publ., Dordrecth, The Netherlands, pp. 425–431.

Lastras, G., Canals, M., Urgeles, R., Hughes-Clarke, J.E., Acosta, J., 2004a. Shallow slides and pockmark swarms in the Eivissa Channel, Western Mediterranean Sea. Sedimentology 51, 837–850.

Lastras, G., De Blasio, F.V., Elverhoi, A., Canals, M., 2004b. Conceptual and numerical modelling of the BIG'95 debris flow, Western Mediterranean Sea. J. Sediment. Res. (submitted for publication).

Latras, G., Canals, M., Urgeles, R., De Batist, M., Calafat, A.M., Casamor, J.L., 2004. Characterization of the recent BIG'95 debris flow deposit after a variety of seismic reflection data, Ebro margin, Western Mediterranean Sea. Mar. Geol. 213. 235–255.

Le Bas, T.P., Masson, D.G., 1997. Automatic registration of TOBI side-scan sonar and multi-beam bathymetry images for improved data fusion. Mar. Geophys. Res. 19, 163–176.

Le Bas, T.P., Masson, D.G., Millard, N.C., 1995. TOBI image processing—the state of the art. IEEE J. Oceanic Eng. 20, 85–93.

Lebreiro, S.M., Weaver, P.P.E., Howe, R.W., 1998. Sedimentation on the Madeira Abyssal Plain: the history of turbidite infill. In: Schminke, H.U., Weaver, P.P.E., Firth, J.V., Duffield, W.A. (Eds.), Proc. ODP, Sci. Results, vol. 157. Ocean Drilling Program, College Station, TX, pp. 523–531.

Lebuis, J., Robert, J.M., Rissmann, P., 1983. Regional mapping of landslide hazard in Québec. Swed. Geotech. Inst. Rep. 17, 205–262.

Lee, H.J., Syvitski, J.P.M., Parker, G., Orange, D., Locat, J., Hutton, E.W.H., Imran, J., 2002. Distinguishing sediment waves from slope failure deposits: field examples, including the "Humboldt slide", and modelling results. Mar. Geol. 192, 79–104.

Leenhardt, O., 1972. Le sondage sismique continu. Masson et Cie, Eds., Paris, France. 164 pp.

Leslie, A.B., Long, D., Stoker, M.S., Bulat, J., 2003. Interaction of down-slope, along slope and glacigenic inputs. AAPG Ann. Meet., Abstr., in http://aapg.confex.com/aapg/sl2003/techprogram/paper_71666.htm.

Lipman, P.W., Normark, W.R., Moore, J.G., Wilson, J.B., Gutmacher, C.E., 1988. The giant submarine Alika debris slide, Mauna Loa, Hawaii. J. Geophys. Res. 93, 4279–4290.

Locat, J., Lee, H.J., 2002. Submarine landslides: advances and challenges. Can. Geotech. J. 39, 193–212.

Locat, J., Mienert, J. (Eds.), Submarine Mass Movements and Their Consequences. Kluwer Acad. Publ., Dordrecth, The Netherlands. 540 pp.

Locat, J., Lee, H.J., Nelson, H.C., Schwab, W.C., Twichell, D.C., 1996. Analysis of the mobility of far reaching debris flows on the Mississippi Fan, Gulf of Mexico. In: Senneset, K. (Ed.), Proc. 7th Int. Symp. Landslides. A.A. Balkema, Rotterdam, Holland, pp. 555–560.

Long, D., 2001. The Western Frontiers Association—evaluating seabed conditions west of the UK. Cont. Shelf Res. 21, 811–824.

Long, D., Bulat, J., 2001a. Seismic surveys of the Afen Slide, Faeroe-Shetland Channel, COSTA. Continental Slope Stability Workshop 1, 17–19 Jan. 2001, Oslo, Norway, Abstr. Vol., p. 14.

Long, D., Bulat, J., 2001b. Update on studies of the Afen Slide, COSTA. Continental Slope Stability Workshop 2, 25–27 Sept. 2001, Brest, France, Abstr. Vol., p. 32.

Long, D., Gillespie, E.J., 1997. Seabed and near-seabed geohazards on the shelf and slope west of Shetland, BGS Tech. Rep. WB/97/19C.

Long, D., Stevenson, A.G., Wilson, C.K., Bulat, J., 2003a. Slope failures in the Faeroe-Shetland Channel. Geophys. Res. Abstr. 5, 04239.

Long, D., Stevenson, A.G., Wilson, C.K., Bulat, J., 2003b. Slope failures in the Faeroe-Shetland Channel. In: Locat, J., Mienert, J. (Eds.), Submarine Mass Movements and Their Consequences. Kluwer Acad. Publ., Dordrecht, The Netherlands, pp. 281–289.

Longva, O., Janbu, N., Blikra, L.H., Boe, R., 2003. The 1996 Finneidfjord Slide, seafloor failure and slide dynamics. In: Locat, J., Mienert, J. (Eds.), Submarine Mass Movements and Their Consequences. Kluwer Acad. Publ., Dordrecht, The Netherlands, pp. 531–538.

Lowe, D.R., 1979. Sediment gravity flows: their classification and some problems of application to natural flows and deposits. Spec. Publ. SEPM 27, 75–82.

Maillard, A., Mauffret, A., 1993. Structure et volcanisme de la fosse de Valence (Méditerranée nord-occidentale). Bull. Soc. Géol. Fr. 164, 365–383.

Maillard, A., Mauffret, A., Watts, A.B., Torne, M., Pascal, G., Buhl, P., Pinet, B., 1992. Tertiary sedimentary history and structure of the Valencia Trough (Western Mediterranean). Tectonophysics 203, 57–75.

Major, J.J., Pierson, T.C., 1992. Debris flow rheology: experimental analysis of fine-grained slurries. Water Resour. Res. 28, 841–857.

Maldonado, A., Palanques, A., Alonso, B., Kastens, K.A., Nelson, C.H., O'Connell, S., Ryan, W.B.F., 1985. Physiography and deposition on a distal deep-sea system: the Valencia Fan (Northwestern Mediterranean). Geo Mar. Lett. 5, 157–164.

Malinverno, A., Ryan, W.B.F., Auffret, G., Pautot, G., 1988. Sonar images of the path of recent failure events on the continental margin off Nice, France. Spec. Pap.-Geol. Soc. Am. 229, 59–75.

Marsset, B., Thomas, Y., Thereau, E., Didailler, S., Marsset, T., Cochonat, P., 2003a. Very high resolution 3D seismic imaging of a complex shelf structure in the Adriatic Sea. In: Locat, J., Mienert, J. (Eds.), Submarine Mass Movements and Their Consequences. Kluwer Acad. Publ., Dordrecht, The Netherlands, pp. 441–448.

Marsset, T., Marsset, B., Thomas, Y., Cochonat, P., 2003b. Detailed anatomy of late-Holocene deposits on the Adriatic Shelf from 3D very high resolution seismic data (TRIAD survey). In: Locat, J., Mienert, J. (Eds.), Submarine Mass Movements and Their Consequences. Kluwer Acad. Publ., Dordrecht, The Netherlands, pp. 449–458.

Masson, D.G., 1994. Late Quaternary turbidity current pathways to the Madeira Abyssal Plain and some constraints on turbidity current mechanisms. Basin Res. 6, 17–33.

Masson, D.G., 1996. Catastrophic collapse of the volcanic island of Hierro 15 ka ago and the history of landslides in the Canary Islands. Geology 24 (3), 231–234.

Masson, D.G., 2001. Sedimentary processes shaping the eastern slope of the Faeroe-Shetland Channel. Cont. Shelf Res. 21, 825–857.

Masson, D.G., 2003. Summary of geophysical techniques. In: Mienert, J., Weaver, P. (Eds.), European Margin Sediment Dynamics, Side-Scan Sonar and Seismic Images. Springer-Verlag, Berlin, pp. 9–16.

Masson, D.G., Kidd, R.B., Gardner, J.V., Huggett, Q.J., Weaver, P.P.E., 1992. Saharan continental rise: sediment facies distribution and sediment slides. In: Poag, C.W., de Graciansky, P.C. (Eds.), Geologic Evolution of Atlantic Continental Rises. Van Nostrand Reinhold, New York, pp. 327–343.

Masson, D.G., Huggett, Q.J., Brunsden, D., 1993. The surface texture of the Saharan Debris Flow deposit and some speculations on debris flow processes. Sedimentology 40, 583–598.

Masson, D.G., van Niel, B., Weaver, P.P.E., 1997. Flow processes and sediment deformation in the Canary Debris Flow on the NW African Continental Rise. Sediment. Geol. 110, 163–179.

Masson, D.G., Canals, M., Alonso, B., Urgeles, R., Huhnerbach, C., 1998. The Canary Debris Flow: source area morphology and failure mechanisms. Sedimentology 45, 411–432.

Masson, D.G., Watts, A.B., Gee, M.J.R., Urgeles, R., Mitchell, N.C., Le Bas, T.P., Canals, M., 2002. Slope failures on the flanks of the western Canary Islands. Earth-Sci. Rev. 57, 1–35.

Mezcua, J., Buforn, E., Udias, A., Rueda, J., 1991. Seismotectonics of the Canary Islands. Tectonophysics 208, 447–452.

Mienert, J., Weaver, P.P.E. (Eds.), European Margin Sediment Dynamics, Side-Scan Sonar and Seismic Images. Springer-Verlag, Berlin. 309 pp.

Middleton, G.V., Hampton, M.A., 1973. Sediment gravity flows: mechanics of flow and deposition. Pacific Section, Short Course Lecture Notes on "Turbidites and Deep Water Sedimentation". SEPM, pp. 1–38.

Middleton, G.V., Hampton, M.A., 1976. Subaqueous sediment transport and deposition by sediment gravity flows. In: Stanley, D.J., Swift, D.J.P. (Eds.), Marine Sediment Transport and Environmental Management. John Wiley, New York, pp. 197–218.

Milliman, J.D., Syvitski, J.P.M., 1992. Geomorphic/tectonic control of sediment discharge to the ocean: the importance of small mountainous rivers. J. Geol. 100, 525–544.

Mitchell, R.J., Markell, A.R., 1974. Flowslides in sensitive soils. Can. Geotech. J. 11, 11–31.

Mohrig, D., Elverhoi, A., Parker, G., 1999. Experiments on the relative mobility of muddy subaqueous and subaerial debris flows, and their capacity to remobilize antecedent deposits. Mar. Geol. 154, 117–129.

Moore, D.G., 1978. Submarine slides. In: Voight, B. (Ed.), Rockslides and Avalanches: 1. Natural Phenomena. Elsevier, Amsterdam, pp. 563–604.

Moore, J.G., Clague, D.A., Holcomb, R.T., Lipman, P.W., Normark, W.R., Toressan, M.E., 1989. Prodigious submarine landslides on the Hawaiian Ridge. J. Geophys. Res. 94, 14465–14484.

Moore, J.G., Normark, W.R., Holcomb, R.T., 1994. Giant Hawaiian landslides. Annu. Rev. Earth Planet. Sci. 22, 119–144.

Morgenstern, N., 1967. Submarine slumping and the initiation of turbidity currents. In: Richards, A.F. (Ed.), Marine Geotechnique. Univ. Illinois Press, Urbana, pp. 189–220.

McQuillin, R., Ardus, D.A., 1977. Exploring the Geology of Shelf Seas. Grahan & Trotman, London, UK, 234 pp.

McQuillin, R., Bacon, M., Barclay, W., 1979. An Introduction to Seismic Interpretation. Graham & Trotman, London, UK, 199 pp.

Muir-Wood, R., 2000. Deglaciation seismotectonics: a principal influence on intraplate seismogenesis at high latitudes. Quat. Sci. Rev. 19, 1399–1411.

Mulder, T., Cochonat, P., 1996. Classification of offshore mass movements. J. Sediment. Res. 66 (1), 43–57.

Mulder, T., Moran, K., 1995. Relationship among submarine instabilities, sea level variations and the presence of an ice sheet on the continental shelf: an example from the Verrill Canyon area, Scotian Shelf. Paleoceanography 10, 137–154.

Mulder, T., Tisot, J.P., Cochonat, P., Bourillet, J.F., 1993. Stabilité des pentes sous-marines dans la Baie des Anges, Nice, France. Approche géotechnique. Rev. Fr. Géotech. 64, 21–30.

Mulder, T., Cochonat, P., Tisot, J.P., Bourillet, J.F., 1994. Regional assessment of mass failure events in the Baie des Anges, Mediterranean Sea. Mar. Geol. 122, 29–45.

Mulder, T., Savoye, B., Syvistki, J.P.M., 1997. Numerical modelling of a mid-sized gravity flow: the 1979 Nice turbidity current (dynamics, processes, sediment budget and seafloor impact). Sedimentology 44 (2), 305–326.

Musson, R.M.W., 1998. Historical seismicity of the Western Frontiers Area, British Geol. Survey Tech. Rep. WL/98/26C.

Nardin, T.R., Hein, F.J., Gorsline, D.S., Edwards, B.D., 1979. A review of mass movement processes and acoustic characteristics and contrasts in slope and base-of-slope systems versus canyon-fan-basin systems. Spec. Publ.-Soc. Econ. Paleontol. Mineral 27, 61–73.

Navarro, J.M., Coello, J., 1989. Depressions originated by landslide processes in Tenerife. ESF Meeting on Canarian Volcanism, Arrecife, Canary Islands.

Nelson, C.H., 1990. Estimated post-Messinian sediment supply and sedimentation rates on the Ebro continental margin, Spain. Mar. Geol. 95, 395–418.

Nelson, C.H., Maldonado, A., 1988. Factors controlling depositional patterns of Ebro Turbidite Systems, Mediterranean Sea. AAPG Bull. 72, 698–716.

Nissen, S.E., Haskell, N.L., Steiner, C.T., Coterill, K.L., 1999. Debris flow outrunner blocks, glide tracks, and pressure ridges identified on the Nigerian continental slope using 3-D seismic coherency. Lead. Edge 18 (5), 595–599.

Norem, H., Locat, J., Schieldrop, B., 1990. An approach to the physics and the modelling of submarine landslides. Mar. Geotechnol. 9, 93–111.

Oldfield, F., Asioli, A., Juggins, S., Langone, L., Rolph, T., Trincardi, F., Wolff, G., Gibbs, Z., Vigliotti, L., Frignani, M., van der Post, K., 2003. A high resolution Late Holocene palaeoenvironmental record from the Adriatic Sea: core RF 93-30. Quat. Sci. Rev. 22, 161–184.

Ollier, G., Cochonat, P., Lenat, J.F., Labazuy, P., 1998. Deep-sea volcaniclastic sedimentary systems. An example from La Fournaise volcano, Reunion Island, Indian Ocean. Sedimentology 45, 293–330.

Ottesen, D., Rise, L., Rokoengen, K., Saettem, J., 2001. Glacial processes and large-scale morphology on the mid-Norwegian continental shelf. In: Martinsen, O.J., Dreyer, T. (Eds.), Sedimentary Environments Offshore Norway–Palaeozoic to Recent, NPF Spec. Publ., 10, 441–449.

Pearce, T.J., Jarvis, I., 1995. High-resolution chemostratigraphy of Quaternary distal turbidites: a case study of new methods for the analysis and correlation of barren sequences. In: Dunay, R.E., Hailwood, E.A. (Eds.), Non-Biostratigraphical Methods of Dating and Correlation, Spec. Publ. Geol. Soc. London, 89, 107–143.

Pelayo, A.M., Wiens, D.A., 1989. Seismotectonics and relative plate motions in the Scotia Sea Region. J. Geophys. Res. 94, 7293–7320.

Piper, D.J.W., Aksu, A.E., 1987. The source and origin of the 1929 Grand Banks turbidity current inferred from sediment budgets. Geo Mar. Lett. 7, 177–182.

Piper, D.J.W., Shor, A.N., Farre, J.A., O'Connell, S., Jacobi, R., 1985. Sediment slides around the epicenter of the 1929 Grand Banks earthquake. Geology 13, 538–541.

Piper, D.J.W., Cochonat, P., Morrison, M.L., 1999. The sequence of events around the epicenter of the 1929 Grand Banks earthquake: initiation of debris flows and turbidity current inferred from sidescan sonar. Sedimentology 46, 79–97.

Prieto, M.J., Canals, M., Ercilla, G., De Batist, M., 1998. Structure and geodynamic evolution of the Central Bransfield Basin (NW Antarctic Peninsula). Interpretation of deposits and sedimentary processes in a glacio-marine environment. Mar. Geol. 149, 17–38.

Prieto, M.J., Ercilla, G., Canals, M., De Batist, M., 1999. Seismic stratigraphy of the Central Bransfield Basin (NW Antarctic Peninsula). Interpretation of deposits and sedimentary processes in a glacio-marine environment. Mar. Geol. 157, 47–68.

Prior, D.B., Coleman, J.M., 1979. Submarine landslides: geometry and nomenclature. Z. Geomorphol. (N. F.) 23, 415–426.

Prior, D.B., Coleman, J.M., 1984. Submarine slope instability. In: Brunsden, D., Prior, D.B. (Eds.), Slope Instability. John Wiley and Sons, Chichester, UK, pp. 419–455.

Pudsey, C.J., Barker, P.F., Larter, R.D., 1994. Ice sheet retreat from the Antarctic Peninsula shelf. Cont. Shelf Res. 14, 1647–1675.

Riba, O., Gali, S., Susagna, M.T., Reguant, S., Canals, M., Mata, J.M., Santanach, P., Serrat, D., Vaquer, R., Marti, J., Melgarejo, J.C., Martinell, J., Colombo, F., 1997. Diccionari de Geologia. Enciclopedia Catalana, Barcelona, 1407 pp.

Riddy, P., Mason, D.G., 1996. The sea floor—exploring a hidden world. In: Summerhayes, C.P., Thorpe, S.A. (Eds.), Oceanography. An Illustrated Guide. Manson Publ., London, UK, pp. 300–313.

Ridley, W.I., 1971. The origin of some collapse structures in the Canary Islands. Geol. Mag. 108, 447–484.

Roberts, J.A., Cramp, A., 1996. Sediment stability on the western flanks of the Canary Islands. Mar. Geol. 134, 13–30.

Rodine, J.D., Johnson, M.A., 1976. The ability of debris, heavily freighted with coarse clastic materials, to flow on gentle slopes. Sedimentology 23, 213–234.

Rokoengen, K., Rise, L., Bryn, P., Frengstad, B., Gustavsen, B., Nygaard, E., Saettem, J., 1995. Upper Cenozoic stratigraphy on the mid-Norwegian continental shelf. Nor. Geol. Tidsskr. 75, 88–104.

Royden, L., Patacca, E., Scandone, P., 1987. Segmentation and configuration of subducted lithosphere in Italy: an important control on thrust-belt and foredeep-basin evolution. Geology 15, 714–717.

Rupke, N.A., 1978. Deep clastic seas. In: Reading, H.G. (Ed.), Sedimentary Environments and Facies. Blackwell Sci. Publ., Oxford, UK, pp. 372–415.

Savage, S.B., 1987. Interparticle percolation and segregation in granular materials: a review. In: Selvadurai, A.P.S. (Ed.), Developments in Engineering Mechanics. Elsevier, Amsterdam, pp. 347–363.

Savoye, B., 1991. Étude des avalanches sous-marines au large de Nice, IFREMER unpubl. report, 11 pp.

Savoye, B. et al., 2004. The 1979 Nice airport slide impacts on the surrounding seafloor revisited (this volume).

Scheidegger, A.E., 1973. On the prediction of the reach and velocity of catastrophic landslides. Rock Mech. 5, 231–236.

Schlosser, P., Suess, E., Bayer, R., Rhein, M., 1988. ^{3}He in the Bransfield Strait waters: indication for local injection from back-arc rifting. Deep-Sea Res. 35, 1919–1935.

Schwab, W.C., Lee, H.J., Twichell, D.C., Locat, J., Nelson, H.C., McArthur, M., Kenyon, N.H., 1996. Sediment mass-flow processes on a depositional lobe, outer Mississippi Fan. J. Sediment. Res. 66, 916–927.

Searle, R.C., 1987. Regional setting and geophysical characterization of the Great Meteor East area in the Madeira Abyssal Plain. Geol. Soc. Spec. Publ. 31, 49–70.

Sharp, J.A., Nobles, L.H., 1953. Mudflow of 1941 at Wrightwood, Southern California. Geol. Soc. Amer. Bull. 64 (5), 547–560.

Sigmond, E.M.D., 1992. Bedrock Map of Norway and Adjacent Ocean Areas. Scale 1: 3 million. Geol. Surv. Norway, Trondheim, Norway.

Simm, R.W., Weaver, P.P.E., Kidd, R.B., Jones, E.J.W., 1991. Late Quaternary mass movements on the lower continental rise and abyssal plain off Western Sahara. Sedimentology 38, 27–40.

Skempton, A.W., Hutchinson, J.N., 1969. Stability of natural slopes and embankment foundations. State-of-the-art report. Proc. 7th Inst. Conf. Soil Mech. Found. Eng., Mexico City, vol. 2, pp. 291–335.

Soler, R., Martinez del Olmo, W., Megias, A.G., Abeger, J.A., 1983. Rasgos básicos del Neógeno del Mediterráneo español. Med. Ser. Geol. 1, 71–82.

Solheim, A., Faleide, J.I., Andersen, E.S., Elverhoi, A., Forsberg, C.F., Vanneste, K., Uenzelmann-Neben, G., Channell, J.E.T., 1998. Late Cenozoic seismic stratigraphy and glacial geological development of the East Greenland and Svalbard–Barents Sea continental margins. Quat. Sci. Rev. 17, 155–184.

Stewart, I.S., Sauber, J., Rose, J., 2000. Glacio-seismotectonics: icesheets, crustal deformation and seismicity. Quat. Sci. Rev. 19, 1367–1389.

Stoker, M.S., Hitchen, K., Graham, C., 1993. The Geology of the Hebrides and West Shetland Shelves and Adjacent Deep-Water Areas, HMSO for the BGS.

Stoker, M.S., Leslie, A.B., Scott, W.D., Briden, J.C., Hine, N.M., Harland, R., Wilkinson, I.P., Evans, D., Ardus, D.A., 1994. A record of late Cenozoic stratigraphy, sedimentation and climate change from the Hebrides slope, NE Atlantic Ocean. J. Geol. Soc. (London) 151, 235–249.

Stuiver, M., Reimer, P.J., Bard, E., Beck, J.W., Burr, G.S., Hughen, K.A., Kromer, B., McCormac, G., van del Plict, J., Spurk, M., 1998. INTCAL98 radiocarbon age calibration, 24000–0 ca, BP. Radiocarbon 40, 1041–1083.

Suess, E., Fisck, M., Kadko, D., 1987. Thermal interaction between backarc volcanism and basin sediments in the Bransfield Strait, Antarctica. Antarc. J. U.S. 22 (5), 46–49.

Sultan, N., Cochonat, P., Canals, M., Cattaneo, A., Dennielou, B., Haflidason, H., Laberg, J.S., Long, D., Mienert, J., Trincardi, F., Urgeles, R., Vorren, T., Wilson, C., 2004. Triggering mechanisms of slope instability processes and sediment failures on continental margins: A geotechnical approach. Mar. Geol. 213, 291–321.

Svendsen, J.I., Mangerud, J., 1990. Sea-level changes and pollen stratigraphy on the outer coast of Sunmore, western Norway. Nor. Geol. Tidsskr. 70, 111–134.

Tappin et al., 1999. Sediment slump likely caused 1998 Papua New Guinea Tsunami, Eos, 80 (30): 329, 334 and 340.

Tappin, D.R., Watts, P., McMurtry, G.M., Lafoy, Y., Matsumoto, T., 2001. The Sissano, Papua New Guinea tsunami of July 1998—offshore evidence on the source mechanism. Mar. Geol. 175, 1–23.

Tinti, S., Maramai, A., Favali, P., 1995. The Gargano promontory: an important Italian seismogenic–tsunamigenic area. Mar. Geol. 122, 227–241.

Totland, T., 2001. Ormen Lange. Developing Large and Long Term Secure Gas Supplies Into a Deregulated Market. Norsk Hydro ASA, Norway. (available at http://www.fun-oil.org).

Trabant, P.K., 1984. Applied High-Resolution Geophysical Methods. Offshore Geoengineering Hazards. D. Reidel Publ., Boston, MA. 265 pp.

Trincardi, F., Correggiari, A., Roveri, M., 1994. Late Quaternary transgressive erosion and deposition in a modern epicontinental shelf: the Adriatic semienclosed basin. Geo Mar. Lett. 14, 41–51.

Trincardi, F., Asioli, A., Cattaneo, A., Correggiari, A., Langone, L., 1996. Stratigraphy of the late Quaternary deposits in the central Adriatic Basin and the record of short-term climatic events. Mem. Ist. Ital. Idrobiol. 55, 39–70.

Urgeles, R., Canals, M., Baraza, J., Alonso, B., Masson, D.G., 1997. The most recent megalandslides of the Canary Islands: the El Golfo debris avalanche and the Canary debris flow, west El Hierro Island. J. Geophys. Res. 102, 20305–20323.

Urgeles, R., Canals, M., Baraza, J., Alonso, B., 1998. Seismostratigraphy of the western flanks o El Hierro and La Palma (Canary Islands): a record of the Canary volcanism. Mar. Geol. 146, 225–241.

Urgeles, R., Masson, D.G., Canals, M., Watts, A.B., Le Bas, T., 1999. Recurrent large-scale landsliding on the west flank of La Palma, Canary Islands. J. Geophys. Res. 104, 25331–25348.

Urgeles, R., Canals, M., Masson, D.G., 2001. Flank stability and processes off the western Canary Islands: a review from El Hierro and La Palma. Sci. Mar. 65 (Suppl. 1), 21–31.

Urgeles, R., Lastras, G., Canals, M., Willmott, V., Moreno, A., Casas, D., Baraza, J., Berne, S., 2003. The BIG'95 debris flow in the NW Mediterranean Sea and adjacent unfailed sediments: geotechnical-sedimentological properties, and age dating. In: Locat, J., Mienert, J. (Eds.), Submarine Mass Movements and Their Consequences. Kluwer Acad. Publ., Dordrecht, The Netherlands, pp. 479–487.

Vanoudheusden, E., Sultan, N., Cochonat, P., 2004. Mechanical behavior of gassy sediments: experimental and theoretical approaches. Mar. Geol. 213. 323–342.

Varnes, D.J., 1958. Landslide types and processes. Spec. Rep.-Natl. Res. Coun., Highw. Res. Board. 29, 20–47.

Vorren, T.O., Laberg, J.S., Blaume, F., Dowdeswell, J.A., Kenyon, N.H., Mienert, J., Rumorh, J., Werner, F., 1998. The Norwegian–Greenland Sea continental margins: morphology and late Quaternary sedimentary processes and environment. Quat. Sci. Rev. 17, 273–302.

Watts, A.B., Masson, D.G., 1995. A giant landslide on the north flank of Tenerife, Canary Islands. J. Geophys. Res. 100, 24487–24498.

Weaver, P.P.E., Kuijpers, A., 1983. Climatic control of turbidite deposition on the Madeira Abyssal Plain. Nature 306, 360–363.

Weaver, P.P.E., Schultheiss, P.J., 1990. Current methods for obtaining, logging and splitting marine sediment cores. In: Hailwood, E.A., Kidd, R.B. (Eds.), Marine Geological Surveying and Sampling. Kluwer Acad. Publ, Dordrecht, The Netherlands, pp. 85–100.

Weaver, P.P.E., Rothwell, R.G., Ebbing, J., Gunn, D., Hunter, P.M., 1992. Correlation and frequency of emplacement and source

directions of megaturbidites on the Madeira Abyssal Plain. Mar. Geol. 109, 1–20.

Weaver, P.P.E., Masson, D.G., Gunn, D.E., Kidd, R.B., Maddison, D.A., 1994. Sediment mass wasting in the Canary Basin. In: Pickering, K.T., Hiscott, R.N., Kenyon, N.H., Ricci Lucci, F., Smith, R.D.A. (Eds.), Atlas of Deep-water Environments: Architectural Style in Turbidite Systems. Chapman and Hall, London, pp. 287–296.

Willmott, V., Canals, M., Lastras, G., Casas, D., 2001. Caracterización sedimentológica de un "debris flow" reciente en el margen continental del Ebro. Geotemas 3 (2), 117–120.

Wilson, C.K., Long, D., Bulat, J., Haflidason, H., 2003a. The morphology, setting and processes of the Afen Slide, COSTA. Continental Slope Stability Workshop 4, 10–13 Febr. 2003, Bologna, Italy, Abstr., p. 24.

Wilson, C.K., Long, D., Bulat, J., 2003b. The Afen Slide—a multistaged slope failure in the Faeroe-Shetland Channel. In: Locat, J., Mienert, J. (Eds.), Submarine Mass Movements and Their Consequences. Kluwer Acad. Publ, Dordrecht, The Netherlands, pp. 317–324.

Yoon, H.I., Han, M.W., Park, B.K., Oh, J.K., Chang, S.K., 1994. Depositional environment of near-surface sediments, King George Basin, Bransfield Strait, Antarctica. Geo Mar. Lett. 14, 1–9.

Zitellini, N., et al., 2001. Source of the 1755 Lisbon earthquake and tsunami investigated. Eos Trans. AGU 82 (285), 290–291.